Interaction between soil and tunnel lining during cross passage construction using artificial ground freezing

W.C.G.W. Catsman

TU Delft

Interaction between soil and tunnel lining during cross passage construction using artificial ground freezing

By

Carmen Catsman

in partial fulfilment of the requirements for the degree of

Master of Science
in Geo-Engineering

at the Delft University of Technology,
to be defended publicly on Wednesday March 21, 2018 at 4:00 P.M.

Thesis committee:

Dr. Ir. W. Broere	TU Delft, Department of Geo-Engineering
Prof. Dr. C. Jommi	TU Delft, Department of Geo-Engineering
Dr. Ir. C.B.M. Blom	TU Delft, Department of Structural Engineering & Gemeente Rotterdam
Dr. Ir. R.B.J. Brinkgreve	TU Delft, Department of Geo-Engineering & Plaxis. BV.
Ir. A. Bäcker	Arthe Civil & Structure

Preface

After months of hard work, I proudly present my master's thesis "*Interaction between soil and bored tunnel lining during construction using artificial ground freezing''*. This thesis has been written to fulfil the graduation requirements of the master program Geo-Engineering at Delft University of Technology.

During these past months the help, support and patience given by my colleagues at Arthe Civil and Structure is very much appreciated. Especially the input of Anne Bäcker gave me a boost when my ideas were frozen. Also, the coffee, stroopwafels and conversation with Kees Blom have substantially improved my work. The guidance and support of my other committee members dr. ir. W. Broere, prof. dr. C. Jommi and dr. ir. R.B.J. Brinkgreve have not gone unnoticed either and I am sincerely grateful for that.

At the moments everything did not go as planned my family and friends were a tremendous support, I cannot thank them enough.

W.C.G.W. Catsman
Capelle aan den IJssel, March 2018

Summary

Frozen soil is a powerful tool for engineering purposes due to its increased strength, stiffness and decreased permeability. Water between the soil particles bonds them together, making it possible to use frozen soil bodies as impermeable barriers and load-carrying structures. Furthermore, during a freeze and thaw cycle different processes cause deformations in the frozen and unfrozen soil. For example; frost heave, consolidation of the unfrozen zone, creep and thaw settlements. These phenomena are often called frost actions. Artificial ground freezing (AGF) is regularly used during the construction of cross passages between bored tunnels. The frost actions are expected to increase the loads acting on the lining of the main bored tunnels. This thesis investigates if a quantitative measure of loads due to frost actions on the main tunnels lining can be given with a numerical model, supporting the physical understanding of frozen soil. The objective is to determine if loads due to AGF may be a governing load case on segments of the bored tunnel lining.

Load situations that influence the interaction between frozen soil and the tunnel lining have been identified for the construction of cross passages using AGF. These load situations are based on the principles of ground freezing, construction stages in cross passage construction with AGF, the behaviour of frozen soils and case studies. The following five load situations are identified: frost heave, enclosure of water in the frozen heart, excavation, construction of the lining and thaw weakening.

The load situations have been investigated for one of the cross passages of the Westerschelde tunnel. The studied cross passage was constructed with AGF at a depth of -28,5 m in boom clay. The monitoring program for the studied cross passage of the Westerschelde tunnel was very extensive. Different types of monitors have been used to measure the soil stresses, deformations, water pressures and temperatures in the soil near the cross passage during construction. Before construction, several frozen and unfrozen soil test were carried out on the boom clay. The constitutive model used in the numerical calculation is the frozen and unfrozen soil model of Plaxis. The model requires seventeen model parameters. Furthermore six thermal parameters and three parameters for the soil freezing characteristic curve are necessary. Not all these parameters could be determined directly from the laboratory test, therefore correlations and default values were used as well. The determined parameter set is optimized and validated with help of available laboratory tests. Simulating these simple soil tests gave the opportunity to explore the capabilities of the model. In later stages the optimisation and validation of the parameters turned out to be crucial to obtain a plausible soil response in the large scale models of the cross passage.

The frozen and unfrozen soil model is only available in a two-dimensional version. Therefore, two numerical models have been made representing the construction of the cross passage: one axisymmetric model and one plain strain model. The model results have been compared to the measured data and to each other. The frozen and unfrozen model is able to describe important features of frozen soil behaviour. For more complex engineering challenges, like cross passages, some assumptions in the model are made that influence the capability of the model to simulate certain load situations. The fact that the deformations are independent of the temperature gradient has a large influence on the lining displacements, but also on pore water pressures inside the frozen cylinder. Beforehand it was already known that the constitutive model is rate independent and thus not capable to take creep into account.

Four of the load situations could be qualitatively analysed with the two numerical models .The enclosure of water in the heart of the frozen cylinder could not be simulated with the numerical models. On the other hand, soil stresses due to frost heave and excavation gave a good quantitative measure. In this research one case is extensively investigation, therefore this research is non-statistical. Henceforward, the conclusion cannot be drawn that this quantitative measure of frost heave stresses

can also be obtained for other cases. A qualitative measure of loads due to frost heave in construction with AGF can certainly be given with these numerical models. Although not all loads due to AGF could be taken into account (i.e. creep, enclosure of water in the frozen heart), one of the most important load situations (i.e. frost heave) could be quantitatively defined for the boom clay. This load situation is worth investigation in AGF projects, since stresses can become 2.5 times higher than initially measured soil stresses. At the start of the project the boom clay was given a frost-susceptibility index of negligible to low. Even with this mild index the stresses due to frost action increased significantly. This factor and index are probably not the same for other soil types. However, this study shows that such large stress increases are a real possibility during cross passage construction with AGF.

Table of contents

List of figures

APPENDIX A

APPENDIX B

APPENDIX C

APPENDIX D

List of tables

List of Symbols

Symbol	Description	Unit
C	Heat capacity	[J/m ^{3}.K]
c_s	Specific heat capacity	[J/kg.K]
E	Youngs modulus	[N/m^2]
e	Void ratio	[-]
e_0	Initial void ratio	[-]
E_f	Frozen soil Young's modulus	[N/m^2]
$E_{f,inc}$	Rate of change in frozen soil Young's modulus with temperature	[N/(m^{2}K)]
$E_{f,ref}$	Frozen Soil Young's modulus at a reference temperature	[N/m^2]
E_{in}	Internal energy	[J]
F_1	Yield criterion due to variation of solid phase	[-]
F_2	Yield criterion due to variation of suction	[-]
G	Soil shear modulus of the mixture	[N/m^2]
G_0	Soil shear modulus in unfrozen state	[N/m^2]
G_e	Gibbs free energy	[J}
K	Soil bulk modulus of the mixture	[N/m^2]
k_t	Rate of change in apparent cohesion with suction.	[-]
K_w	Water bulk modulus	[N/m^2]
L	Latent heat	[kg/ m^3]
L_w	Latent heat of water	[J/kg]
m	Yield parameter	[-]
M	Slope of the critical state line	[-]
P	Pressure	[Pa]
p^*	Mean effective stress	[N/m^2]
p^*_c	Critical stress	[N/m^2]
p^*_y	Pseudo pre-consolidation stress for unfrozen conditions	[N/m^2]
p^*_{y0}	Initial pre-consolidation stress for unfrozen conditions	[N/m^2]
p_{at}	Atmospheric pressure	[N/m^2]
p_{ice}	Ice pressure	[N/m^2]
p_{ref}	Parameter for the pressure dependency of ice thawing temperature	[N/m^2]
p_w	Pore water pressure	[N/m^2]
q	Flow rate	[J/m^2.s]
q^*	Deviatoric stress	[N/m^2]
Q_1	Plastic potential function	[-]
r	Coefficient related to the maximum soil stiffness	[-]
S	Entropy	[J/K]
s_c	cryogenic suction	[N/m^2]
$s_{c,seg}$	Segregation threshold value	[N/m^2]
$(s_{c,seg})_{in}$	Initial segregation threshold value	[N/m^2]
S_{ice}	Ice saturation	[-]
S_n	Salinity	g/l
S_{uw}	Unfrozen water saturation	[-]
T	Temperature	K
t	time	[s]
T	Current temperature	[K]

T_f	Freezing/melting temperature	[K]
T_k	Reference temperature for solvents	[K]
T_{ref}	Reference temperature	[K]
V	Volume	[m^3]
w	Water content	[m^3/m^3]
w_u	Unfrozen water content	[m^3/m^3]

GREEK SYMBOLS

Symbol	**Description**	**Unit**
$\alpha_{,x,y,z}$	Thermal expansion coefficient in x,y,z direction	[1/K]
α	Parameter for the pressure dependency of ice thawing temperature	[-]
β	Parameter controlling the rate of change in soil stiffness with suction	[m^2/N]
γ	Plastic potential parameter	[-]
γ_w	Unit weight of water	[N/m^3]
$d\varepsilon$	Increment of strain	[-]
$d\varepsilon^m$	Increment of st rain due to solid phase stress variation	[-]
$d\varepsilon^{me}$	Increment of elastic strain due to solid phase stress variation	[-]
$d\varepsilon^{mp}$	Increment of plastic strain due to solid phase stress variation	[-]
$d\varepsilon^p$	Increment of plastic strain	[-]
$d\varepsilon^s$	Increment of strain due to suction variation	[-]
$d\varepsilon^{se}$	Increment of elastic strain due to suction variation	[-]
$d\varepsilon^{se}$	Increment of plastic strain due to suction variation	[-]
$d\varepsilon^e_q$	Increment of elastic shear strain	[-]
$d\varepsilon^e_v$	Increment of elastic volumetric strain	[-]
κ	Elastic compressibility coefficient of the soil mixture	[-]
κ_s	Elastic compressibility coefficient for suction variation	[-]
κ_0	Unfrozen soil elastic compressibility coefficient	[-]
λ	Elasto-plastic compressibility coefficient for a frozen state	[-]
λ_0	Elasto-plastic compressibility coefficient for an unfrozen state	[-]
λ_s	Elasto-plastic compressibility coefficient for suction variation	[-]
λ_{s1}	Thermal conductivity	[W/(mK)]
λ_r	Parameter for fitting unfrozen water saturation curve	[-]
$d\lambda_1$	Plastic multiplier regarding the loading-collapse yield surface	[-]
$d\lambda_2$	Plastic multiplier regarding the grain segregation yield surface	[-]
ν_f	Frozen Soil Poisson's ratio	[-]
ρ_b	Dry bulk density of the unfrozen soil	[kg/m^3]
ρ_r	Parameter for fitting unfrozen water saturation curve	[N/m^3]
ρ_s	Density of the solid material	[kg/m^3]
ρ_{ice}	Density of ice	[kg/m^3]
σ	Total stress	[N/m^2]
σ^*	Solid phase stress	[N/m^2]
ϕ	Residual or critical angle of friction	[^{o}]

List of abbreviations

Abbreviation	**Definition**
AGF	Artificial Ground Freezing
BC	Boom clay
CP	Cross passage
FUS model	Frozen and unfrozen soil model
GS yield surface	Grain segregation yield surface
LC yield surface	Load collapse yield surface
M1	Model 1
M2	Model 2
NATM	New Austrian Tunnelling Method
SFCC	Soil Freezing Characteristic Curve

1 Introduction

Frozen soil is a powerful tool for engineering purposes due to its impermeability and high strength. Water between the soil particles bonds the particles together, making it possible to use frozen soil bodies as impermeable barriers and load-carrying structures. For more than a century, artificial ground freezing (AGF) has been used for underground constructions works. AGF was developed by the German engineer Friedrisch Poetsch in order to safely construct shafts through water bearing soils down to hard rock and coals seams. Nowadays, AGF is used in many other geotechnical applications such as groundwater control systems, temporary excavation support and soft soil stabilisation. (Shuster, 2000; Chang & Lacy, 2008; Haß&Schäfers, 2006). Another important advantage is that AGF is an environmentally friendly method, because it leaves no residual products in the subsurface after the frozen soil body has served its purposed and thaws. The frozen body can be designed in many shapes and can be used in any soil type containing a limited amount of pore water

1.1 Application of the artificial ground freezing method

AGF is based on heat withdrawal from the soil. A frozen body can be formed in many shapes depending on the freeze pipe configuration. A closed ended freeze-pipe is placed in the soil. An inner pipe or supply pipe is inserted into this freeze pipe. The cooling medium flows through the supply pipe and backs up through the freeze pipe. On the way up, heat is exchanged between the soil and the cooling medium. A continuous flow of cooling medium causes a frozen ring around the freeze pipe (Figure 1.1). This ring grows and when several freeze pipes are placed in sequence their columns will merge into one large frozen ground mass. Two different cooling systems can be used to freeze the ground, the direct and indirect freezing method. A combination of these two systems is also possible.

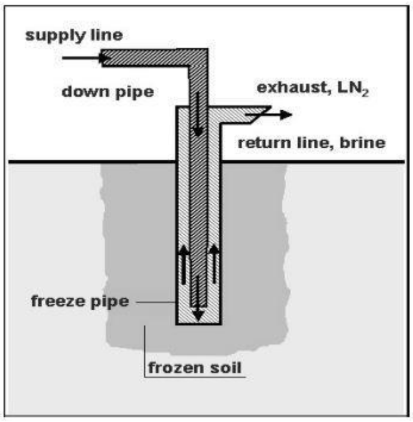

Figure 1.1: Coolant flow through freeze pipe (Haß & Schäfers, 2006).

1.1.1 Direct freezing method

In this system, heat is extracted from the soil through direct vaporisation of a cryogenic fluid in the freeze pipe. The cryogenic fluid is often liquid nitrogen (LN_2) which starts to vaporise at -196 ^{0}C. The LN_2 is pumped through the freezing pipes from a storage tank. Because this is an open system, the cold nitrogen gas is directly released into the atmosphere after its cycle through the freeze pipes (Figure 1.2a). The relative high speed of freezing is an advantage of direct freezing. Due to the very low temperature, a frozen body can be formed in days. The liquid nitrogen is not re-used in this system, which makes it an expensive method if used for longer periods. Also, the delivery of the LN_2 must be scheduled precisely to maintain the frozen body. Because of the advantages and disadvantages of the direct method, it is mostly used for short-term projects or limited volumes of soil (Haß & Schäfers, 2006).

1.1.2 Indirect freezing method

The indirect method is a closed system with brine as a cooling medium. Brine is water with an additive to lower the freezing point, this additive is usually calcium chloride (Johansson, 2009). After the brine is pumped through the freezing pipes, it returns to the freezing plant station for re-cooling (Figure 1.2b). Thus, the indirect freezing method is a closed system. The temperature of the brine varies from -25 ^{o}C to -37 ^{o}C. Although brine freezing takes about five times longer than freezing LN_2, indirect freezing is less expensive when the freezing time becomes longer (Figure 1.3), where the cost relation (cost LN_2/ cost brine) is indicated. The cost of brine becomes less than LN_2 when the freezing time is longer or excavation is larger.

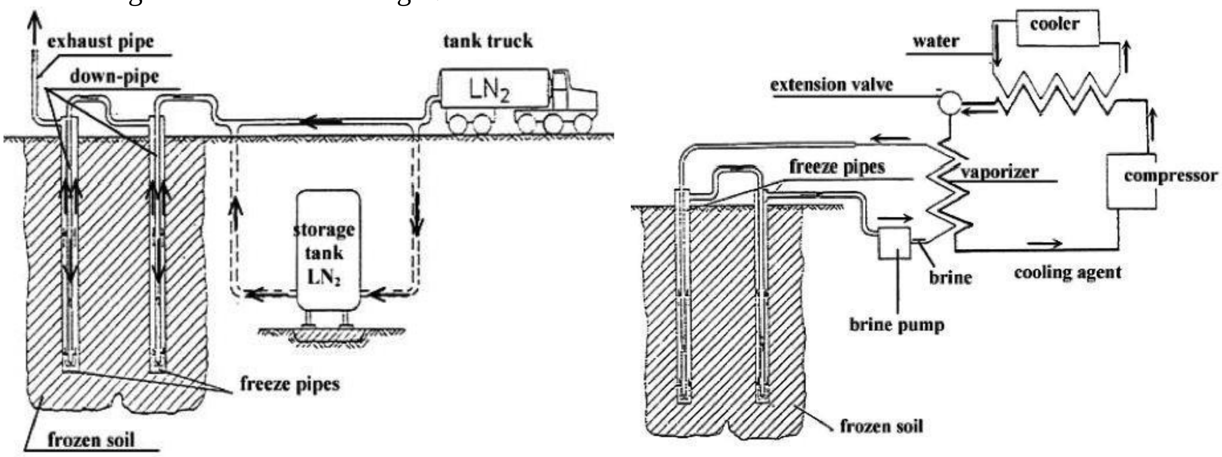

a. Direct freezing **b. Indirect freezing**

Figure 1.2 Freezing systems

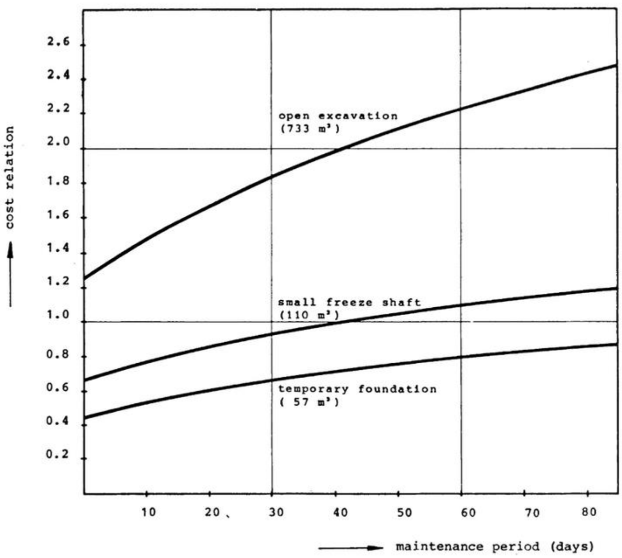

Figure 1.3: Cost relation between brine freezing and liquid nitrogen. (Stoss & Valk, 1979)

1.1.3 Combination of direct and indirect freezing

Best of both indirect and direct freezing can also be combined. Initial freezing of the soil body can be done with liquid nitrogen, leading to rapid formation of a frozen body. The maintenance of the frozen body with brine will follow, resulting in lower freezing cost during a longer maintenance period. For the combination system, it is a possibility to use the same freeze pipes both for the liquid nitrogen and brine. However, adaptions have to be made when switching from one system to the other. The disadvantage of using the same pipe system is that during the adaption no heat can be extracted from the soil and the soil body will start thawing.

Another option is to install two independent systems. More freezing pipes need to be installed, but the transition of methods can be realised without adaptions. The frozen body can be maintained continuously. Two independent systems also give extra security. In case of unexpected problems with the frozen body, freezing can be speeded up using the direct freezing system. Also, a back-up is always present when one of the two systems fails.

1.2 Artificial ground freezing in cross passage construction

AGF is regularly used during the construction of cross passages between bored tunnels (Figure 1.4). Due to safety concerns bored tunnels are often constructed in pairs, one tube for each traffic direction. This reduces the risk of frontal collisions between trains or cars. Cross passages are an extra safety measure and offer the possibility to escape from one tunnel tube into the other in case of a calamity. Construction of cross passages from ground level is not a possibility in every project, since tunnels are often built underneath rivers or densely built up areas. The result is a situation where the cross passages have to be constructed from within the tunnels, which is challenging when the bored tunnels are located in soft soils underneath the ground water level. Soil between the tunnel tubes needs to be stabilized and water prevented from rushing in when a hole is made in the lining of the bored tunnel. In the Netherlands, AGF proved to be a reliable construction method when constructing the 26 cross passages of the Westerschelde tunnel in 2000. The method was adopted for many other cross passages in the Netherlands.

Several construction stages can be distinguished when constructing a cross passage from within the main tunnel (Figure 1.5):

1. Freezing
2. Maintenance
3. Excavation
4. Construction of the lining
5. Thawing

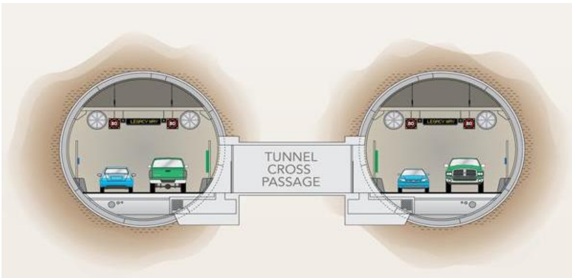

Figure 1.4: Cross passage between two tunnel tubes

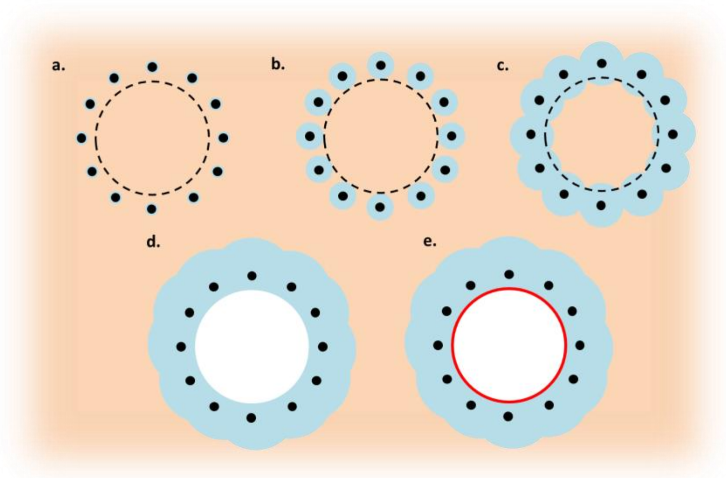

Figure 1.5: Schematic view of artificial ground freezing stages during cross passage construction. a. Installation of the freeze pipes b. Growing of the columns around the freeze pipes c. Closing of frozen ring d. Excavation of the cross passage e. Installation of the lining

1.2.1 Freezing

To freeze the soil between two tunnels, freezing pipes will be placed in a circular pattern (Figure 1.5a). Besides placement of the freezing lances, installation of temperature sensors is important to keep track of the temperature and growth of the frozen body. Special pipes can be placed to measure the temperature. Depending on the distance between the two tunnels the pipes can be placed through the segment lining from either one tube or both tubes (Figure 1.6). First frozen columns around the freeze pipe will be formed (Figure 1.5b), which later will merge into a frozen ring (Figure 1.5c). Indirect freezing with brine is often employed to freeze cross passage. The closed system is safe to use in the enclosed space of the start tunnel. Liquid nitrogen can also be used, but the vaporised nitrogen gas cannot be vented inside the tunnel. Therefore more adaptions have to be made to this system in order to meet the safety regulations. (Groot et al., 2009)

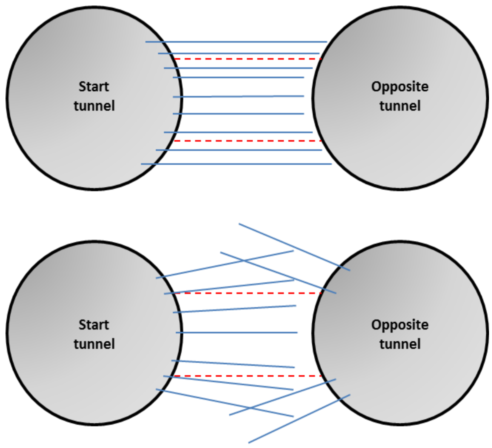

Figure 1.6: Possible freeze pipe configurations

1.2.2 Maintenance

The freezing temperature can be lowered when the frozen body has grown to its required size and is watertight. At this point, it is not necessary to let the frozen body grow any bigger. Freezing is only necessary to preserve the already frozen soil. Temperature sensors in the ground or sound waves can be used to check whether the volume of frozen soil is big enough. The wave velocity of unfrozen and frozen soil differs and is respectively 400-1600 m/sec and 1200-4800 m/sec. The water tightness of the connection between the frozen cylinder and the two tunnel tubes can be checked by placing a water pressure sensor inside the heart of the frozen cylinder. As soon as the frozen cylinder is watertight, the water is trapped inside the frozen cylinder and between the bored tunnels. The water cannot move as it expands upon freezing and the pore water pressure inside the heart of the cylinder increases. Furthermore, energy costs are reduced by increasing the freezing temperature.

1.1.1 Excavation

During excavation of the cross passage the frozen body has to fulfil its role as load bearing and impermeable structure (Figure 1.5e). Before excavation, a gap has to be made in the lining of the main tunnel. The gap reduces the strength of the lining and stresses must be redistributed through other segments. Due to the extra loading of the segments near the gap, often special segments (e.g. steel segments) are used to compensate the higher stresses. The position of the gap relative to the segments influences how stresses are redistributed around the gap (Figure 1.7) Making the gap in the tunnel lining can be done from both bored tunnels. When lack of space is a concern, the gap is made from the opposite tunnel, in order to prevent interference with the freezing system in the start tunnel

Excavation of the frozen soil is often done with the New Austrian Tunnelling Method (NATM). Sections will be excavated one by one, assuming the frozen soil can be stable without support for some time (Figure 1.8). After excavation of each section, shotcrete is placed as a temporary support. In NATM, the time between the excavation and placing of the shotcrete is crucial. The longer is waited to install the lining, the more the frozen soil may deform. According to the convergenceconfinement method the more elastic deformations in the soiled are allowed, the necessary support pressure by the lining decreases. The deformations allows to soil to redistribute the stresses around the excavation.

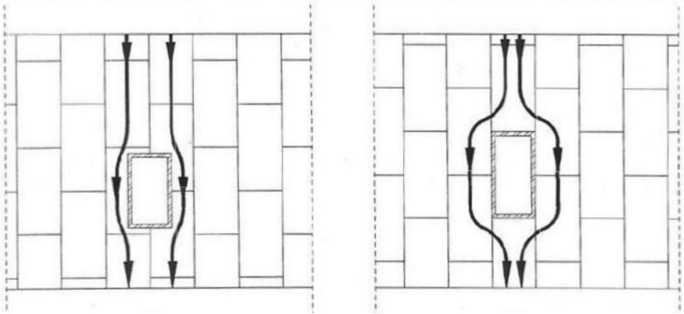

Figure 1.7: Different redistribution of stresses around the gap. (Van der Meer, 1999)

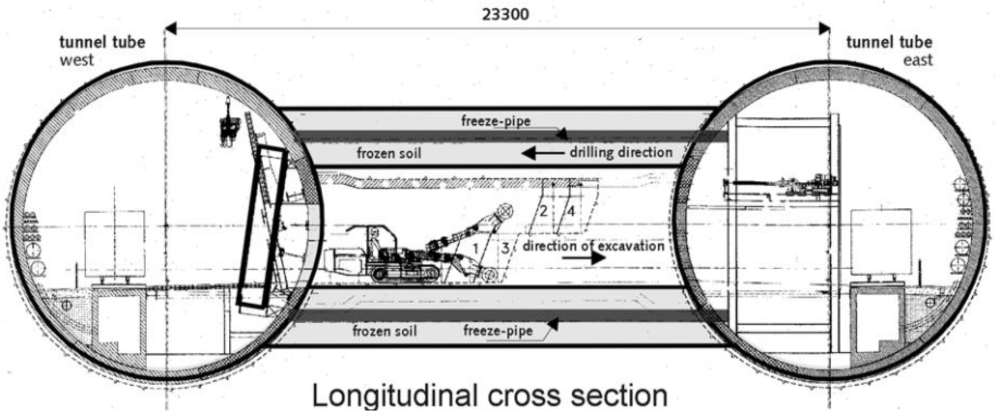

Figure 1.8: Sequential excavation with NATM in a cross passage (Heijboer, Van den Hoonaard, & Van de Linde, 2004)

1.1.2 Construction of the lining

During excavation, a temporary shotcrete lining is made. Spraying the shotcrete directly on the frozen soil may lead to insufficient hardening, due to the cold temperature of the soil. Insulation can be placed first against the frozen walls to prevent the shotcrete from falling off. Before the final lining is made an impermeable membrane will be applied to prevent leakage. Leakage between the connection of the cross passage and main tubes is also a hazard. Making a rigid connection between the two gives less risk of leakage but a flexible connection with an expansion joint offers room for settlements after thawing of the soil. Small deformations can be sustained without cracks in the joints. Fabrication of the final lining can be done in several ways i.e. shotcrete and reinforcement, cast in place concrete or prefab elements (Figure 1.5e).

1.1.3 Thawing

When the construction in the cross passage is finished, freezing can be stopped. Freezing pipes can be extracted from the soil. In time it becomes clear if the cross passage is completely water proof. It may take a while before any leakage will be noticed. Temperature measurements by Johansson (2009) showed areas of frozen soil still present even 12 months after shutting down the cooling device. Accelerated thawing is also possible, by turning the freeze pipes into warming pipes. Pumping warm water through the system will thaw the frozen body faster. In some conditions the ice will turn into water faster than the soil can discharge, causing excess pore water pressures. This may lead to extra settlements.

1.2 Difficulties with artificial ground freezing

Shuster(2000) described problems that could be encountered during AGF. He divided these problems into four categories; structural considerations, groundwater considerations, ground movement considerations and construction considerations. From these categories important difficulties for AGF as an aid in tunnelling are summed up below:

- *Ground movement*

  Water expands upon freezing, also in soils. That is why an expansion of soil during freezing can be expected, this is called frost heave. When frost heave is restricted, high pressures can arise nearby structures, for example the lining of the main bored tunnels. Furthermore, a volume decrease can be seen when the soil thaws again. This may lead to (non- uniform) settlement near the cross passage. Apart from frost heave and thaw weakening, there are more processes that deform the soil during freezing and thawing. Andersland & Ladanyi (2004) use the term *frost action* to refer to processes during freezing and thawing of soil. These frost actions can influence the construction process and nearby structures.

- *Water movement*

  Water flow near the frozen body supplies heat to the system. If the energy supply from this source exceeds the energy the freezing pipe can extract, the soil body melts. Zones of high permeability may easily go undetected during soil investigation. The consequence of this water flow is that the frozen body will thaw, does not close or has weak zones. Flow velocities larger than 2 m/day for brine freezing and 6 m/day for liquid nitrogen freezing might cause problems with the frozen body (Andersland & Ladanyi, 2004).

- *Water quality*

  Solvents in frozen soil depress the freezing point, for example salt water or hydrocarbons. Longer freezing times have to be taken into account in salt water environments. As a consequence of a lower freezing point, a higher unfrozen water content is present in the soil. At a certain sub-zero temperature the strength and stiffness in frozen soil with salt water will be lower than a frozen soil with fresh water, due to the higher unfrozen water content.

- *Water quantity*

  Frozen soil is stronger than unfrozen soil, due to of the transformation of water into ice. Strength or stability of the soil is not increased if the water saturation is too low. The strength of the frozen soil is closely related to the saturation. The strength and stiffness increase in the soil will be limited with saturations lower than 10%, therefore the benefits of AGF will be limited (Shuster, 2000).

- *Enclosure of water in frozen cylinder*

  When AGF is used for the construction of cross passages, the frozen columns will eventually merge and form a closed cylinder (Figure 1.5c). Water inside this cylinder is now trapped between the two main tunnel tubes. Further growth of the frozen cylinder in radial direction causes pressure on the enclosed (still unfrozen) water in the pores, because volume expansion is restrained by the main tunnels and frozen cylinder itself. Placing a drainage pipe in the middle of the cylinder and opening a valve in the main tunnel, can help to release the water pressure on the main tunnels and cylinder (Report F100-E-02-0.79, 2002). A sensor was placed inside the cylinder to measure the increasing water pressures when the frozen body is fully closed. It is important to start draining at an early stage after closure, because when the soil is frozen drainage does not reduce frost heave loads.

- *Boundary effect*

  A good connection between the frozen body and the tunnel is required to be able to open the lining without an ingress of water and soil. Heat exchange can take place between the segments of the main tunnel and the adjacent soil, especially with steel segments. Therefore the temperature of the main tunnels lining can be too high to make a solid connection with the frozen body. In this situation the lining forms a temperature boundary for the frozen body due to higher temperatures in the main tunnels. Insulation of the main tunnel lining around the freeze pipes and cooling with ice from inside of the main tunnel have been used to enable the connection between the frozen body and main tunnels (Report F100-E-02-0.79, 2002).

- *Irregularities frozen body*

Different soil types have different thermal behaviour, as a consequence of their minerology and degree of saturation. Varying soil types in one freezing area can therefore cause irregularities in the diameter of the frozen column around the freeze pipes(Figure 1.9). To ensure the right thickness and bearing capacity of the frozen body, these irregularities have to be taken into account (Chang & Lacy, 2008). Temperature sensors can be used to verify the thickness and shape of the frozen body.

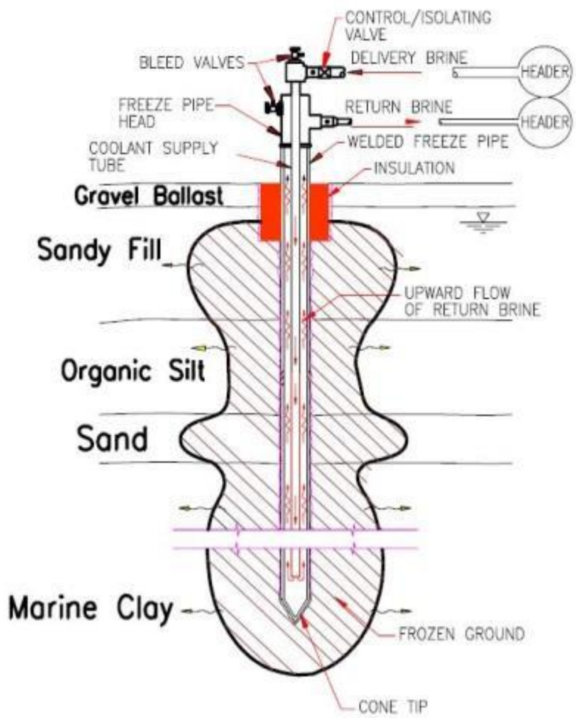

Figure 1.9: Irregular diameter of frozen column (Chang & Lacy, 2008)

1.3 Problem description

When AGF is used in order to construct a cross passage between two tunnels, frost actions are expected to influence the soil stresses and properties . Consequently this influences the loads acting on the lining of the main tunnels. In literature, little can be found on the (frozen) soil tunnel lining interaction. Frost heave is more often mentioned as an influence on cross passages than thaw settlement. However, according to Shuster (2000) thaw settlement is larger than the initial heave by an order of 20-25%. Fully thawing of the frozen soil body take several months. The consequences of these frost actions on the cross passage and the main lining are hard to predict. Understanding the physical soil behaviour due to frost actions is essential to understand the interaction between frozen soil and the lining.

Design with AGF often consists of a thermal analysis to determine the shape and temperature profiles of the frozen soil body and a structural analysis to evaluate whether or not the frozen soil is stable during construction. However, there is no generally accepted engineering method to reliably quantify the loads on structures due to frost actions. Therefore, governing risks as a consequence of the frost actions are sometimes needed to be mitigated since the consequences to adjoining structures are not well-known.

A new material model for frozen soils was recently implemented in the finite element program Plaxis (Plaxis, 2016). This material model is based on the constitutive material model for rate-independent behaviour of saturated frozen soil developed by Ghoreishian, Amari, Grimstad, Kadivar and Nordal (2016). It is expected that by using a numerical model with the new material model of Plaxis, the freeze action loads acting on the adjoining structures are predicted more reliable. This expectation results in the following problem statement on which I will reflect in this thesis:

Problem statement:
Can a quantitative measure of loads due to frost actions on the bored tunnel lining be given with a numerical model, supporting the physical understanding of frozen soil.

Objective
To determine if loads due to AGF may be a governing load case on the segments of a bored tunnel lining.

1.4 Methodology

In order to answer the problem statement, this question has been decomposed in different sub-questions. First a literature study is done to answer the following sub-questions to understand the behaviour of frozen soil:

1. *What soil behaviour (stress-strain, stiffness and deformations) can be expected of soil during freezing and thawing?*

2. *What interaction can be expected between the (frozen) soil and lining of the main tunnel and cross passage is during different stage of cross passage construction with AGF?*

These questions will lead to hypotheses about soil and lining behaviour during construction with AFG, which will be tested with the Plaxis unfrozen and frozen material model. For this purpose, numerical models will be made of the cross passages of the Westerschelde tunnel where the cross passage were constructed with AGF in 2000. Before the construction of these cross passages, laboratory tests were done on the soil and extensive monitoring took place for two cross passages of the Westerschelde tunnel. The availability of monitoring data makes it possible to quantitatively compare the measured results to the model results. With the numerical model, the aim is to answer the following sub-questions:

3. *What are the similarities and differences between modelled soil behaviour and the measured soil behaviour (stresses, pore water pressure, deformations and temperature?*

4. *Are there any unexpected phenomena noticed in the numerical models?*

1.5 Limitations

Limitations of this thesis that were determined beforehand:

- Research will be done for artificial freezing in soft soils and not in rock.
- Behaviour of soil is described for a situation where the soil is not previously exposed to multiple freeze-thaw cycles. Multiple freeze-thaw cycles have influence on the soil behaviour, and can occur due to natural freezing of the top soil layer.
- The frozen and unfrozen model is a new constitutive model in Plaxis. Many features of frozen soil are captured however, creep behaviour cannot be taken into account.
- The model can only be used for fully saturated soils.
- The frozen and unfrozen model is only available in 2D. Calculations can only be made based on axisymmetric or plane strain assumptions.

1.6 Document structure

Chapter 2:	Changes in soil behaviour are described when the soil freezes. Different phenomena occurring during freezing (i.e. frost actions) are explained as well.
Chapter 3:	The interaction between frozen soil and the bored tunnel lining is described by different load situations. These load situations are based upon the principles of ground freezing, construction stages in cross passage construction with AGF, the behaviour of frozen soil and experiences during different AGF projects.
Chapter 4:	Parameters are determined for the frozen and unfrozen model for boom clay. The parameters are optimised and validated by comparing numerically modelled soil tests to laboratory tests from the Westerschelde project.
Chapter 5:	Two numerical models are made of the studied cross passage from the Westerschelde tunnel. The numerical models are compared with each other, the expected interaction from chapter 3 and with measurements taken during construction of the cross passage.
Chapter 6:	Discussion
Chapter 7:	Conclusion and recommendations

2 Behaviour of frozen soil

First the thermal properties of soil are discussed in paragraph 2.2. These properties determine the speed of freezing. The properties of frozen soils are different from unfrozen soils, due to the presence of ice in the voids. The change in soil properties is described in paragraph 2.2. During a freeze and thaw cycle different processes cause deformations in the frozen and unfrozen soil. The physical processes causing these deformations are discussed in paragraph 2.3.

2.1 Thermal properties of soil

In contrast to natural ground freezing, artificial ground freezing can be controlled in order to create the frozen body in a desired shape. The rate of the temperature change can be controlled by controlling the amount of energy extracted from the ground by the freezing pipes. Heat capacity, thermal conductivity and latent heat are important thermal properties. These parameters change with temperature, soil type, water/ice content, degree of saturation. Solvents have an important influence on thermal properties as well.

2.1.1 Heat capacity

The heat capacity C (J/m^3K) of the soil is the amount of energy per volume-unit necessary to raise the temperature one Kelvin. The specific heat capacity c_s (J/kg.K) is the necessary amount of energy per mass unit to raise the temperature 1 Kelvin.

$$C = \rho_d * c_s \qquad 2.1.1$$

The heat capacity of the soil depends on the specific heat capacity of all components, grains, water and ice. For the unfrozen, frozen or partially frozen soil the heat capacity can be calculated by taking the specific heat capacity of the different components and weighting them by their mass fractions (Andersland & Ladanyi, 2004).

$$C_{soil} = \rho_d \left(c_{s,k} + c_{s,w} * \frac{w}{100} \right) + \left(c_{s,i} * \frac{w - w_u}{100} \right) \qquad 2.1.2$$

Where:

ρ_d	dry density	(kg/m^3)
$c_{s.k}$	Specific heat capacity of the grains	(kJ/kg.K)
$c_{s,i}$	Specific heat capacity of ice	(kJ/kg.K)
$c_{s,w}$	Specific heat capacity of water	(kJ/kg.K)
w	Total water content	-
wu	Unfrozen water content	-

The heat capacity is thus a function of the frozen and unfrozen water content, and they are both not constant during a freezing process. The specific heat capacity of ice (at 0^oC) is approximately 2.09 kJ/kg.K and of water (0^oC) 4.22 kJ/kg.K. Consequently, the heat capacity decreases when the unfrozen water content decreases.

2.1.2 Thermal conductivity

Just as heat capacity, different components of the soil have different thermal conductivities. The thermal conductivity (λ in W/m.K) influences the rate of heat transfer through a medium. This increases when the dry density and degree of saturation increase (Andersland & Lananyi, 2004). The rate of heat transference through a soil per unit area (q in J/m^2.s) is given by:

$$q = -\lambda * \frac{dT}{dx} \qquad 2.1.3$$

Where dT/dx is the thermal gradient (^{o}C/m). Heat flows from high to low temperatures, which is indicated by the minus sign. The thermal conductivity can be measured during laboratory tests. Instead, it can also be calculated with the method of Johansen (1975) which is based on the thermal conductivity of minerals, fraction of frozen/unfrozen water, temperature and dry density.

2.1.3 Latent heat

The amount of energy that must be extracted from water to turn it into ice or the amount energy that must be absorbed by ice to return into water is called latent heat. For soils, the amount of latent heat will depend on the water content. The mass latent heat for water (L_w) is 333.7 kJ/kg. The latent heat for soil (L in kJ/m^3) can be calculated with the dry density of the soil and the (ρ_d) , total water content (w) and unfrozen water content (w_u) according to the following formula:

$$L = \rho_d L_w * \frac{w - w_u}{100} \qquad 2.1.4$$

2.1.4 Solvents

Heat capacity, thermal conductivity and latent heat are all influenced by the volume of ice and water in the soil. Solubles such as salts depress the freezing point and consequently the volume of unfrozen water at certain temperatures. When salt water freezes, the salt is expelled from the ice into the unfrozen water. Resulting in an increased salt content in the remaining unfrozen water, depreciating the freezing point even further. This process stops at -21o C as salt (NaCl) crystalizes at its eutectic temperature. A lower freezing point increases the creep rate (Anderland & Ladanyi, 2004). The amount the freezing point depreciates (ΔT), can be calculated using the empirical equation of Veili and Grishin (Andersland & Ladanyi, 2004):

$$\Delta T = T_k \left[\frac{Sn}{1000 + Sn}\right] \qquad 2.1.5$$

Where:

Sn	Salinity	(g/l)
T_k	Reference temperature for solvents +57^{o}C for sea water, +62^{o}C for NaCL and +31,5 ^{o}C for $CaCl_2$	(^{o}C)

Material properties, like strength and stiffness, are dependent on the freezing temperature. In the design of the frozen body it is important to take into account different material properties in a saline environment with respect to properties that would be taken into account in a fresh water environment at the same temperature.

2.2 Changing properties

The changing soil strength, stiffness and permeability becomes very beneficial during construction. The changes of these two important soil properties during freeze-thaw cycle will be discussed together with the parameters influencing them:

2.2.1 Strength

Frozen soil consists of solid grains, ice, unfrozen water and gasses. In a saturated state the pores are filled with unfrozen water and ice. Due to strong molecular forces unfrozen water surrounds the solid grains. Water in the middle of the pores is free to freeze. Despite a small fraction of water form a thin film around the grains, the behaviour of frozen soil is primarily directed by the ice. Ice strengthens the soil since it can resist shear forces (unlike water). This means that in frozen condition, loads can be spread over the ice skeleton and soil skeleton. However, ice under pressure melts. Due to this pressure melting phenomenon, ice deforms and transfer loads from the ice to the soil skeleton. Deformation and redistribution of stresses under the same loading indicate that frozen soil is sensitive to creep. For that reason, frozen soil has a long term strength and a short term strength.

Ice between the grains bonds them together and increase cohesion with decreasing temperature. The strength of the soil is increased due to an increase in cohesion, while the internal angle of friction barely changes at sub-zero temperatures (Report NITG 98-22-B, 1996). Because ice in the pores increases the cohesion, the strength of frozen soil very much depends on the amount of ice present in the soil. This already starts with the initial water content. Figure 2.1 shows an uniaxial compression test on frozen silt with different water contents. Higher water content results in a higher compressive strength. In addition, plastic and brittle behaviour in the frozen silt can be observed between varying water contents. Figure 2.2 shows an optimum water content for fine sand. The strength of a ‘’frozen’’ soil with very little water in the voids (<10%) is the same as an unfrozen soil. With increasing moisture content, the strength increases until full saturation of the voids is reached (Shuster, 2000). At larger moisture content, the soil is oversaturated and the grains are separated decreasing the strength until the compressive strength of 100% ice is reached.

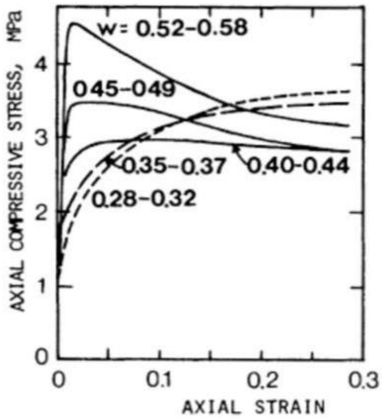

Figure 2.1: Stress-strain curve of silt frozen at -1.67°C with varying total water content (Sayles & Carbee ,1980).

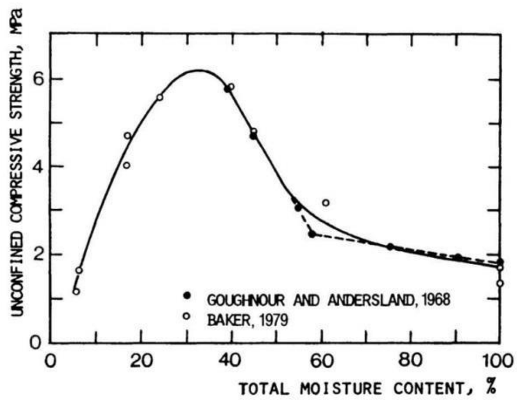

Figure 2.2: Effect of total moisture content on the unconfined compressive strength of frozen fine sand at -12°C and at a strain rate of 2.2 x 10^{-6} s^{-1} (Baker, 1979)

Upon freezing there are several factors that have influence on the ice content in the pores: soil type, temperature, load and time.

- *Soil type*
  The strength of unfrozen soil is different for each soil type. It depends on the friction between the particles, cohesion (in clays) and dilatancy (in sands), stress conditions, stress history and loading conditions. These factors are all important in frozen soil as well. New is the extra strength increase due to the ice. Soils with a higher fine content and a higher specific surface area hold more unfrozen water since more minerals are coated with an unfrozen water film. Sands have a smaller specific surface area than clay and have a larger ice content at the same sub-zero temperature.

The difference in compression strength between frozen sand and clay at a temperature of -12^{o}C is shown in Figure 2.3. Compressional strengths of both clay and sand increase when frozen, because the cementation by the ice reduces the compressibility of the soil skeleton (Andersland & Ladanyi, 2004). The strength of the sand in Figure 2.3 increased 8.5 times in frozen state. Although both compressive strengths of sand and clay have increased, the sand is approximately a factor 2 stronger. This large difference is mainly because the amount of unfrozen water in clay remains higher than in sand. So, an increase in ice content will decrease the compressibility of the soil, resulting in a higher compressional strength.

- *Temperature*

Decreasing sub-zero temperatures increase the ice content within the pores, because the pre-melting film becomes thinner. Therefore, frozen soil becomes stronger until a certain peak temperature at very low temperatures. The strength increase is not only due to ice content. Also ice becomes stronger at lower temperatures. Figure 2.4 shows the uniaxial compression strengths of different materials with varying temperatures. The strength goes up with decreasing temperature. A large increase in strength can be observed for clay between -80 ^{o}C and -100 ^{o}C, Even the pre-melting film starts to freeze at this range of temperatures. Before reaching these low temperatures, the frozen sand is stronger than the frozen clay. Different compressional strengths are shown for ice. This varies among others with crystal structure, rate of freezing, chemical compositing, temperature (Sayles, in Shelman et al, 2014).

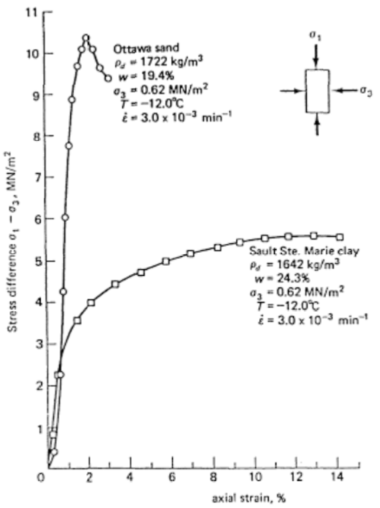

Figure 2.3: Stress-strain curves for unconfined compression tests on different materials (Andersland & Ladanyi, 2004).

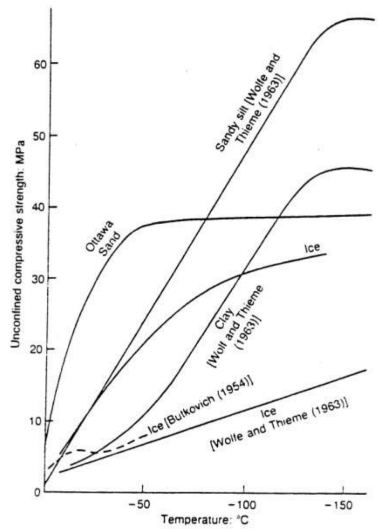

Figure 2.4: Uniaxial compression strength of different materials at different temperatures. (Sayles, in Shelman et al, 2014).

- *Load (rate)*

Strength of frozen soil becomes higher with higher confining pressures, just as for unfrozen soil. When frozen soil is loaded, ice melts at the contacts with the grains increasing the unfrozen water content. This reduces the strength of the frozen soil. (Ghoreishian Amari et al., 2016).

Also, the strain rate has influence on the behaviour of frozen soil. Figure 2.5 shows the relationship between the strength of a frozen silt at different strain rates in compression and tension. This shape of the curve and the separation of the compressional and tensional strength is the same as for ice, however the strain rate at separation is about four times higher. As already can be seen from Figure 2.1 and Figure 2.3 behaviour of frozen soil can be plastic and brittle. Clays behave primarily plastic, only at temperatures below -110^{o}C even molecular bound water freezes and the clay starts to behave brittle. In sands brittle or plastic behaviour can be related to the strain rate (Figure 2.6) (Anderland & Ladanyi, 2004).

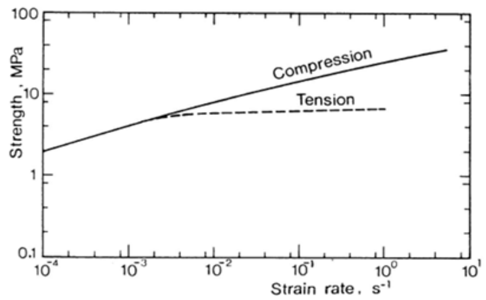

Figure 2.5: Relationship between strength and strain rate for a frozen silt at -9.4^{0}C.

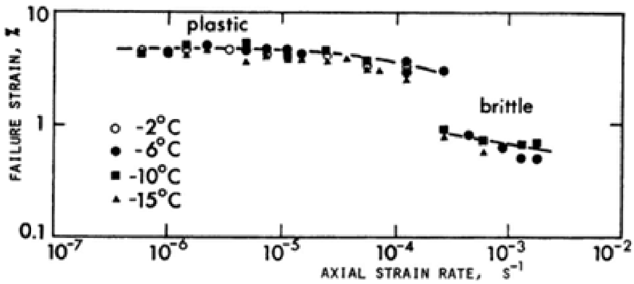

Figure 2.6: Failure strain vs strain rate for a frozen sand.

- *Time*

Frozen soil has a long term strength and short term strength due to creep. Sayles (1968) did extensive testing on creep in sands. Figure 2.7 shows time dependence of the strength of Manchester fine sand at different temperatures. The instantaneous strength can be almost ten times larger than the long-term strength and is therefore important to consider during design.

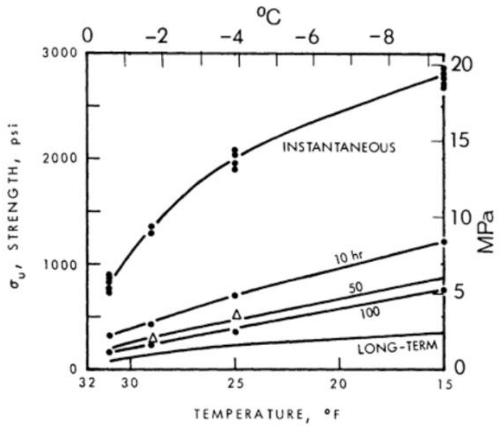

Figure 2.7: Temperature – time dependence of uniaxial compressive strength for Manchester fine sand. (Sayles, 1973).

Upon thawing the strength of the soil changes again and does not return exactly to its original strength. Often a reduction in strength can be observed, called thaw weakening. Figure 2.8 shows over-consolidated clay in unfrozen and post-thawed condition. The peak strength of the over-consolidated clay in unfrozen state due to inter-particle bonding is damaged during freezing and disappears in the post-thawed clay

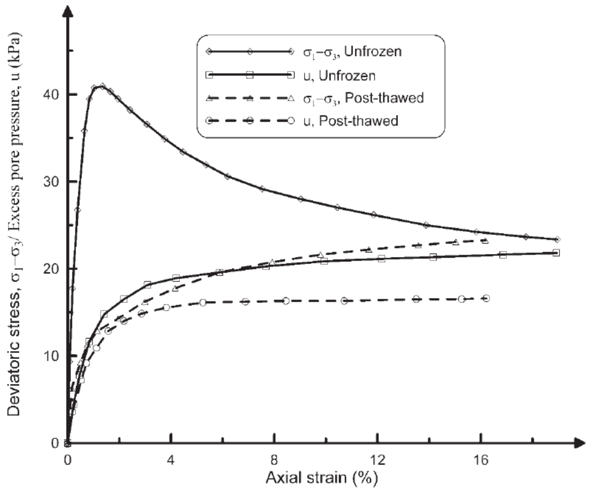

Figure 2.8: Triaxial compression tests for unfrozen and post-thawed over consolidated clay (Leroueil et al, 1991)

Qi, Ma, & Song (2008) investigated properties of a post-thawed silt and found that changes in cohesion and friction angle can be related to the dry unit weight of the soil. In Figure 2.9 is shown that the cohesion decreases at dry unit weight above 16.4 kN/m^3 and the friction angle increases. There is a critical dry unit weight for both cohesion and friction where freezing and thawing does not have influence on these parameters. Given the combination of change in friction angle and cohesion, freezing and thawing does not always have to result in a lower strength.

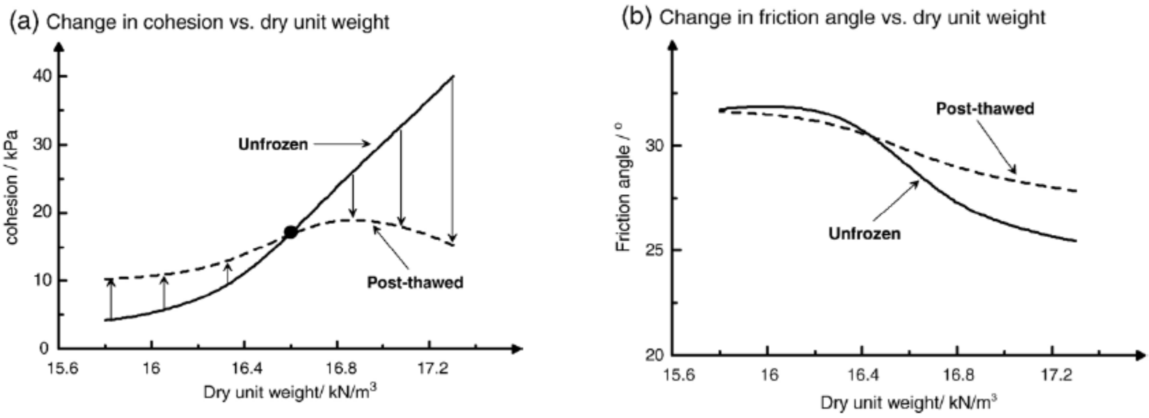

Figure 2.9: Changes in cohesion and friction as a function of dry unit weight. (Qi, Ma, & Song, 2008)

2.2.2 Stiffness

Stiffness of frozen soil depends among other things on temperature, confining pressure, strain rate and time. Johnston (1981) (in Anderland & Ladanyi, 2004) presented empirical formula's for frozen soils at sub-zero temperatures and 200 kPa confining pressure.

- Frozen sand (with grain sizes between 50-250 μm, w = 17-19%, temperatures (T) between 0°C and -10°C.

$$E = 500\ (1+4.2 * |T|) \tag{2.2.1}$$

- Frozen silt (with grain sizes between 5-50 μm, w = 26-19%, temperatures (T) between 0°C and -5°C.

$$E = 400\ (1+3.5* |T|) \tag{2.2.2}$$

- Frozen clay (with grain sizes smaller than 5μm, w = 46-56%, temperatures (T) between 0°C and-5°C.

$$E = 500\ (1+0.46* |T|) \tag{2.2.3}$$

Kong & Campbell (1987) recommended to use an instantaneous E-modulus of ice of:

$$E = 6600\ (1-0.012T) \tag{2.2.4}$$

Where T is the temperature in °C. Based on these formula the elasticity moduli (Table 2.1) of these soils and ice are calculated at -0 °C, -5°C and -10°C (if the formula covered the range until -10°C).

Table 2.1: Calculated Young's Moduli at 0 °C and -5 °C

	E (MPa) at -0°C	**E (MPa) at -5°C**
Sand	500	11000
Silt	400	7400
Clay	500	1650
Pure ice	6600	6466
Concrete	30000	30 000

2.2.3 Permeability

As soon as water starts to turn into ice, the permeability in the soil pores decreases because of ice plugging the pore. The ice inside the pores can be considered to be totally impermeable. Still, water can flow a little through the connecting pre-melting films around the grains. The temperature decides the thickness of the pre-melting films and thus influences permeability. For engineering purposes, this decrease in permeability is enough to consider the frozen body impermeable.

Freezing can cause structural changes to the soil due to frost heave. The volume change of ice turning into water changes the structure of the soil again, especially in soils consisting of clay (Johansson, 2009). Figure 2.10 shows this structural change before and after freezing. Figure 2.10a shows a silty clay, where clay particles have different directions between the silt particles. The silt grains have influence on the deformability and the clay on the permeability. During freezing pore volume increases due to expansion of water. After a freeze and thaw cycle, the space between the silt particles is almost the same as before freezing, since size of the silt particles the compaction. The clay particles however, have been rearranged and have become more densely packed. This leaves more pore volume and thus an increased permeability.

Figure 2.10b shows a silty clay and the silt particles floating between the clay particles. Degree of compaction is in this case not influenced by the silt particles. The clay particles control in this case both compressibility and permeability. After thawing, the clay can settle and the void ratio is decreased. However, shrinkage fissures and cracks at the places where ice lenses were formed increase the permeability significantly (Othman & Benson, 1993). More about the formation of ice lenses is explained in section 2.3.1. The increase in clay permeability is smaller for larger overburden pressures, since this can cause the fissures to close (Figure 2.11)

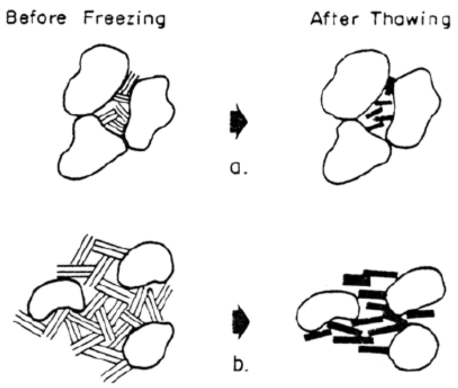

Figure 2.10: Structural transformation of soil. a. Clayey silt b. Silty clay. (Johansson, 2009)

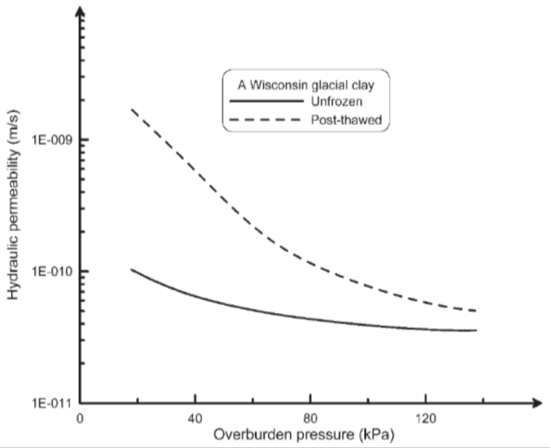

Figure 2.11: Hydraulic permeability for unfrozen and post-thawed clay (Othman & Benson, 1993))

2.3 Deformations during freezing and thawing of soil

During a freeze and thaw cycle different processes cause deformations in the frozen and unfrozen soil. The following processes will be discussed:

- Frost heave
- Consolidation of the unfrozen zone
- Creep
- Thaw settlement

2.3.1 Frost heave

When a soil is subjected to sub-zero temperatures the volume of the soil will expand i.e. heave. Frost heave occurs in both natural frozen soils as well in artificial frozen soils. This phenomenon has been studied for years, especially for natural soils in cold regions. Heave in natural soils can have detrimental effect on roads and foundations. In artificial frozen ground heave occurs as well and influences the surrounding soil and structures. Frost heave in frozen soils is caused by two mechanisms; the in-situ phase change and the formation of ice lenses. Ice lenses play the biggest role in the generation of frost heave.

In-situ phase change

At a temperature lower than 0^{o}C fresh water starts to freeze. The ice fuses the grain particles together increasing their combined strength and making the system impermeable for seepage water. In most materials, a decrease in temperature causes shrinkage of the material. At lower temperatures molecules vibrate less, resulting in a smaller average separation between the molecules. An increase in temperate leads to more active molecules needing a larger average separation and thus the volume of the material expands. An exception to this behaviour is water. The volume of water shrinks until a temperature of 4^{o}C. The density of water is the highest at this temperature. Below this temperature, water expands due to the tendency of hydrogen bonds to get stronger with lower temperatures. Hydrogen bonds fixate the water molecules at temperatures below 0^{o}C in an open hexagonal form, creating a distance between the molecules larger than the distance between water molecules before the fixation of the hydrogen bonds (Figure 2.12). Ice behaves more like common materials and shrinks when the temperature is lowered. Still, the shrinkage of ice at decreasing temperatures is smaller than the expansion of water upon freezing (Figure 2.13). Upon freezing, water can expand up to 9% of the its original volume. This can result in an increase of 3.6% of the total soil volume with a porosity of 0.4 in saturated soils (Chang,& Lacy, 2008). In unsaturated soils, this volume change would be less depending on the initial water content.

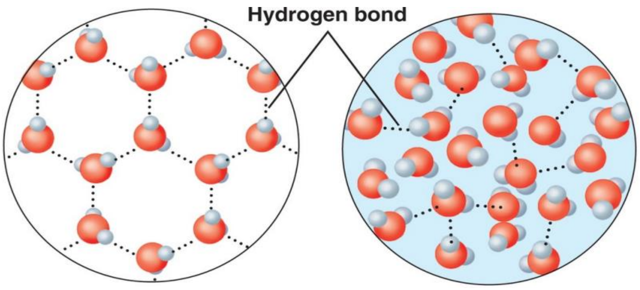

a. Ice, with stable hydrogen bonds. **b. Liquid with hydrogen bonds constantly breaking and reforming.**

Figure 2.12: Fixation of water molecules

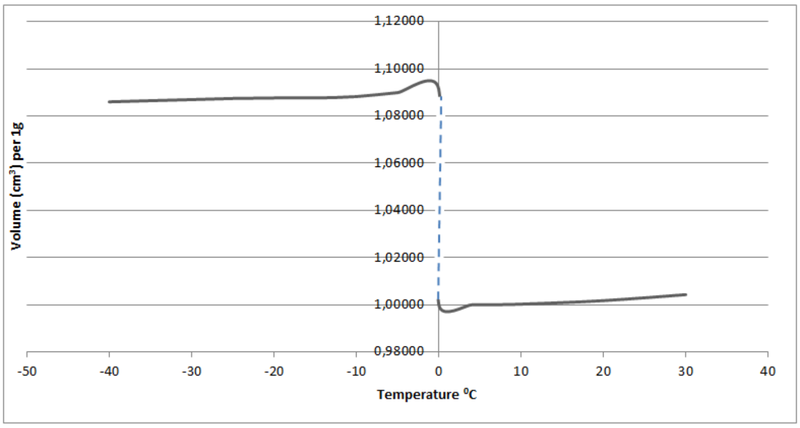

Figure 2.13: Volume of water and ice as function of temperature. (Based on Greenwood & Earnshaw, 1997)

At sub-zero temperatures, water in the middle of the pores will solidify first. When water starts to freeze in the middle of a pore, the pore pressure increases. This pressure will cause the still unfrozen water to flow out of the pore in order to neutralize the pressure in the pore. This leaves less water in the pore to freeze. Consequently, expansion of the pore volume will be very small or zero. Drainage of pore water can only take place if the drainage is faster than the freezing rate which can be the case in sands or gravels with high hydraulic conductivities (Andersland & Ladanyi ,2004; Wettlaufer and Worster, 2006; Rempel, 2010). In less permeable soils like clays, the drainage of water is unlikely and a large volume increase (up to 9% of the pore volume) due to the in-situ phase change can be expected.

Ice lens formation
The water-ice phase change is one process that can cause frost heave. The other process that causes additional elevation of the soil is the formation of ice lenses. Ice lenses are bands of clear ice in the soil. In order to understand how ice lenses are formed within the soil, a closer look to the soil near the freezing front must be taken. Three different zones can be distinguished near the freezing front; frozen zone, frozen fringe and unfrozen zone (Figure 2.14). The frozen fringe is the transition zone between the frozen zone and unfrozen zone and consists of partially frozen pore ice. Above the frozen fringe pore water can accumulate, forming an ice lens. Ice can grow, because water is sucked from the unfrozen zone through the frozen fringe toward this ice lens. The pore water moves through unfrozen water films (i.e. pre-melting films), that are wrapped around the soil grains. The pre-melting films are bonded to the grains by molecular forces. In the frozen fringe these pre-melting films thus act as conduits trough which water can migrate toward the ice lens.

The migration of the water from the unfrozen zone, through the frozen fringe, toward the ice lens is called cryogenic suction. This water flow is induced by a suction gradient that develops over the frozen fringe in response to the temperature gradient (Hohmann,1997). The temperature of the frozen fringe decreases from 0^oC at the freezing front to a lower segregation temperature at the end of the frozen fringe (Figure 2.15). The thermodynamic potential or Gibbs free energy (G_e) states that the amount of free energy (J/g) decrease with decreasing temperatures.

$$G_e = E_{in} + PV - TS \qquad \textit{2.3.1}$$

Where:

E_{in}	Internal energy	(J)
P	Pressure	(Pa)
V	Volume	(m^3)
T	Temperature	(K)
S	Entropy	J/K

Water near pore ice is colder than water in pores without pore ice and thus a difference in free energy is established over the frozen fringe. This gradient in thermal potential causes the suction gradient over the frozen fringe and the water to migrate from the warm side to the cold side of the frozen fringe (Sheng, Zhang, Yu, & Zhang, 2013). Ice lenses are formed in bands perpendicular to the temperature gradient and direction of water migration (Andersland & Ladanyi,2004; Azmatch, Sego, Arenson, & Biggar, 2012; Rempel, 2010).

Ice lenses can grow when the rate of freezing does not exceed the rate of water flow from the unfrozen zone and if the pressure of accumulated ice is greater than the pressure acting on the body of soil as a whole. The pressure exercised by the ice is relieved by heaving of the soil in the direction of least resistance. Restraining the frost heave, leads to a built up of frost heave pressures.

When the balances are not favourable ice lens growth stops. For example, when the freezing front further penetrates the ground. In this situation, the frozen fringe becomes thicker and the temperature on the warm side of the ice lens decreases. As a consequence, the unfrozen water content and permeability near the warm side of the ice lens decreases (almost linear with temperature). At a critical segregation temperature, water will no longer be able to move through the unfrozen water films which reduces and eventually stops the growth of the ice lens (Sheng et al, 2013).When favourable circumstances are present again, a new ice lens can be initiated in the frozen fringe between the previous ice lens and the freezing front (0°C isotherm)

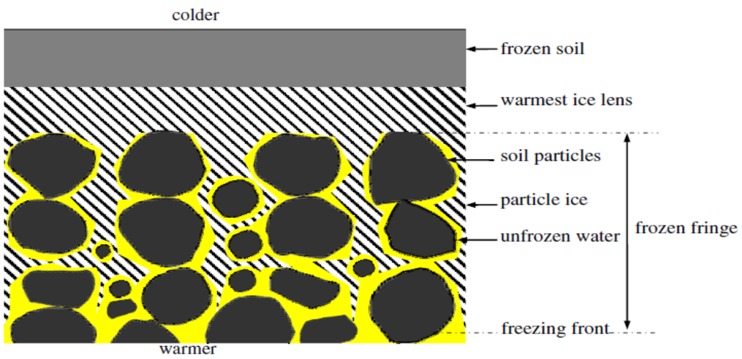

Figure 2.14: Schematic view of particles in the frozen fringe with unfrozen water films around the particles (Sheng, Zhang, Yu, & Zhang, 2013)

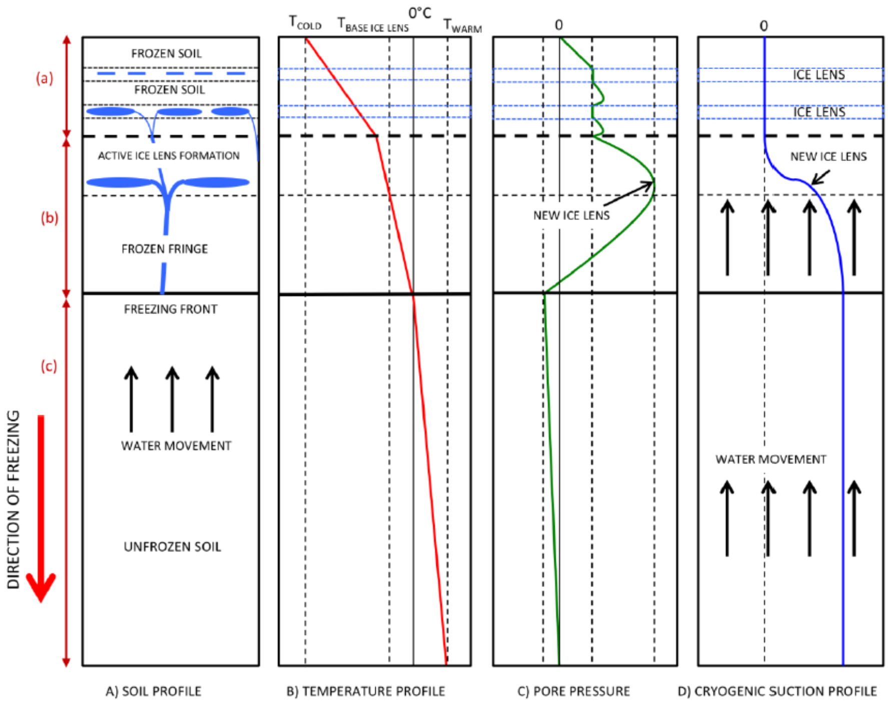

Figure 2.15: 1D soil column a. Partly frozen soil column. b. Temperature distribution. c. Pore water pressures d. Cryogenic suction. (Steiner, 2016)

As said before the initiation of ice lenses is governed by the balance between the rate of heat removal, the upward movement of soil water and confining pressures. The ability of water movement trough the frozen fringe (i.e. hydraulic conductivity) depends inter alia on the degree of saturation and the intrinsic permeability. The degree of unfrozen water saturation is higher in soils with higher fine contents. More fines correspond to a larger surface area, wrapped by pre-melting films. More pre-melting films form larger and better connected system of conduits for water to migrate to the ice lens. Both silt and clay have a high fine content. Still the hydraulic conductivity of clay is low. This can be explained by means of the intrinsic permeability which is a measure of the ability of a soil to let a fluid pass. The intrinsic permeability depends on the shape and configuration of the pores. Silts have a far higher intrinsic permeability than clays and thus a higher hydraulic conductivity. The sensitivity to ice lens formation in a soil is often determined based on fine content This is called the frost-susceptibility of the soil. However, a soil classified in a low class of frost susceptibility can still generate a significant amount of heave under favourable environmental conditions (Groundwater supply, overburden, temperature gradient and cooling rate).

By attracting additional water from the unfrozen zone to form by cryogenic suction, the soil can expand more than the 9% of the in-situ expansion of the water-ice phase change. Both in-situ phase change and formation of ice lenses are a cause of frost heave. However the main part of the heave is caused by the ice lenses (Zeinali, Dagli, & Edeskär, 2016). Depending on several conditions mentioned, the thickness of the ice lenses can vary from microscopically small to up to a meter under the right circumstances.

Parameters influencing frost heave:
In the previous paragraph, different parameters have been mentioned regarding the magnitude of frost heave. An overview is given of these parameters and their influence on frost heave.

- Soil type:
  A high degree of saturation and intrinsic permeability contribute to larger hydraulic conductivity of a soil. The higher the hydraulic conductivity the easier water can migrate through the frozen fringe toward an ice lens. The volume change of the soil due to in-situ phase change depends on the initial water content of the soil.
- Groundwater:
  In order for ice lenses to grow, water has to be supplied through the frozen fringe. If the availability of water is limited, ice lens growth will be small. Heave will in that situation be primarily caused by the in-situ phase change.
- Freezing rate:
  High temperature gradients increase the freezing rate. Ice lenses growth is restricted if the freezing rate is higher than the velocity at which the water can migrate through the unfrozen water films to supply water to the ice lens.
- Overburden:
  The larger the overburden, the larger the pressures that have to be overcome to separate the soil particles. Larger overburdens repress ice segregation and thus frost heave.

2.3.2 Consolidation of the unfrozen zone

Frost heave in the frozen zone and frozen fringe have influence on the unfrozen zone. Only few studies on frost heave take unfrozen zone into account the. Recently, Zhang et al. (2016) investigated the relationship of frost heave and consolidation of the unfrozen zone. They were able to measure pore water pressures in the unfrozen zone of different soils in one dimensional soil columns. Their experiments support the theory that consolidation in the unfrozen zone consists of two components; compression-induced consolidation and vacuum-induced consolidation. The first is caused by the pore compression due to frost heave stress. The pore pressure increase in the unfrozen zone and water is extruded from the pores in this early stage of freezing. In the later stage of freezing, vacuum-induced consolidation results from cryosuction. The pore pressure decreases in the unfrozen zone because water is migrating from the unfrozen zone to the frozen fringe or frozen zone. Freezing normally consolidated soil causes local consolidation in the area around the frozen body which results in over consolidation (Arenson, Xia, Sego, & Biggar, 2005).

The tests of Zhang et al. (2016) were done on silty clay samples and sandy soil. The silty clay samples first showed an increase and later a decrease in pore water pressure, triggering compression-induced consolidation and vacuum-induced consolidation. In the sandy soil samples, no increase in pore water pressure was measured, so no compression-induced consolidation will occur. Furthermore ice lens formation in sand is very limited (low fine content, high permeability, low unfrozen water content), therefore no vacuum-induced consolidation is induced in the unfrozen zone. Johansson (2009) describes the situation when clay is frozen. Unlike sand, water cannot flow away during freezing in clay and a pressure is built up in the pores due to the expansion when phases change. Dissipation of pore pressures will be low, because water flows slowly. Therefore compaction-induced consolidation occurs very slowly. Vacuum-induced consolidation will be limited because migration of water through the frozen fringe is also limited, due to the low permeability of clay. Deformations due to consolidation in the unfrozen zone can reduces the volume expansion caused by frost heave.

2.3.3 Creep

Frozen soil deforms under constant loading (i.e. creep). When a load is applied on frozen soil this load concentrates the stress between the soil particles at their point of contact with the pore ice. This pressure on the ice causes it to melt. As ice melts, pre-melting films become thicker and water can migrate better through the frozen soil. Ice melting and water movement causes breakdown of the ice and structural bonds of the soil grains causing plastic deformations of the pore ice and rearrangement in the particle arrangements (Sayles, 1968).

Deformation characteristics for frozen soil are the same as the classical creep curve for metals (Sayles, 1968). In frozen soil primary, secondary and tertiary creep can be distinguished (Figure 2.16a). The strain rate is different in these periods. During primary creep, the strain rate is decreased after which a constant strain rate can be expected during secondary creep. The strain rate can increase fast during tertiary creep, after which failure can occur (Figure 2.16c).

Time, temperature and confining pressure have influence on creep in frozen soils. Plastic and organic soils creep significantly at low stress levels, in contrast to granular and low plasticity soils that may only experience primary creep under high stress levels (Shuster, 2000). Figure 2.16b shows a typical secondary creep curve of sand saturated with ice at a constant temperature. For lower stresses the same soil will show only primary creep behaviour and will approach a limited deformation. Creep decreases strength and stiffness of the frozen soil in time.

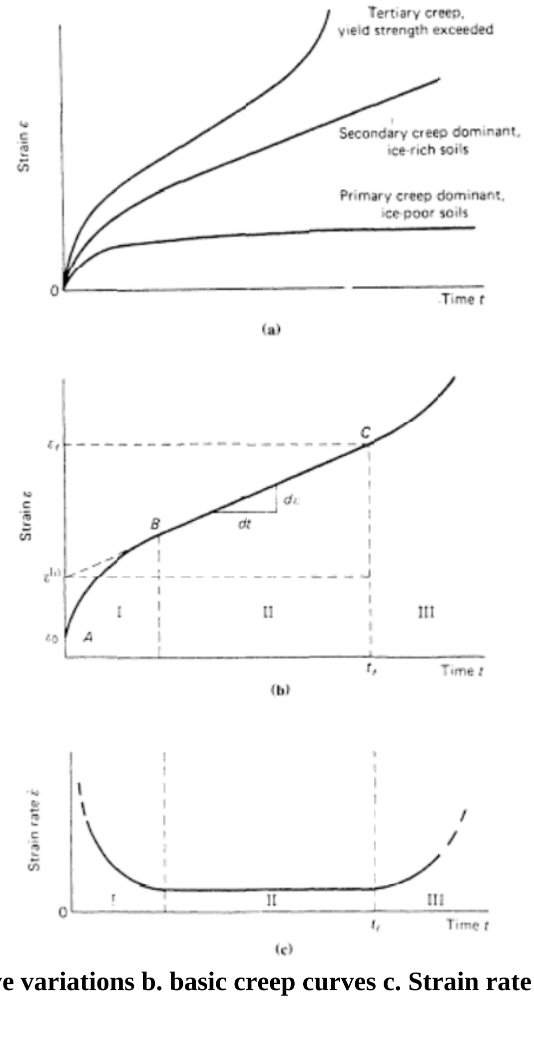

Figure 2.16: a. Creep curve variations b. basic creep curves c. Strain rate curve (Chang& Lacy, 2008)

2.3.4 Thaw settlements

The water-ice phase change and formation of ice lenses during freezing causes an expansion of the soil, while during thawing this process is reversed. During freezing extra water is accumulated in the frozen soil due to cryogenic suction, leading to excess pore water pressures upon thawing. The amount of excess pore water results from the balance between the rate of pore fluid generation (melting) and the ability of the thawed soil to expel water (consolidation). Thawing at a slow rate allows melted water to drain from the soil with the same rate. When this is not the case, excess pore water can reduce the shear strength of the soil during thawing i.e. thaw weakening.

Freezing can cause structural transformations especially to clays, and often cracks and fissures are observed (Figure 2.17). During thawing the soil rearranges and adapts to the new void ratio (Anderland & Landanyi, 2004). Often, the volume changes during thaw causes settlements. The amount of settlement is influenced by the self-weight of the soil, amount of additional pressure and the density of the soil (Zhou& Tang,2015). Shuster (2000) reports that because of thaw, plastic strains can be 20-25% larger than the initial frost heave. The thaw settlements do not necessarily have to be larger than the frost heave deformations.

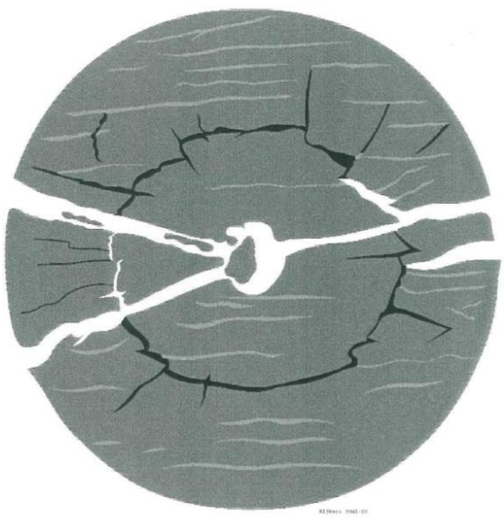

Figure 2.17: Structure of a clay sample after freezing, thawing and drying of the sample. (Report NITG 98-22-B., 1996)

Conclusions of chapter 2

This chapter answers the first sub-question of this thesis:

> *What soil behaviour (strength, stiffness and deformations) can be expected of soil during freezing and thawing?*

The ice saturation is the most important factor influencing frozen soil behaviour. The soil properties that are influenced most, are the strength, stiffness and permeability.

- *Increase of strength and stiffness of the soil*: Ice in the pores of the soil increases the strength by enhancing the cohesion between the soil particles. Unlike water, ice can sustain shear forces, resulting in an increase in stiffness of the soil.
- *Impermeability of the soil*: the pores are plugged by the ice, leading to a decrease in permeability.

During a freeze and thaw cycle, different processes cause deformations in the frozen and unfrozen soil.

- *Frost heave*: Frost heave is caused by two mechanisms; the in-situ change from water into ice and the formation of ice lenses. Due to the in-situ phase change, the volume of the pores can expand up to 9% relative to their initial volume. Ice lenses may cause even more expansion, because water might be attracted from the unfrozen zones due to cryogenic suction. Whether or not ice lenses form and to what extent this causes deformations, depends on different factors; soil type, availability of ground water, freezing rate and overburden. Most of these factors cannot be influenced during a project with AGF, exept the freezing rate. Higher freezing rates restrict ice lens growth.
- *Consolidation of the unfrozen zone*: the extraction of water from the unfrozen zone due to cryogenic suction can lead to consolidation of the unfrozen zone. The volume expansion caused by frost heave may be reduced by the consolidation of the unfrozen zone.
- *Creep*: Ice will deform under constant loading, i.e. creep. The instantaneous strength can be almost ten times larger than the long-term strength and is therefore important to consider during design.
- *Thaw settlement*: the volume expansion due to freezing of the soil is reversed during thawing. The water volume in the pores can be larger than at onset, due to the formation of ice lenses. Therefore upon thawing, excess pore water pressures may be the result. This can lead to thaw settlement, that influences nearby structures. Additionally, thawing can cause structural deformations of the soil. In clays, cracks and fissures can occur causing large volume changes and increase the permeability.

3 Interaction

The expected interaction between the (frozen) soil and lining of the main tunnel and cross passage is discussed in this chapter. This is based on the principles of ground freezing, construction stages in cross passage construction with AGF, the behaviour of frozen soil and experiences during different AGF projects. Background information about several case studies can be found in Appendix A. Five load cases have been identified during cross passage construction, where loads are caused by usage of AGF. For each load case the expected behaviour of the lining is described. A visualisation of the deformations and loads is shown in Figure 3.6. The deformations in each situations are drawn relative to the original situation, since the deformations are a qualitative estimate. Also, the original tunnel shape is kept round, because a final oval form of a bored tunnel depends inter alia on the cover, water pressures, diameter of the tunnel and stiffness of the lining.

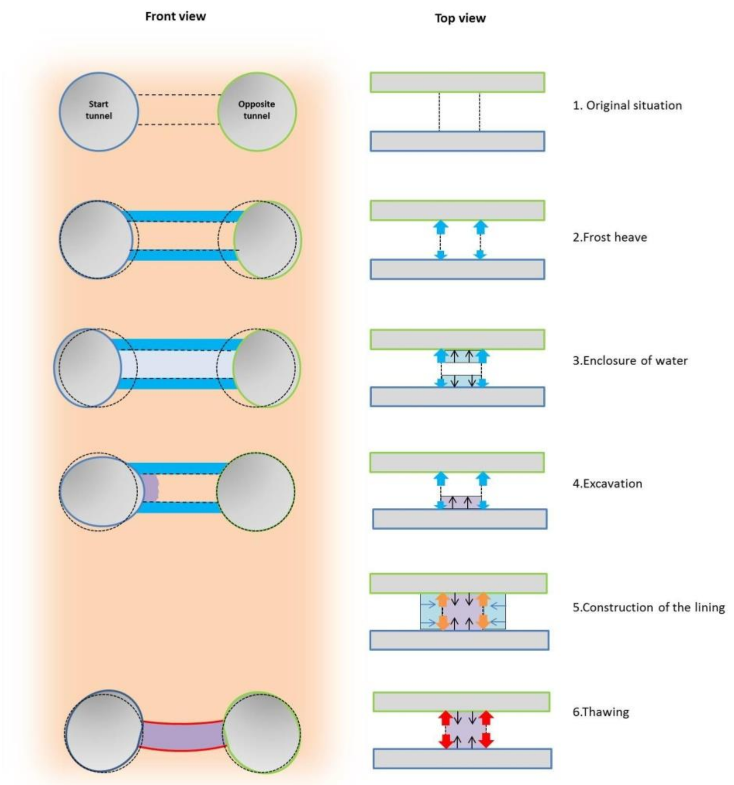

Figure 3.1: Expected deformations and loads during different load cases.

3.1 Load situation 1: Frost heave

The two components leading to frost heave are the in-situ phase change and ice segregation. The frost heave loads induced on the main bored tunnels depend highly on the permeability of the soil and freezing rate. Triaxial tests were done on frozen clay and sand before construction on the cross passages of the Westerschelde tunnel. They confirmed that frost heave is significant in radial direction and less significant in axial direction to the freezing front (Coté et al., 2000). The larger deformation in radial direction is caused by the formation of ice lenses perpendicular to the temperature gradient. Cryogenic suction develops over the frozen fringe as response to the temperature gradient, consequently water flows is induced toward the frozen fringe. Thus, soil expands in the direction of the temperature gradient (Figure 3.1). This is beneficial for the two main bored tunnels, since with small expansions in axial direction the force pushing on the tunnel lining would be limited.

Looking closer at the freeze pipe configuration, most freeze pipes lay (almost) parallel to the cross passage. However, often freezing lances are not bored through the lining of the opposite tunnel but stop at the grouting layer around the tunnel. The temperature gradient around the tip is not completely parallel to the freeze pipe and can cause heave loads on the lining of opposite tunnel (Figure 3.2). This behaviour has been measured at the Westerschelde tunnel. Figure 3.3 shows the deformation of the lining of cross passage 2, located in Boom clay. The maximal deformations of the lining of the cross passage was 18 mm. The graph shows the deformation when it was 16 mm. These deformations are caused by frost heave. Characteristic about the graph is its ''camel'' shape. The two peaks in the graph are the places were the tip of freezes pipes were located.

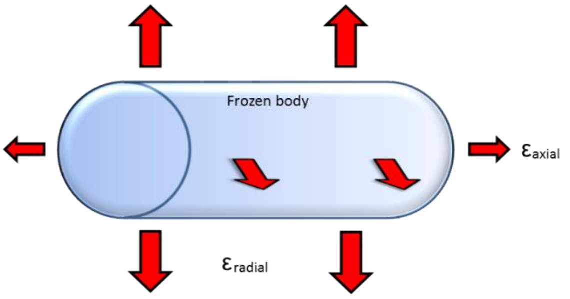

Figure 3.2: Axial and radial stress development in artificial frozen ground between bored tunnels (Rijkers et al., 2000).

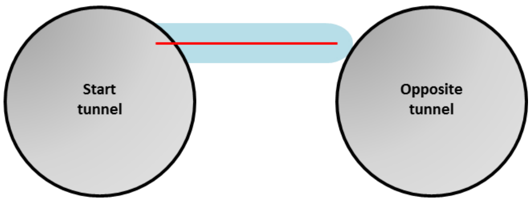

Figure 3.3: Shape of the frozen column around the freeze pipe (Report F100-E-02-0.79, 2002).

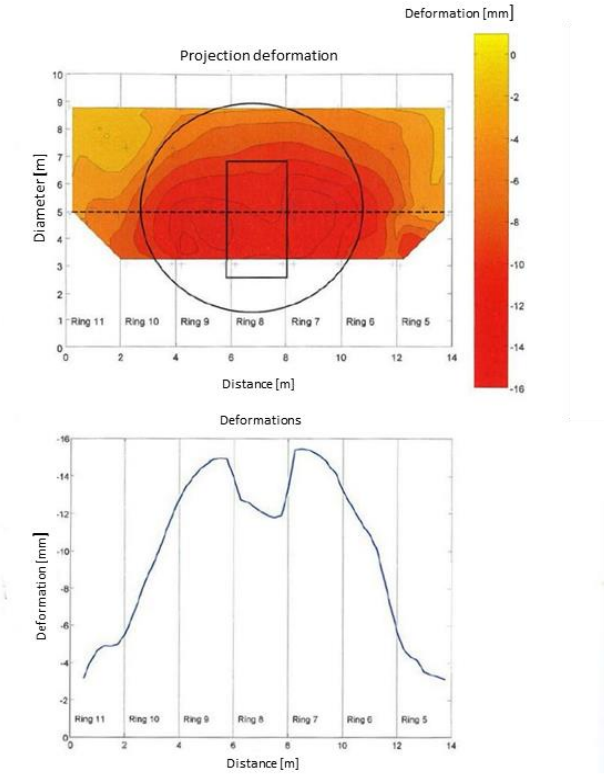

Figure 3.4: Deformation tunnel lining at cross passage 2 in clay of the Westerschelde tunnel (18th of August 2000) (Report F100-E-02-0.79, 2002).

In other projects too, an increase in pressure on the lining was measured during freezing, excavation and thawing. For instance in the Shanghai Yangtze River tunnel, special pat-type earth pressure gauges were placed on the segments to measure pressure differences on the tunnel lining. The maximum increase in pressure in this project was 186 kPa during freezing (Han, Ye, & Xia, 2015). When the cross passage diameter is large compared to the bored tunnels, the deformations caused by the tip of the freeze pipe will not only be horizontal. During the cross passage construction at the Pannerdensch Canal tunnel, the horizontal tunnel diameter increased 7-9 mm, while the vertical diameter decreased 6-8 mm (Mortier & Tuunter, 2004).

3.2 Load situation 2: Enclosure of water

During freezing, it is very important for the frozen body to form a watertight connection with the two main tunnels in order to create an impermeable structure. This occurs (Figure 1.4c) in the freezing stage where a frozen cylinder is formed, but the heart of the soil is unfrozen. The water enclosed in the unfrozen heart expands upon freezing. Expansion is prevented between the two main tunnels and the frozen cylinder. Freezing of this part of the soil can stress and/or deform the tunnel lining as well as the frozen cylinder itself. At the Westerschelde project, pressure inside the frozen cylinder was released by opening a valve of the drainage pipe that was placed together with the freeze pipes. Timing for opening the valve is important. If the valve is opened too early, the frozen cylinder is not connected to the main tunnels and water is not yet enclosed. When the inner cylinder is already partly frozen, pressure within the frozen body will not diminish when the valve is opened.

Cross passage 1 of the Westerschelde project was made in sand. Pressures in the heart of the unfrozen cylinder are shown in Figure 3.4. At point A, a slight increase of 0.2 Bar was measured indicating the closure of the frozen heart. However, water pressure did not increase further. Temperature sensors near the main tunnel lining indicated that the soil directly behind the segments was not frozen. The water tightness was tested by opening the valve of the drain, which is clearly visible by a drop in water pressure around date 6/24. Water did not stop running, indicating that the frozen cylinder was not watertight indeed. The valve was closed and dry ice was placed against the segments in the main tunnel. After a couple of days, a significant increase of water pressure (Point B) confirmed the frozen cylinder was now water tight. Figure 3.5 shows this phenomenon even better, because of the sudden increase in water pressure when the frozen cylinder is closed.

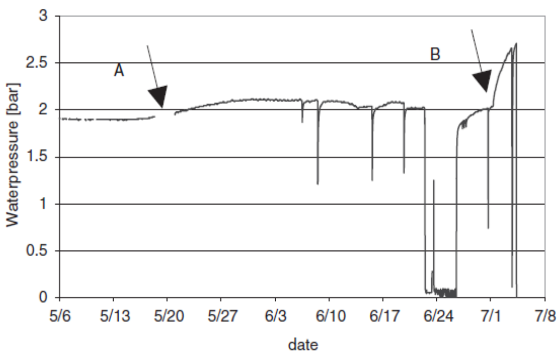

Figure 3.5: Development of the water pressures in the unfrozen cylinder in sand at the Westerschelde tunnel (Rijkers, Hemmen, Naaktgeboren & Weigl, 2006).

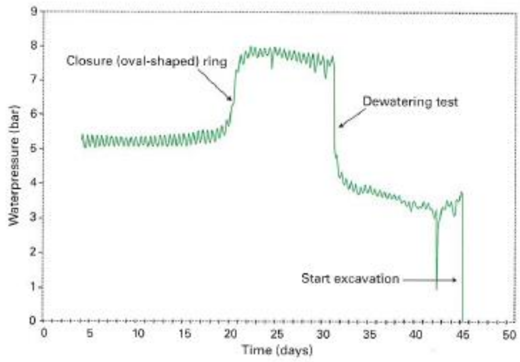

Figure 3.6: Development of the water pressures in the unfrozen cylinder in sand at the Westerschelde tunnel (Heijboer, Van den Hoonaard, & Van de Linde, 2004).

3.3 Load situation 3: Excavation

Upon excavation the frozen body becomes a structural support system and stresses are redistributed in the frozen soil. The strength of the frozen soil adjacent to the excavation can be slightly reduced due to exchange of heat between the air in the excavation and the frozen soil.
In a situation without the cross passage, soil will provide the support pressure in order to keep the segments together. When excavation is started, local stress on the tunnel lining is released. In response, the tunnel lining is expected to deform in the direction of the stress release. The deformation is restricted by the frozen cylinder and the cylinder is loaded in axial direction. Additional stresses in the lining of the main bored tunnel will also be caused by opening up the lining, however this is not a consequence of frozen soil–structure interaction.

3.4 Load situation 4: Construction of the lining

During the construction of the inner lining of the cross passage the main influence on the bored tunnel lining will probably be creep. Frozen soil under a constant loading creeps. Stresses are redistributed between the frozen soil, the lining of the bored tunnels and the newly installed lining of the cross passage. Additionally, concrete that is curing releases a lot of heat. This heat is melting the soil, decreasing the strength and stiffness. This behaviour was taken into account for the construction of the cross passages of the Pannerdensch Canal tunnel by assuming a short term strength twice as small as the long term strength (Mortier & Tuunter, 2004). From creep tests at the Westerschelde a decrease in stiffness of approximately 30% was observed. When less load can be carried by the frozen cylinder, the newly installed lining has to take this job. Inward deformations could be the case when a temporary lining of shotcrete is made and it is not completely cured yet.

3.5 Load situation 5: Thaw weakening

As the freezing system is shut down, the soil will start thawing gradually. The strength of the (frozen) soil decreases and the frozen body turns from a structural support system to a load on the cross passage. Not much information is available on how the cross passage will be loaded: gradually, stepwise or all at once. Only in one project, the Bothnia line, measurements taken of the tunnel roof of load increase when the clay soil was thawing were published. These measurements showed an gradual increase on the tunnel roof (Johansson, 2009).
During thawing, the soil will also settle. An increase of load on the tunnel roof and (non-uniform) settlements can lead to a rotation of the cross passage relative to the main bored tunnels. Depending on the kind of connection between the cross passage and main tunnel, the main bored tunnels will experience additional stresses with a fixed connection. With a flexible connection, displacements can cause problems to the water tightness of the seals.

Additionally, the lining of the cross passage will expand when the concrete becomes warmer. Extension in axial direction could result in a load on the main bored tunnel. A simple calculation can be made to calculate the expansion of the lining of a 10 m long cross passage, when brine freezing is applied with a temperature of -30°C and a unfrozen soil temperature of +10°C.

$E_{concrete,}$ = 15 000 MPa
$\Delta T = +10\ ^oC - (-30\ ^oC) = +40\ ^oC$
Expansion coefficient concrete = $\alpha \approx 1 * 10^{-5}$ per °C
Length cross passage = 10 m

Hooke's law:
$\varepsilon = \alpha * \Delta T \quad = 4.0 * 10^{-4}$
$u = \varepsilon * L \quad = 0.004$ m

This means an expansion of 2 mm at either end of the cross passage. When the connection between cross passage and main tunnel is flexible and a little space is left for expansion, this should be no problem.

3.6 Conclusions of chapter 3

This chapter answers the second sub-question of this thesis:

What interaction can be expected between the (frozen) soil and lining of the main tunnels during different stage of cross passage construction with AGF?

Five load situations describing the expected interactions between the frozen soil and the lining of the main tunnel have been identified.

- *Load situation 1: Freezing*
  The expansion due to freezing is the largest in the direction of the temperature gradient. When freeze pipes are placed from one bored tunnel to the other, the tip of the freeze pipes can cause deformations and inward deformations to the lining of the opposite tunnel.
- *Load situation 2: Enclosure of water*
  As soon as the frozen soil around the freeze pipe fuses into a frozen cylinder, water flow through the frozen cylinder is prevented. Water in the core of the frozen cylinder is due to

expand during freezing. However, this is prevented by the two main bored tunnels and the frozen cylinder. The excess pore water pressure will increase the load on the lining of the main bored tunnel and the inside of the frozen cylinder.

- *Load situation 3: Excavation*
  Upon excavation, the frozen body becomes a structural support system and stresses are redistributed in the frozen soil. When the soil behind the lining of the bored tunnel is excavated, the lining loses some of its support pressure resulting in an outward deformation of the lining. This deformation is restricted by the frozen cylinder and the cylinder is loaded in axial direction.
- *Load situation 4: Construction of the lining*
  During the construction of the inner lining of the cross passage, the main influence on the bored tunnel lining will probably be creep. Stresses are redistributed between the frozen soil, the lining of the bored tunnels and the newly installed lining of the cross passage. Additionally, concrete that is curing releases a lot of heat. This heat is melting the soil, decreasing the strength and stiffness. Both phenomena may lead to an additional loading on the lining of the cross passage and bored tunnels. Inward deformations could occur when a temporary lining of shotcrete is made and it is not completely cured yet.
- *Load situation 5: Thawing.*
  A volume decrease will occur in the thawing phase. An increase of load on the tunnel roof and (non-uniform) settlements can lead to a rotation of the cross passage relative to the main bored tunnels. Also, the frost heave loads decrease when the soil thaws and an additional outward deformation of the lining of the bored tunnels is expected.

4 Parameter determination, optimisation and validation.

The expected interaction between the frozen soil and lining of the bored tunnels has been described. The next step to investigate whether this behaviour can be numerically modelled is the evaluation of frozen and unfrozen soil (FUS) model in Plaxis. This soil model is capable of describing the change in mechanical behaviour of saturated soils at different temperature, and consequently also the transition between frozen and unfrozen soils. The FUS model describes many features of frozen soil such as the influence of ice content, cryogenic suction, ice segregation and pressure melting, However, the model is rate-independent and cannot take mechanisms like creep into account. The model uses two additional stress-state variables; the solid phase stress and cryogenic suction. The solid phase refers to the soil grains and ice, consequently the pores contain only water. Total formulation and a parameter description of the FUS model can be found in APPPENDIX B.

The capability of the model to simulate changes in strength, stiffness and deformations when soil freezes starts with the appropriate input parameters. Seventeen input parameters are required for this model, together with a soil freezing characteristic curve (SFCC). The SFCC is the relationship between temperature and the amount of unfrozen water in the freezing soil. Cross passage 2 of the Westerschelde project was constructed in Boom clay. For this projects several frozen and unfrozen soil test were carried out on BC by Jessberger(1998). Hence, the laboratory data are used to obtain a parameter set for boom clay (BC) in the FUS model. Once a selection of parameters is made, the same laboratory tests will be simulated numerically. Simulating simple soil tests provide the opportunity to explore the capabilities of the model. Optimizing the parameters and validating the results to real laboratory data serve as a way to assure plausible results in the next stage when the FUS model will be applied to model a cross passage between two bored tunnels. In the next paragraphs the determination of the parameter set will be explained(§4.1), as well as the optimisation of the parameters to fit the measured data (§4.2) and the validation of the final parameter set in relation to the laboratory tests(§4.3). A comprehensive description of the characteristics of boom clay at the Westerschelde project can be found in APPENDIX A1.

4.1 Parameter determination for boom clay

The seventeen model parameters of the FUS model can be divided into elastic parameters, strength parameters and parameters controlling virgin loading under isotropic stress state and cryogenic suction variation (Aukenthaler, 2016). Besides these model parameters, six thermal parameters and three parameters for the SFCC curve are determined for boom clay (BC). Table 4.1 shows a brief description of all parameters that have to be determined. Some of these parameters are well known and can be easily associated with specific soil behaviour, like E_f, $E_{f,inc}$, v_f, k_t, G_0, M. Other parameters are more difficult to grasp. Most of these parameters originate from the Barcelona Basic model for example β, $\lambda_{0,}$ r, p_c^*, p_{y0}^*, $\lambda_{s,}$ κ_{s}.. These model specific parameters are more thoroughly explained and visualised in section B.5 to make the parameters more understandable and to see their influence on soil behaviour. All model parameters can be obtained from several laboratory test in frozen and unfrozen conditions. Table 4.2 summarises which tests are necessary to obtain which model parameter. Not every test is commonly executed during site investigation, especially not the ones that have to be executed in frozen conditions. This is also the case in the Westerschelde project, not all of these tests were performed. Hence, not all model parameters could be obtained from the laboratory tests. The parameters that could not be determined with the executed soil tests are to be determined by correlations or a default value is chosen. Default values are obtained from other clay soils described in literature. The colour coding in Table 4.1 indicates how a parameter is determined; with laboratory tests (green), with correlations (orange) or with a default value (red). The following three sections are dedicated to explain the determination of each parameter.

Table 4.1: Input model parameters

Elastic parameters	Symbol	Unit
Stiffness frozen	$E_{f,ref}$	N/m^2
Stiffness increase with temperature	$E_{f,inc}$	N/m^2
Poisson ratio frozen soil	v_f	-
Unfrozen shear modulus	G_o	N/m^2
Elastic compressibility coefficient for cryogenic suction variation	κ_s	-
Unfrozen elastic compressibility coefficient	κ_0	-
Strength parameters		
Slope of the critical state line	M	-
Increase in apparent cohesion	k_t	-
Segregation potential	$(S_{c,seg})_{in}$	N/m^2
Yield parameter	m	-
Plastic potential parameter	γ	-
Parameters controlling virgin loading under isotropic stress state and cryogenic suction variation		
Rate of change in soil stiffness with cryogenic suction	ß	m^2/N
Elasto-plastic compressibility coefficient for unfrozen state	λ_0	-
Coefficient related to the maximum soil stiffness	r	-
Reference stress	p^*_c	N/m^2
Elasto-plastic compressibility coefficient for cryogenic suction variation	λ_s	-
Initial pre-consolidation stress for unfrozen conditions	P^*_{y0}	N/m^2
Thermal parameters		
Thermal conductivity	λ_{s1}	W/m/K
Specific heat capacity	c_s	J/kg/K
Density of solid material	ρ_s	Kg/m^3
Solid thermal expansion coefficient, x-direction	α_x	1/K
Solid thermal expansion coefficient, y-direction	α_y	1/K
Solid thermal expansion coefficient, z-direction	α_z	1/K
Parameters for fitting the SCFF curve		
Parameter for fitting the SCFF curve	λ_r	-
Parameter for fitting the SCFF curve	ρ_r	N/m^3
Parameter for the pressure dependency of ice thawing temperature ($7 \leq \alpha \leq 9$)	α	-

Determined with laboratory test
Determined with correlations
Default parameters used

Table 4.2: Laboratory test to determine model parameters (Aukenthaler et al, 2016)

Type for laboratory test	Model parameters to determine the state variables
Oedometer test (or isotropic compression tests) in frozen and unfrozen conditions	The v:ln p plane provides data to find the parameters p^*_{y0}, furthermore the parameters β, κ_0, r and p^*_c can be determined either by the sequential calibration procedure proposed by Gallipoli, Onza & Wheeler (2010) (isotropic compressions tests) or by Zhang, Alonso & Casini (2016) (temperature controlled oedometer tests). The latter reformulation for the present constitutive model in Aukenthaler (2016). The parameters λ_0 can be determined by taking the compression index C_c of the oedometer test in an unfrozen state into account. $\lambda_0=C_c/\ln(10)$
Simple shear test in unfrozen state	Obtain G_0 and M
Unconfined axial compression test at an arbitrary reference temperature at a frozen state.	Determine $E_{f,ref}$ and v_f
Unconfined axial compression test at a different temperature at a frozen state	Determine $E_{f,inc}$ and k_t.
Frost heave test (freezing-thawing cycle)	Obtain $(s_{c,seg})_{in}$, λ_s, and κ_s by plotting the results in the v: $\ln(sc+p_{at})$ plane

4.1.1 Parameters determined with laboratory tests

The laboratory tests executed on BC during the Westerschelde project were among others (frozen & unfrozen) triaxial compression tests, uniaxial compression tests and frost heave tests. An overview of the mechanical properties obtained from frozen and unfrozen triaxial tests is given in Table 4.4. The increase in stiffness and strength with temperature were obtained during this test. Parameter $E_{f,ref}$ is the frozen Young's modulus and represents the stiffness at the reference temperature (=273.16K = 0°C). The increment in stiffness with temperature is encountered by the parameter $E_{f,inc}$. The increase in strength in frozen soil is associated with an increase in cohesion, which is captured by the parameter k_t. Table 4.4 shows that the value of $E_{f,ref}$ = 40 MPa. $E_{f,inc}$ can be calculated:

$$E_{f,inc} = \frac{\Delta E}{\Delta T} = \frac{300\ MPa - 40\ MPa}{0\ ^oC - -20\ ^oC} = 13.0\ \text{MPa}/^oC \qquad 4.1.1$$

The value of $E_{f,inc}$ is the same for the two types of BC layers (BC1 and BC2). Parameter k_t can be calculated the same way and is 0.09 for BC1 and 0.12 for BC2. A value for k_t of 0.12 was chosen to start with. Report NITG 98-22-B pointed out that the pre-consolidation stress in unfrozen conditions was determined with an oedometer test and lies between 1.0 and 2.0 MPa. The initial value for p_{y0}^* is chosen between these two values at 1.5 MPa. This report also mentioned the determined bulk modulus; ρ_s = 2700 kg/m³. The values for the parameters determined with laboratory test are shown in Table 4.4.

Table 4.3: Mechanical properties Boom Clay (After Report F100-E-02-0.79(2002) & Report CO-380950/11 (1998)).

Soil type	Mechanical parameter	Unit	0°C	-10°C	-20°C
BC1	Young's modulus (2 days) with σ_3= 0.3 MN/m²	MPa	40	170	300
	Poisson ratio	-	0,35		
	Cohesion	MPa	0,015	0,94	1,88
	Angle of internal friction	o	27,5	9	9
BC2	Young's modulus(2 days) with σ_3= 0.3 MN/m²	MPa	40	170	300
	Poisson ratio	-	0,35		
	Cohesion	MPa	0,015	0,93	2,4
	Angle of internal friction	o	27,5	5,2	5,2

Table 4.4: Parameters determined with laboratory tests

Parameter description	Symbol	Value	Unit
Stiffness of frozen soil	$E_{f,ref}$	40.0E6	N/m²
Soil Stiffness increase with temperature	$E_{f,inc}$	13.0E6	N/m²
Increase in apparent cohesion	k_t	0.12	-
Density of solid material (Bulk modulus)	ρ_s	2700	kg/m³
Initial pre-consolidation stress for unfrozen conditions	P^*_{y0}	1.5E6	N/m²

4.1.1 Parameters determined with correlations

Six of the parameters can be determined with correlations. The unfrozen Poisson ratio (ν) and unfrozen Young's modulus from Table 4.3 can be used to determine the unfrozen shear modulus (G_0):

$$G_o = \frac{E}{2(1+v)} = \frac{40MPa}{2(1+0.35)} = 14.8\ \text{MPa} \qquad 4.1.2$$

The slope of the critical state line (M) can be estimated by using the critical friction angle (φ') in the formula of Muir Wood (1991) suggested by Aukenthaler (2016), with a critical friction angle of 20° for low plasticity clay (Ortiz et al., 1986). This results for triaxial compression in:

$$M = \frac{6\ sin\varphi'}{3-\sin\varphi'} = \frac{6\sin 20}{3-sin20} = 0.77 \qquad 4.1.3$$

The thermal conductivity (λ_{s1}) and specific heat capacity (c_s) of the soil can be determined in the laboratory but can also be calculated based on the minerology of the soil. The minerology of the clay was determined in the laboratory, after which λ_{s1} and c_s were determined with the method of Johansson (1995) (section 2.1.2).

The reference stress (p_c^*), is the stress at which the soil volume equals the initial specific volume of the soil (1-e). The porosity was determined in a borehole during with a device measuring the density of the electrons in soil layers. At a depth of -25.5 m the porosity(n) was 48% (Report F100, 2002). The void ratio and thus the initial specific volume can be determined from the porosity, since e = n/(1-n). This gives a void ratio of 0.9, at a depth of -25.5 m and with a volumetric weight of 19.0 kN/m^3 results in a reference stress of 500kPa.

The SFCC curve has an important role in the model, since the amount of unfrozen water influences the strength and the stiffness of the soil. Aukenthaler, Brinkgreve & Haxaire (2016) developed a simple approach to calculated the SFCC curve based on particle size distribution and void ratio. This approach is proved to give very similar SCFF curves relative to measured data. An SCFF curve can be given directly in the form of a table in Plaxis. However, when entering a user defined curve the unfrozen water saturation is not updated when pressure increases. Consequently, pressure melting cannot occur. When no user defined table is user-defined, the SFCC curve is calculated in Plaxis 2016 based on the approach of Nishimura, Gens, Olivella & Jardine (2009). In this approach the unfrozen water content (S_{uw}) is calculated by using the cryogenic suction (s_c) and consequently temperature:

$$S_{uw} = [\ 1 + (\frac{s_c}{\rho_r})^{\left(\frac{1}{1-\lambda_r}\right)}]^{-\lambda_r} \qquad 4.1.4$$

$$s_c \ = \ \rho_{ice} * \ L_w + * \frac{T}{T_f} \qquad 4.1.5$$

$$T_f \ = T_{ref}(\frac{p_{ice}}{-p_{ref}} + 1)^{\frac{1}{\alpha}} \qquad 4.1.6$$

where:

λ_r	Parameter for fitting the unfrozen water saturation curve	[-]
ρ_r	Parameter for fitting the unfrozen water saturation curve	N/m^2
ρ_{ice}	Density of ice (918.9 kg/m^3)	Kg/m^3
L_w	Latent heat of fusion for water (3.34E5J/kg)	J/kg
T	Current temperature	K
T_f	Freezing/melting temperature	K
T_{ref}	Reference temperature (273.16K)	K
p_{ice}	Ice pressure	N/m^2
p_{ref}	Reference pressure, at which is assumed that water no longer freezes (-395 MPa)	N/m^2
α	Parameter for the pressure dependency of ice thawing temperature ($7 \leq \alpha \leq 9$)	[-]

When this approach is used the unfrozen water saturation is updated for pressure melting, since extra pressure lowers the reference temperature(T_f), leading to a higher unfrozen water content (eq. 4.6). The values for α, ρ_r and λ_r have to be estimated. Hence, these parameters are chosen in such way that the SFCC curve in Plaxis is similar to the SFCC based on the particles size distribution and void ratio for BC. Figure 4.1 shows the SFCC for both approaches. With the following parameter values chosen, α =9, ρ_r = 1.3E5 N/m^2, λ_r = 0.25, the SCFF curve generated in Plaxis is similar to the SCFF curve based on particle distribution and void ratio. In Plaxis 2017 the SCFF curve based on the particle size distribution can directly be generated, without having to enter the three fitting parameters. All values for parameters determined with correlations are summarised in Table 4.5.

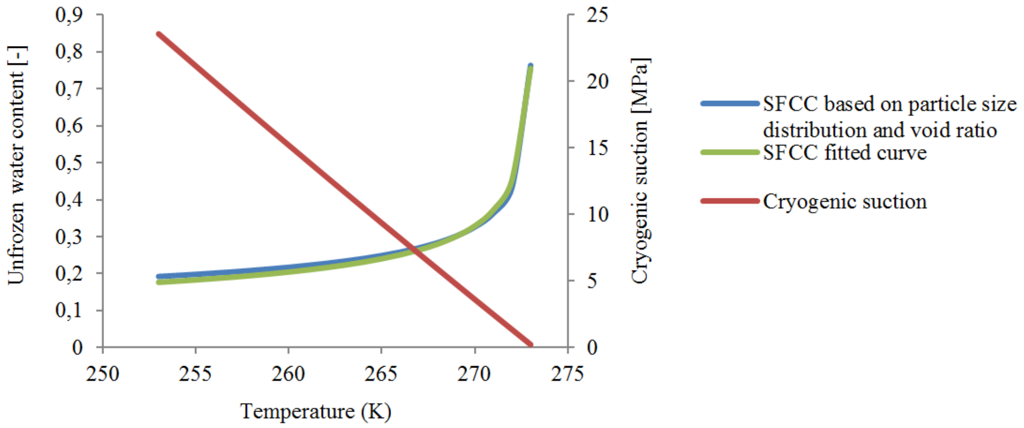

Figure 4.1: Saturated freezing characteristic curve and cryogenic suction

Table 4.5: Parameters determined with correlations

Parameter description	Symbol	Value	Unit
Slope of the critical state line	M	0.77	-
Unfrozen shear modulus	G_0	14.8	MPa
Reference pressure	p^*_c	500E3	N/m^2
Thermal conductivity	λ_{s1}	1.9	W/m/K
Specific heat capacity	c_s	920	J/kg/K
Parameter for fitting the unfrozen water saturation curve	λ_r	1.3E5	[-]
Parameter for fitting the unfrozen water saturation curve	ρ_r	0.25	N/m^2
Parameter for the pressure dependency of ice thawing temperature ($7 \leq \alpha \leq 9$)	α	9.0	-

4.1.2 Parameters with default values

For the remaining parameters default values will be chosen, since they were not obtained during a laboratory test and no correlation is available. The elasto-plastic compressibility coefficient in unfrozen state (λ_0) and the elastic compressibility coefficient for mean net stress (κ_0) can be determined from an unfrozen oedometer test. However, this test was not available for the boom clay from Westerschelde project. Therefore, values for λ_0 and κ_0 were calculated from compression and swelling indices Cc and Cs from oedometer test on Boom Clay from Belgium described by Deng et. all. (2011). Initially calculated values for are; λ_0 = 0.15 and k_0=0.08.

Most of the parameters that are more difficult to determine originate from the Barcelona basic model (BBM). Tests to find these parameters are not very common, especially because tests have to be executed in a frozen state. The elasto-plastic compressibility coefficient for cryogenic suction variation (λ_s), rate of change in soil stiffness with cryogenic suction (β), the ratio between the elasto-plastic compressibility coefficient in unfrozen state and at infinite suction ($r=\lambda(\infty)/\lambda(0)$), the elastic compressibility coefficient for cryogenic suction variation (κ_s) and the solid thermal expansion coefficients ($\alpha_{x,y,z}$) are initially chosen after the clay soil described by Aukenthaler (2016). This gives the following values for these parameters: λ_s = 0.1, β=0.6E-6 $(N/m^2)^{-1}$, r=0.60, κ_0 = 0, κ_s=0.005, $\alpha_{x,y,z}$ = 5.2E-6.

Aukenthaler (2016) recommends to use a value of the Poisson ratio for frozen soil close to the Poisson ratio of ice, which is ν_{ice} = 0.31. Aukenthaler (2016) also suggested to use the values for the estimated by Rempel(2007) for the initial threshold value for grain segregation. The proposed values for $s_{c,seg}$ for clay is 3.5 MPa for clay. For both parameters m and γ is chosen for a value of 1.0. The unfrozen water content is taken fully into account in the LC yield curve and the flow rule (eq. B.11 and eq. B.23).

Table 4.6: Parameters with default values

Parameter description	Symbol	Value	Unit
Elasto-plastic compressibility coefficient for unfrozen state	λ_0	0.15	-
Elasto-plastic compressibility coefficient for cryogenic suction variation	λ_s	0.08	-
Rate of change in soil stiffness with cryogenic suction	ß	0.6E-6	m^2/N
Coefficient related to the maximum soil stiffness	r	0.60	-
Unfrozen elastic compressibility coefficient	κ_0	0.08	-
Elastic compressibility coefficient for cryogenic suction variation	κ_s	0.005	-
Yield parameter	m	1.0	-
Plastic potential parameter	γ	1.0	-
Frozen Poisson ratio	v_f	0.31	-
Segregation threshold	$s_{c,seg}$	3.5	MPa
Solid thermal expansion coefficient, x, y, z-direction	$\alpha_{x,y,z}$	5.2E-6	1/K

4.2 Parameter optimisation

This paragraph describes the steps taken in the optimisation process, while the next paragraph will explain the exact way of modelling and the validation of the model. The determined parameters are supposed to reasonably fit the results of the used laboratory test (unfrozen & frozen triaxial compression test, uniaxial compression test and frost heave test). This makes sure that different strength, stiffness and deformation behaviour is resembled properly, or it is known whether certain behaviour is underestimated or overestimated. The optimisation has been an iterative process, where the starting point was the initially determined parameter set. The parameters have been evaluated and optimised to a test where the influence of the parameter on the soil behaviour could be clearly seen. It does not mean that the parameter has only influence on the test it was optimised on. One parameter can have influence on more than one soil test, so when a parameter is adapted, there must be checked if the changes in parameters cause a large deviation in their results. The optimised parameters are therefore a compromise to approach all measured data.

The first test that optimised was the unfrozen triaxial compression test. By starting with the unfrozen test many parameters that influence freezing behaviour can be avoided. This leaves five unfrozen parameters to assess, M, G_0, κ_0, λ_0, P^*_{y0}. The parameter M is a strength parameter, increasing M leads to an increase in deviatoric stresses and slightly larger strains before the peak strength occurs. G_0 has influence on the elastic range of the stress-strain diagram, with increasing or decreasing G_0 the stiffness in the elastic range can be controlled very well. Although parameter k_o influences the unfrozen elastic compressibility, the ratio between κ_0 and λ_0 influences the plastic strains as can be seen in see eq. B16 t/m B19). The larger the ratio is between κ_0/λ_0 the more distinctive hardening or softening behaviour can be seen in the stress-strain diagram. The parameter P^*_{y0} is the threshold stress at which the volumetric changes become plastic instead of elastic (Figure B.5). This parameter also influences hardening and softening behaviour. Softening indicates an overconsolidated soil, where the ratio between confining pressure and the pre-consolidation stress (σ_3/ P^*_{y0}) is smaller than 1. If this ratio is larger than 1, hardening can be expected.

The second test used to optimise the parameters is the frozen uniaxial compression test, executed at different sub-zero temperatures. The stiffness of the soil around the freezing point ($E_{f,ref}$) and the soil stiffness increase ($E_{f,in}$) and strength increase (k_t) with decreasing temperatures can be checked with this test (Table 2.1Table 4.4). Also, the influence of the frozen Poisson ratio (v_f) can be investigated. The initially chosen parameters $E_{f,ref}$ and $E_{f,in}$ gave the right amount of stiffness and stiffness increase, while the k_t value was found to be low and thus was raised. The influence of v_f turned out to be very small and the initial value similar to the Poisson ratio of ice was maintained. The different temperatures used in this test also offer the possibility to investigate if the right amount of unfrozen water is kept in the pores at a certain temperature and thus also the parameters λ_r, ρ_r and α. The parameters m and y have both influence on the amount of unfrozen water content that is taken. Parameter m does this as an exponent in the LC yield surface (eq. B.11) and y as an exponent in the plastic potential function (eq. B.23). The value has to lie between 0-1. When a value of 1.0 is chosen the unfrozen water content will be taken into account as given in the SFCC curve. In case a lower value is chosen, more unfrozen water content will be taken into account, leading to a lower strength and more plastic behaviour. For this project the choice was to stay with the unfrozen water content given in the SFCC curve.

In the frozen triaxial test the influence of p_c*, $s_{c,seg}$, r and β can be examined. The higher $s_{c,seg}$ the more cryogenic suction is necessary to initiate frost heave deformations. The dilatation of the soil due to the occurrence of ice segregation results in softer behaviour of the soil. With a high value of $s_{c,seg}$ the strength of the soil can be significantly increased, since the elastic range is smaller. Changing parameter $s_{c,seg}$ is tempting to optimise to fit the stress-stain curve in frozen conditions, since it is an uncommon parameter where little can found on the range of the parameter. The values suggested by Aukenthaler(2016) range from 0.55 MPa to 3.5MPa in Clay, therefore was chosen to not increase the sc,seg value to optimise the strength of frozen soil. The pc* is the stress state at which the volume is equal to the initial volume (Figure B.5). The larger difference between pc*and p*y0 means a larger stress range over which the volume responses elastically. The effect of changing this parameter is small in the frozen triaxial tests. The influence of pc* can better be visualised on the normal compression lines and the LC yield curve in figures B.7d and B.8.

The compressibility of soil decreases when the suction increases. Equation B.13 describes the change in compressibility compared to the compressibility at zero suction (λ_0). The equation is dependent on parameters r and β. The decrease in stiffness due to suction cannot go on forever. Therefore, a minimum compressibility at infinite suction is captured by parameter r ($r=\lambda(\infty)/\lambda(0)$). It determines the maximum compressibility of the soil when the suction becomes very large. The parameter β determines how much the compressibility changes with different suctions. By increasing the r the change in compressibility between infinite suction and no suction becomes smaller, leading to less hardening. The influence of parameters β and r are small in the stress-strain diagram. The influence of both parameters can be better visualised on the normal compression lines and the LC yield curve in figure B.7 and B.8.

The frost heave test will give more insight in the deformations generated by the model. The compressibility coefficient due to cryogenic suction is represented by parameters λ_s and κ_s. The elastic region is dominated by k_s, where suction causes a volumetric decrease of the soil (Figure B.9). Whereas λ_s causes a volumetric increase when the cryogenic suction is higher than the segregation threshold ($s_{c,seg}$). Their size thus defines the magnitude of the volumetric decrease or increase. These two parameters are very important for the magnitude of frost heave.

Thermal parameters can also be verified with the frost heave test. The freeze time can be accelerated or slowed down with the thermal conductivity and specific heat capacity. The solid thermal expansion coefficient is the amount the solids shrink when they are frozen, in general this value should be very small. On the contrary, the solid thermal expansion coefficient can also be used as a mean to model a dominant direction of frost heave if desired.

The final test that was modelled was the thawing test. Although, there was no data to optimise this test it gave the opportunity to explore the model during thawing. The volumetric behaviour during thawing is influenced by three mechanisms. Firstly, the parameter k_s causes a volume increase during thawing in the elastic region. Aukenthaler(2016) suggested that selecting a low value of k_s will let other mechanisms dominate thawing behaviour. A small negative value was chosen for this parameter, making sure a volume decrease during thawing is obtained in the elastic region. More is explained and visualised about the effect of changing the sign of k_s in section B.5. Secondly, consolidation affects the volumetric behaviour during the increase of temperature. The hydraulic properties and the rate of thawing control the consolidation. Thirdly the stress conditions are important. When the segregation threshold is passed during freezing, the GS-yield curve shifts upward and consequently the LC-yield surface moves inward. During thawing the LC-yield curve can be hit, causing plastic strains. Whether and when this occurs depend on the chosen unfrozen pre-consolidation stress, stress condition and the rate of thawing. The volume of the frozen soil does not necessarily have to return to its original size, it can become smaller due to plastic strains or remain at a larger volume when the LC-yield curve is not hit.

4.3 Parameter validation

The method of modelling and the validated results in relation to real soil tests will be discussed for each tests. Only for the numerical tests demonstrating thaw settlement no real soil data available are to compare the results with.

4.3.1 Triaxial compression test

Triaxial tests are modelled for BC in unfrozen conditions (T= +20^{o}C) and in frozen conditions (T=-10^{o}C). This undrained consolidated triaxial test is modelled similarly to the real triaxial tests conducted in the laboratory. First the sample was consolidated for 48 hours in an unfrozen state, where pore water was allowed to drain. The confining pressure varied each test. In the frozen triaxial tests the soil is cooled down to the desired temperature, during which freezing water was allowed to drain as well. Finally the sample is sheared with a rate of 0.1%/min, without drainage of water. An axisymmetric model is used with the geometry shown Figure 4.2. The left and bottom boundary are normally fixed, whereas the top and right boundary are free. Only a quarter of the original triaxial cell is modelled due to symmetry of the x-axis and y-axis.

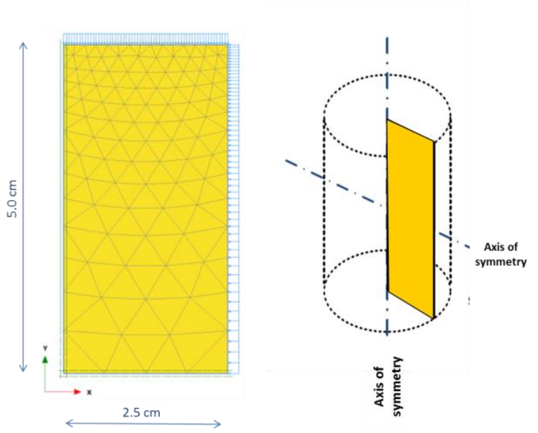

Figure 4.2: Model mesh and geometry for compression triaxial test.

Figure 4.3 shows stress-strain diagrams calculated with the numerical model for different temperatures at a confining pressure of 0.5 MPa. The stiffness and strength increase nicely with decreasing temperatures. In Figure 4.4a an unfrozen triaxial test is shown with measured and calculated data at three different confining pressures: 0.5, 1.0 and 2.0 MPa. The measured unfrozen triaxial test shows slight softening behaviour at the two lower confining pressure and hardening at a confining pressure of 2.0 MPa. The softening behaviour at the two lower confining pressures is also observed in the calculated data, but the softening is larger and occurs at lower strains. The obtained stresses are for a confining stress of 0.5 MPa larger than the measured stresses, while at a confining pressure of 1.0 MPa the calculated stresses approach the measured stresses better. Calculated stresses at the confining pressure of 2.0 MPa are a little lower than the measured stresses, although the stiffness response in the elastic region is very similar. In the frozen triaxial compression test the stress-strain response of the frozen soil is quite accurately resembled by the numerical model. The stiffness response in the elastic region is very similar and hardening increases with higher confining pressures. At the confining pressures of 1.0 MPa and 2.0 MPa the yield point lies at a lower stress than at the measured data, therefore the deviatoric stresses in the plastic range are a little lower. The stresses that will occur at the depth of the cross passage that will be modelled, are a little more than 0.5 MPa. The soil behaviour at this confining pressure is well described in the stress-strain diagram.

The model also shows the phenomenon of pressure melting. The boundaries are closed during shearing, consequently pore water pressures increase. At larger confining pressures, larger shear forces can be sustained by the soil. Larger shear forces lead to higher pore water pressures. The consequence is a decrease in ice saturation. Shearing with a confining pressure of 2.0 MPa causes a decrease in pore water pressure of approximately 0.7% (Figure 4.5). The SCFF curve (Figure 4.1) is not very steep at lower temperatures, so the decrease in ice saturation corresponds to freezing at -9^{o}C instead of -10 ^{o}C. This does not influence the strength and stiffness significantly. However at low sub-zero temperatures the SCFF curve is very steep and an increase in confining pressures causes a large decrease in ice saturation and thus strength. If equation 4.7 is filled in constants, the following equation is left:

$$T_f = T_{ref}(\frac{p_{ice}}{-p_{ref}} + 1)^{\frac{1}{\alpha}} = 273.16K\,(\frac{p_{ice}}{+395\,MPa} + 1)^{\frac{1}{9}}\,\frac{K}{MPa} \quad 4.7$$

The equation gives the prediction that approximately 13.0 MPa is necessary to depress the freezing point of ice by 1K.

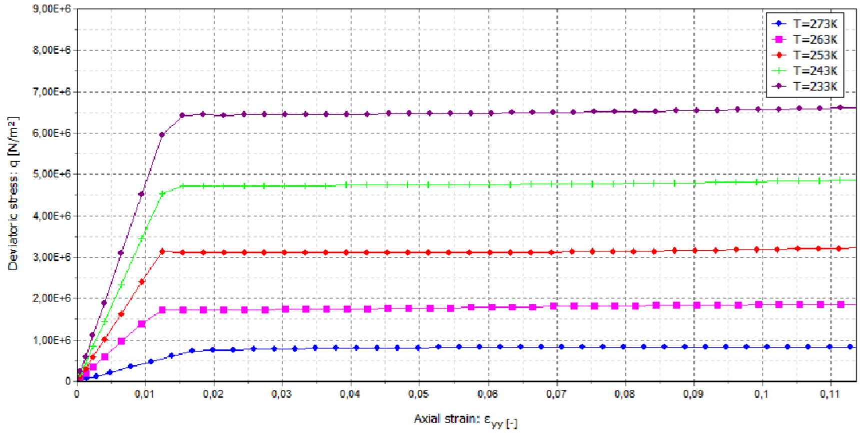

Figure 4.3: Stress-strain diagram for different temperatures for constant confinement (σ_3=0.5 MPa).

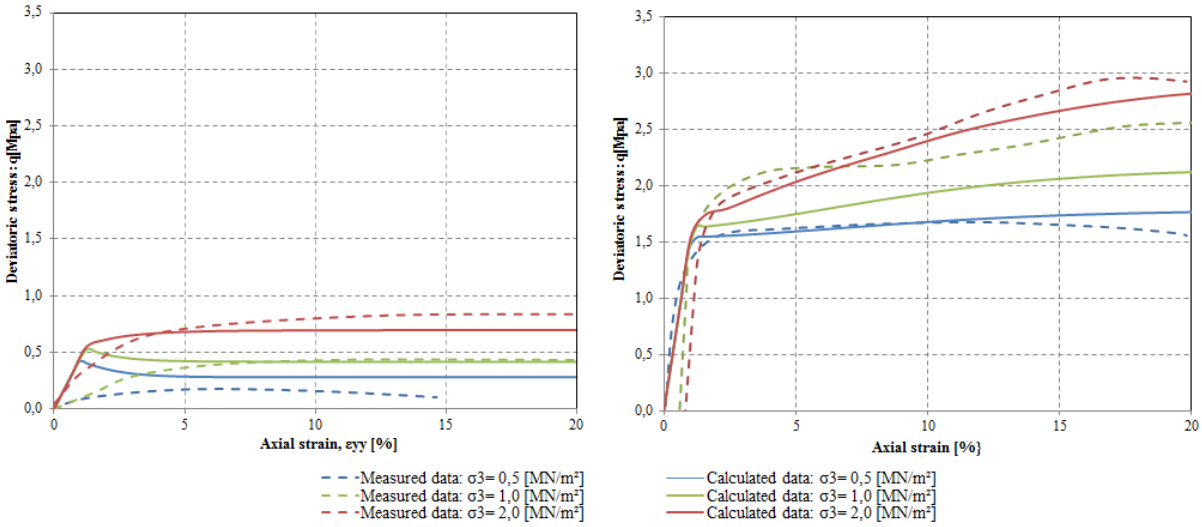

Figure 4.4 Stress-strain relation for measured data (Jessberger + Partner, 1998) and calculated data at for different confining pressures (a) Temperature is +20°C (b) Temperature is -10°C

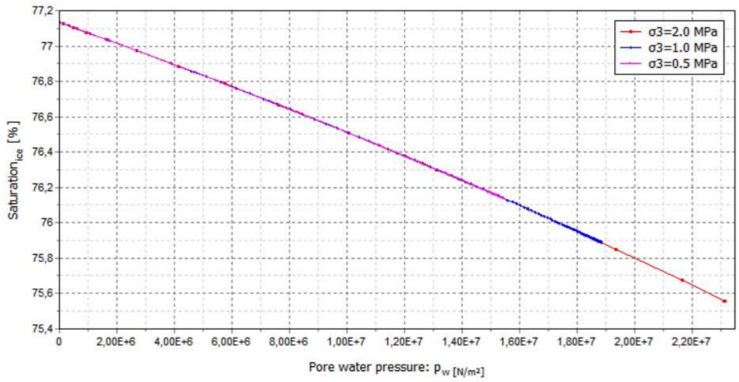

Figure 4.5: Pressure melting at -10°C for different confining pressures.

4.3.2 Uniaxial compression test

Uniaxial compression tests have been calculated for different temperatures. Again an axisymmetric model is used with a geometry as presented in Figure 4.6. Firstly, the sample is frozen to the desired temperature without constraining the volumetric expansion of the sample. Afterwards, the top of the sample is loaded with a rate of 1%/min in drained conditions. The load was subsequently applied in the model with a prescribed displacement. This resulted in Figure 4.7, the peak strength at different temperatures is shown in combination with the measured data from the Westerschelde project. The calculated maximal load the sample is able to withstand lies close to the lower boundary of the measured loads. The individual stress-strain curves for the different temperatures can be found in APPENDIX C.

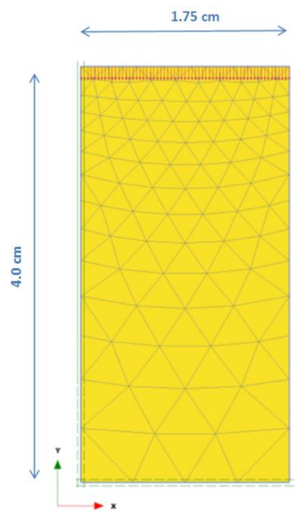

Figure 4.6: Model geometry uniaxial test

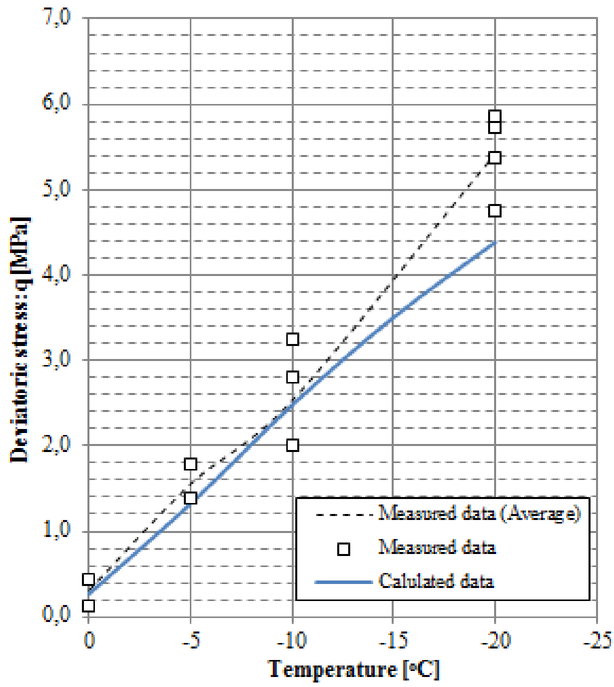

Figure 4.7: Uniaxial compression test for measured data (Jessberger + Partner, 1998) and calculated data.

4.3.3 Heave test

To investigate volume changes during freezing, a special triaxial cell was used during laboratory heave tests for the Westerschelde project. In the centre of the cylindrical sample a small freeze pipe was placed in vertical direction (Figure C2). The numerical model made to calculated deformations due to frost heave is resembling the heave test carried out in the laboratory. The model geometry is shown in Figure 4.6. The left vertical boundary serves as temperature boundary (i.e. freeze pipe) and the temperature around the model is kept constant at 5^{o}C. The sample is consolidated, with a total pressure of 620 kPa and a backpressure of 420 kPa. In the next phase, the freeze pipe is activated and the sample is frozen at -15^{o}C or -30^{o}C. Drainage during freezing is allowed in vertical and horizontal direction. Horizontal drainage was possible in the laboratory test by placing filter paper at the right boundary of the sample.

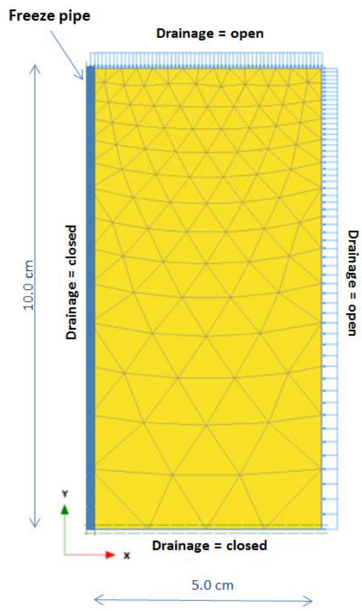

Figure 4.8: Model geometry heave test

Paragraph 2.1.1 was already mentioned that ice lenses are formed in bands perpendicular to the temperature gradient. Thus, in this test the largest deformations can be expected to be in horizontal direction. The magnitude of heave deformations in clay also depend on the layering of the clay (i.e. stratigraphy). Clay expands more easily perpendicular to the layering than parallel to the layering. Thus, the largest possible expansion could be measured when the freeze pipe was positioned parallel to the layering just as a horizontal freeze pipe would do in the soil. For this reason, the soil samples in the laboratory were placed in the triaxial cell such that the layering was parallel to the freeze pipe. Consequently, the radial deformations in the laboratory test are larger than the axial deformation. The deformations in the numerical model are independent of the layering or temperature gradient. Therefore different solid thermal expansion coefficients have been used in the model to capture the difference in deformation between the x and y direction. The results of the calculated deformations due to frost heave are visualised in Figure 4.9a. In Figure 4.9b can be seen that the displacements in the direction of the temperature gradient (i.e. horizontal displacements) are indeed the largest. The vertical displacements are approximately 2-3 times smaller than the horizontal displacements (Figure 4.9c).

In Figure 4.10 the calculated displacements are shown relative to four deformation measurements around the sample during the laboratory frost heave tests. The size of the radial deformations measured are very similar to the calculated deformations at -30^{o}C. When the test is carried out at -15^{o}C, the deformations approximate the lower end of the measured data. The radial deformations at -15^{o}C in the calculated data are lower than at -30^{o}C. This is the other way round in the heave test in the laboratory, which can be explained by the fact that the frozen fringe contains less ice at -15^{o}C. Consequently, it is easier for water to migrate through the frozen fringe to the frost front and to form ice lenses. In the numerical model there is no frozen fringe and no formation of ice lenses. The soil expands as a whole due to cryogenic suction. With decreasing temperatures the cryogenic suction increases, causing the soil to expand. This explains the larger deformations at lower temperatures.

Furthermore, for both the radial deformations and axial deformations the numerical model shows first a contraction and then a dilation due to frost heave occurs (Figure 4.11). The soil in the vicinity freezes and expands, consequently the still unfrozen soil is pushed together. When the soil starts to freeze and the segregation threshold is passed the soil start to expand. The calculated deformations approach the measured deformations, especially at -15^{o}C. At 30^{o}C the rate of deformations slows down after a few hours. In these first few hours most heave occurs. Afterwards the ice saturation is so high that no more heave can occur. The decrease of deformations can be explained by the use of the solid expansion coefficient. The colder the soil gets, the more the solid shrinks, lowering the deformations in time until the temperature becomes constant.

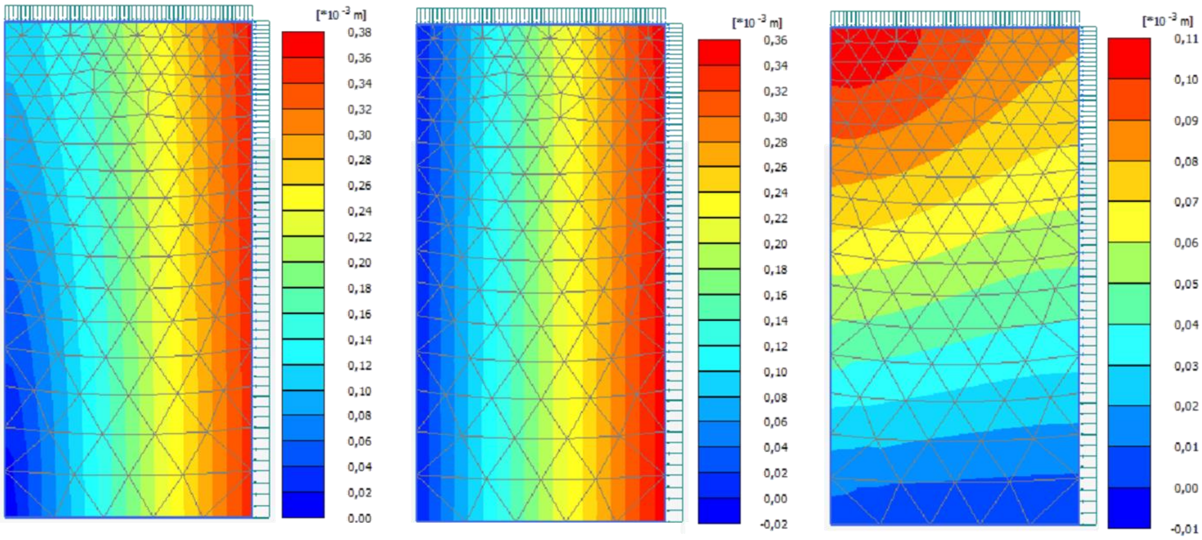

a. Total displacements ` **b. Horizontal displacement** **c. Vertical displacement**

Figure 4.9: Displacements in the sample due to frost heave at -30^{o}C.

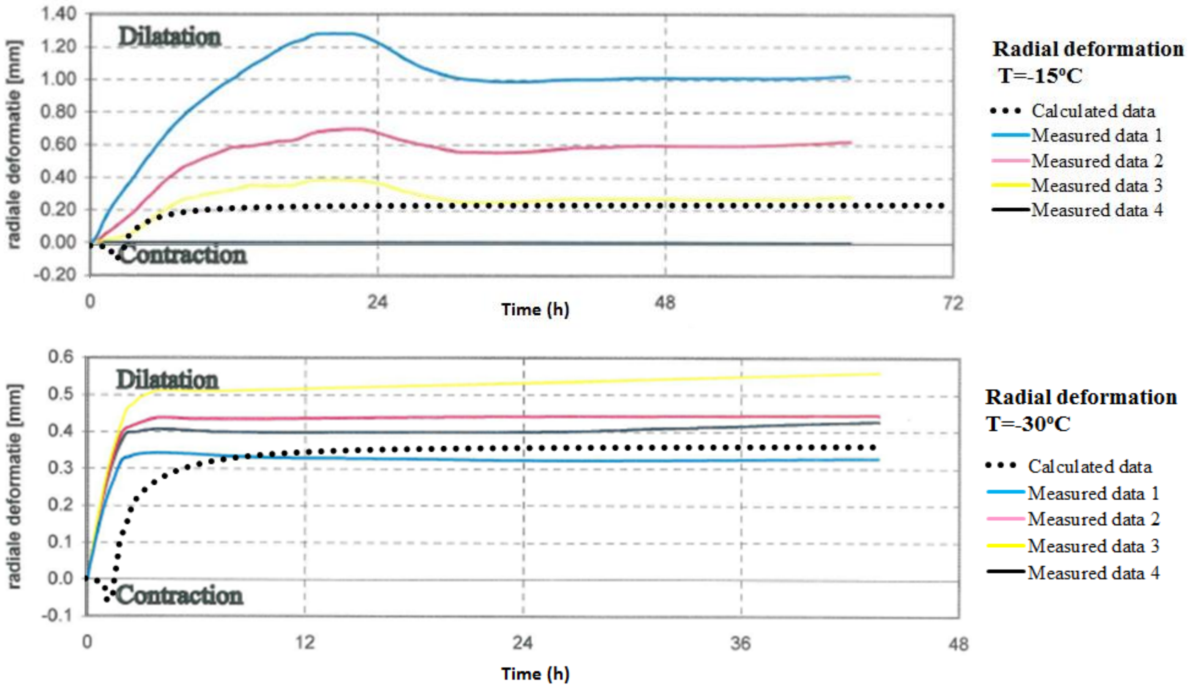

Figure 4.10: Radial deformation in heave tests of measured data (Report NITG 98-22-B, 1996) and calculated data at -15°C and -30°C.

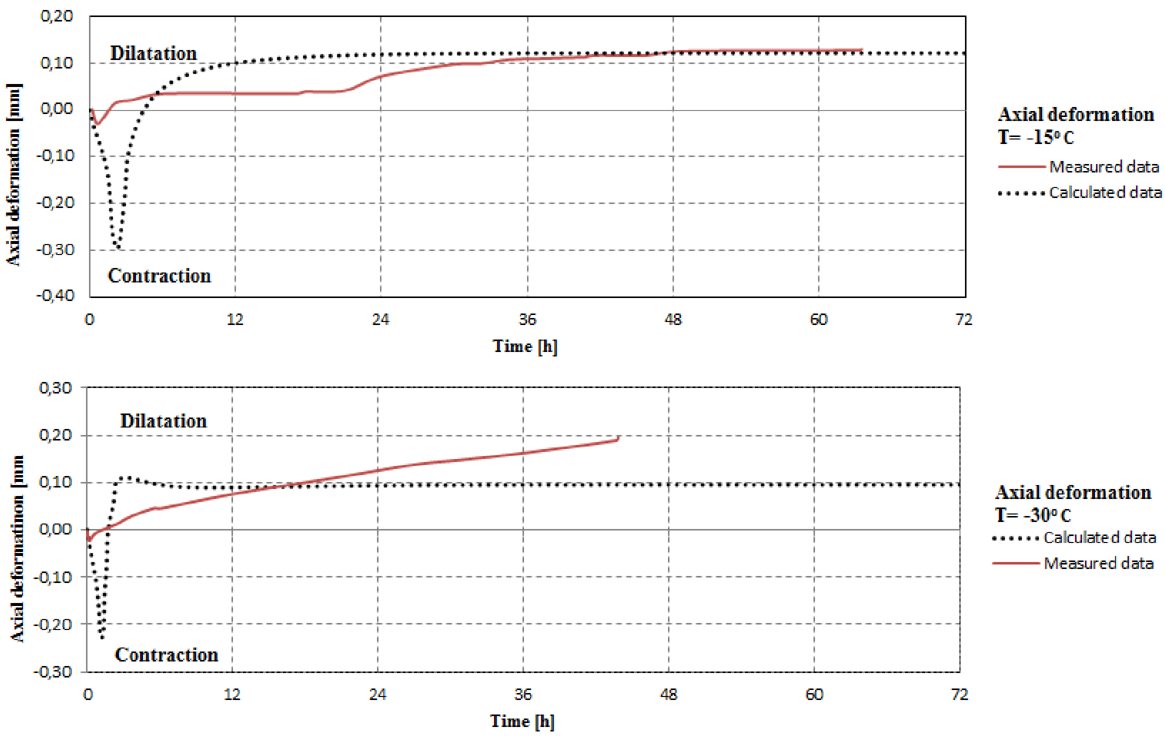

Figure 4.11: Axial deformation in heave tests of measured data (Report NITG 98-22-B, 1996) and calculated data at -15°C and -30°C

4.3.4 Thaw tests

During thawing of a soil sample, ice turns into water and the volume decreases. The volume does not necessarily go back to its original volume, it can be smaller and larger than its original volume. because thawing may induce additional settlements. To demonstrate this, the model of the heave test is used. The sample is completely frozen at the end of the heave test. Subsequently the freeze pipe (temperature boundary) is turned off and the temperature around the sample will be constant. Figure 4.12 shows the volumetric strain of a gauss point in the middle of the sample during freezing and thawing. The arrows indicate the direction of the freeze-thaw cycle. During freezing the soil expands gradually with decreasing temperaturec, while at thawing the largest volume decrease takes place just before 0^{o}C. The final displacements are influenced by the rate of thawing. When the ambient temperature is higher, the final volumetric change is larger. The faster ice turns into water, the more pore pressure will build up in the clay, as the hydraulic conductivity is lower than the thawing rate (Figure 4.14). Larger pore pressures cause more settlement of the soil. Also the confining pressure influences the final volumetric change as shown in Figure 4.13. Larger confining pressure causes a larger volumetric strain during thawing.

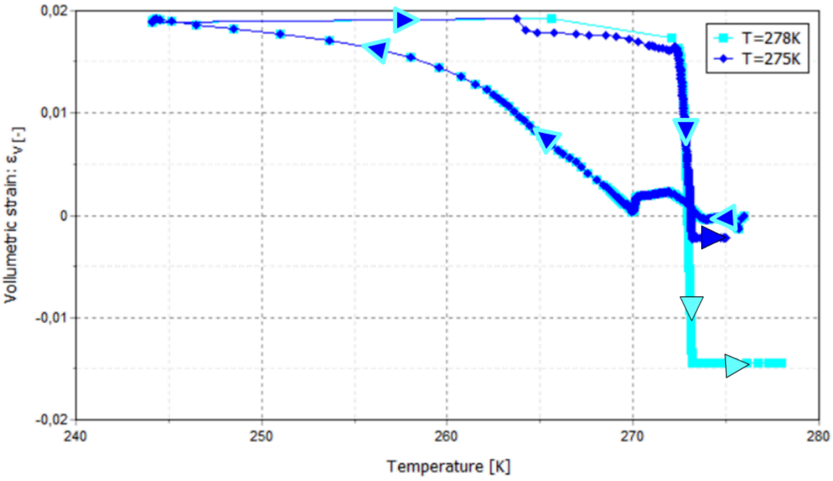

Figure 4.12: Volumetric strain at two different thawing temperature (for gauss point in the middle of the sample)

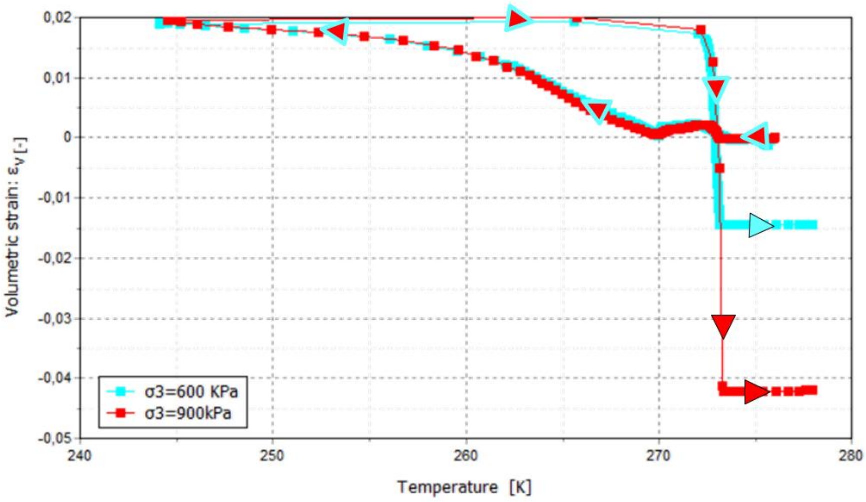

Figure 4.13: Volumetric strain at two different confining pressures (for gauss point in the middle of the sample)

4.4 Conclusions of chapter 4

The capability of a numerical model to simulate changes in strength, stiffness and deformations when soil freezes starts with the appropriate input parameters. The frozen and unfrozen soil model in Plaxis requires seventeen model parameters, six thermal parameters and three fitting parameters to determine the SCFF curve. Three steps have been taken to gain a reliable parameter set which can be used at a later stage to model cross passage construction with AGF.

- *Parameter determination*: the parameters can be determined with laboratory tests (Table 4.2). Not every laboratory test was available to determine the parameters for the Westerschelde project. Some of the unknown parameters could be determined with correlations. For the remaining parameters default values can be chosen. These default values were mostly obtained from the works of Aukenthaler (2016) and Ghoreishian Amari (2016), who described the determination of parameter sets for various soil types.
- *Parameter optimisation*: most of the model parameters are difficult to associate with specific (frozen) soil behaviour. Furthermore, a single parameter does not necessarily control one feature of (frozen) soil behaviour. Often combinations of these parameters control specific soil behaviour. Parameter optimisation on laboratory tests is a must to require the desired frozen soil features in large scale numerical models.
- *Parameter validation*: It is challenging in this constitutive model to obtain a parameter set in which all frozen soil features are equally well described. The validation of the final parameter set against laboratory tests gives an indication if frozen soil behaviour is underestimated or overestimated.

5 Cross passage models

Two numerical models have been made representing the construction of cross passage 2 of the Westerschelde tunnel (Figure A2). The studied cross passage was constructed with AGF at a depth of -28,5 m in boom clay. Brine was used as a cooling medium for the 22 freeze pipes with a temperature of approximately -36 to -38°C.

The frozen and unfrozen (FUS) model is only available in 2D, therefore two different cross sections are made to evaluate the soil behaviour during cross passage construction with AGF (Figure 5.1). Model 1 (M1) is a cross section taken in the XY-plane and plane strain conditions are adopted. Model 2 (M2) is a cross section with axisymmetric conditions. Under these conditions a real cross section is modelled, but a cylinder of soil is in z- direction. Axisymmetric conditions were chosen over plane strain models in the XZ or YZ-plane. The frozen soil would be simplified as straight slabs instead of a cylinder. The axisymmetric conditions were assumed to be a better approximation of reality.

The two models offer the possibility to investigate the expected interaction between the frozen soil and the lining of the bored tunnels, described in chapter 3. The calculations from the numerical models can also be compared to measurements of temperature, soil stresses, water pressures and deformations made near cross passage 2 during construction. Comparing the two models with each other will also give information about the validity of the models. First the method of modelling will be discussed in section 5.1, after which the results of the models will be evaluated in section 5.2 and finally an overview of the differences between the two models will be given in section 5.3.

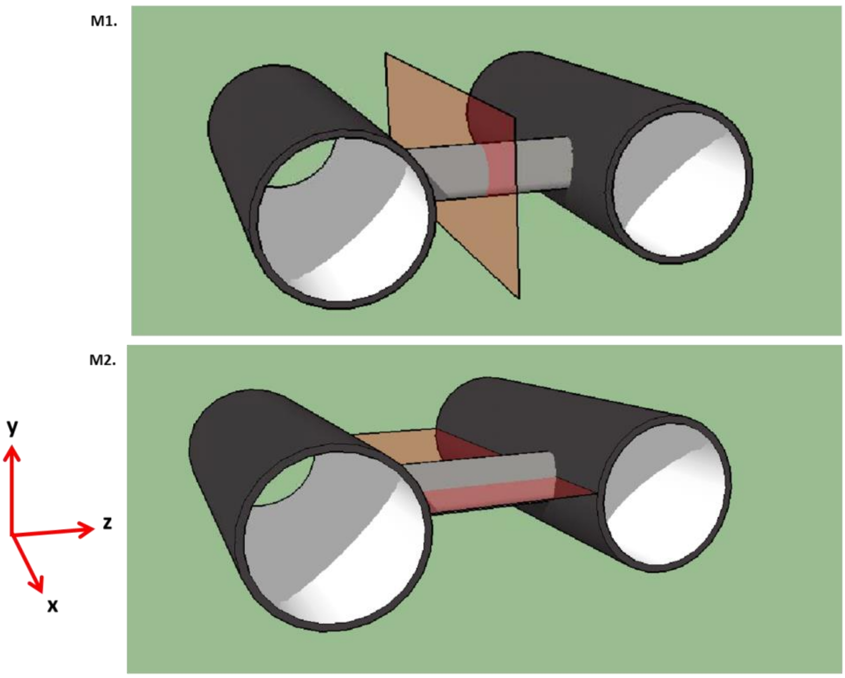

Figure 5.1: Schematic overview of the cross passage and the cross sections used for numerical model 1 (M1) and model 2 (M2).

5.1 Method of modelling

For both models the same construction phases have been modelled, all corresponding to the construction steps taken during the real construction process:

1. Freezing phase: the freeze pipes are activated. Their temperature is -37°C and they cool the soil by means of convection for 73 days. The thermal transfer coefficient of the freeze pipes was set to 2845.9 W/m^2/k. (van der Meijden, 2003). The initial soil temperature is 10°C.
2. Excavation phase: the frozen soil in the centre of the frozen cylinder is deactivated. The duration of this phase is 3.5 days and the freeze capacity remains 100%.
3. Shotcrete phase: of the shotcrete 0.25 m is applied as a temporary lining. The lining is given a temperature of 1°C, to simulate the heat transfer from the cross passage to the ice. The duration of this phase is 3.5 days and the freeze capacity remains 100%.
4. Final lining phase: the final concrete lining of 0.4 m is placed and additional measures are taken to finalize the cross passage, this takes 34 days. The temperature of the lining is kept at 1°C. During construction of the cross passage the freeze capacity was lowered to 33% of the original to maintain the frozen body. In the model this is expressed as a temperature increase in the freeze pipes to a temperature of -13°C.
5. Thawing phase: the freeze pipes are deactivated. This phase lasts 91 days, however in the models it took longer to let the soil thaw fully. Therefore the duration was increased to let the whole soil thaw.

The lining properties used in M1 and M2 have been summarised in Table 5.1.

Table 5.1: Lining properties

	Bending stiffness (EI) [N/m^2/m]	**Axial stiffness (EA) [N/m]**	**Plate thickness (d) [m]**	**Specific weight (w) [N/m/m]**	**Poisson ratio (ν) [-]**
Shotcrete	10.0 E6	2.0 E9	0.25	5564	0.15
Final lining (incl. shotcrete)	120 E6	10.0 E9	0.40	8900	0.15

5.1.1 Model 1

Model 1 is a plane strain model of the front view of the cross passage. The model consists of 22 freeze pipes and the gap that will be excavated is already visible in Figure 5.2. The rectangle around the cross passage is present to refine the mesh. Figure 5.3 gives a closer view of the freeze pipe configuration. The soil profile in the model is simplified to be all boom clay. In reality the boom clay starts at -23 m in the area of the cross passage, there is a sand layer above the BC (Figure A5). The sand above the cross passage is not taken into consideration, since the freeze and thaw process takes place in the boom clay in which the cross passage is constructed. The phreatic level is set to surface level. The possibilities and limitations of this model are summed up below.

Possibilities:

- Evaluate the freezing process, freezing time and thickness of the frozen ring.
- Evaluate pore water pressures inside the frozen cylinder.
- Evaluate change in stresses around frozen cylinder with a stress increase in the vertical direction due to gravity.
- Evaluate deformations around the frozen cylinder in XY direction.

Limitations

- Strains and deformations in z-direction are assumed to be zero, while the main bored tunnels are able to deform.
- Influence of freezing on bored tunnels cannot be evaluated (z-direction)

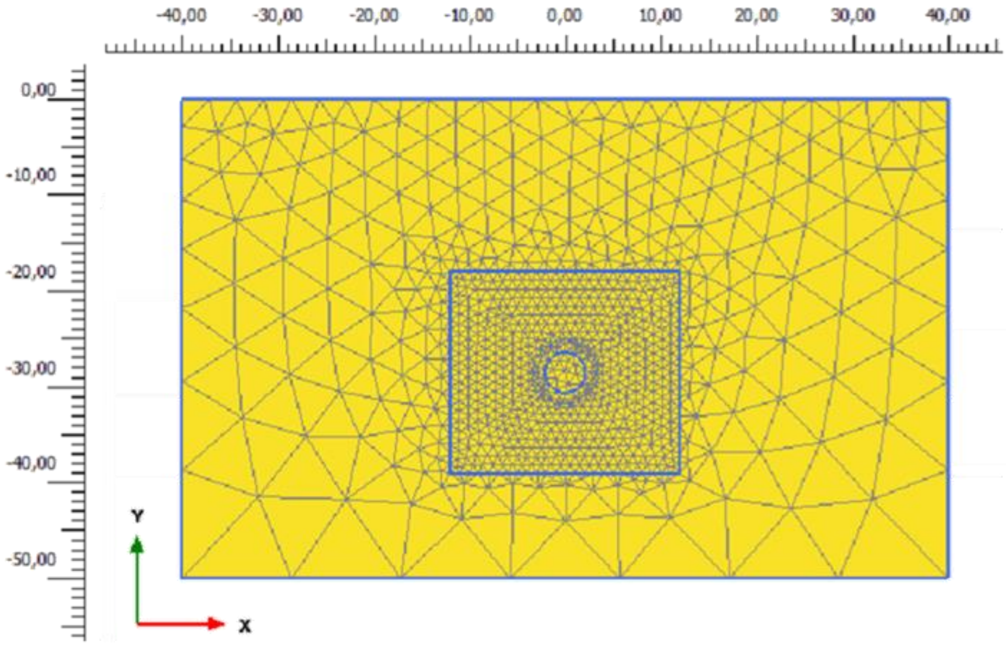

Figure 5.2: Geometry model 1 (1985 elements, 15983 nodes)

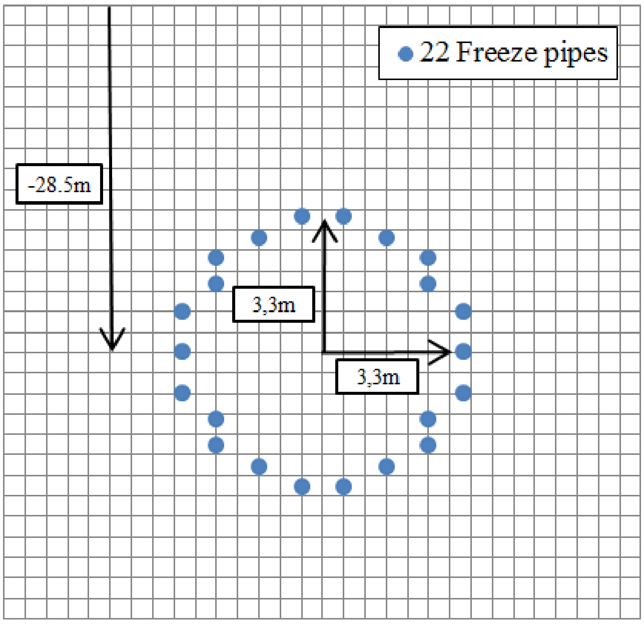

Figure 5.3: Freeze pipe configuration

5.1.2 Model 2

The second model is an axisymmetric model with the cross section taken in the (XZ-plane). The geometry of model 2 is shown in Figure 5.4. The geometry is very similar to the geometry of the triaxial compression test modelled in paragraph 4.3.1. By choosing to make this model axisymmetric a cylindrical representation of the frozen body and excavation can be made. The boundary around which the model rotates must be the vertical axis and cannot be changed to the horizontal axis. In the case of the cross passage the vertical direction is the z-direction. In this XZ-plane the stresses are constant, therefore the gravity is set to zero. Although the stress conditions around the cross passage are not constant, there has to be a constant stress imposed on the borders of the model. The choice was made to take the stress conditions in the middle of the cross passage at -28.5m depth. The water conditions are controlled as a user-defined water pressure.

The left and bottom boundary are normally fixed and the loads at the top and right side of the model are used to control the stress conditions in the sample. Due to symmetry only half the width of the cross passage is modelled. The left boundary is the symmetry boundary, in this case the middle of the cross passage. A freeze pipe is placed from the start tunnel until 0.15 m from the opposite tunnel. The line between the freeze pipe and the symmetry boundary indicates the size of the gap that has to be excavated. The opposite tunnel has been modelled with a plate, the properties are described in Table 5.2. The start tunnel has not been modelled as a plate, because this boundary cannot deform in z-direction.

The construction phases are similar to model 1. The only difference is that for this model an extra phase is added prior to the freezing phase, to generate the desired stresses in the soil (σ'=138.1 kPa and p=285 kPa). The possibilities and limitations of this model are summed up below.

Possibilities:

- Evaluate displacements and forces on opposite tunnels during construction.
- Evaluate a circular excavation and frozen ring.
- Evaluate pore water pressures inside the frozen cylinder.
- Evaluate stresses changes around the frozen cylinder

Limitations:

- Bored tunnel as a plate and not a circular lining
- The start tunnel is not taken into consideration.
- The ring of freeze pipes is a continuous ring instead of separate freeze pipes.
- Stress conditions remain constant around the cross passage, the model only applies to the XZ-plane and not to the whole cylinder.

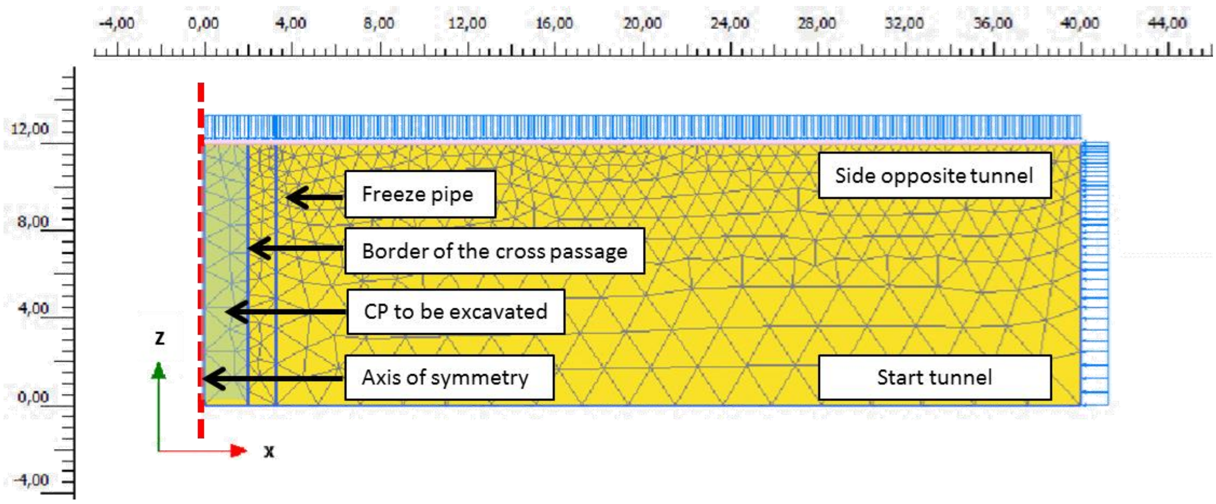

Figure 5.4: Geometry model 2 (804 elements, 6637 nodes)

5.2 Model results

The monitoring program for the studied cross passage of the Westerschelde tunnel was very extensive. Different types of monitors have been used to measure the soil stresses, water pressures and temperatures in the soil near the cross passage during construction. The location of these monitors is visualised in section A1.2.

5.2.1 Temperature distribution

The temperature distribution around the cross passage is nicely shown in M1 in Figure 5.5a. The temperature is the lowest around the ring of freeze pipes (-37^{o}C), logically the lowest temperatures give the highest ice content(Figure 5.5b.) The heart of the frozen body is still a little unfrozen after 73 days of freezing in M1, while in M2 the heart had just frozen but has only 7% ice saturation (Figure 5.6). The white circle in Figure 5.5 and Figure 5.6 indicates the frost line. From the freeze pipe to the frost line, the ice is approximately 1.5 m thick in M1. In M2 this thickness is 2 m. Although the two models have the same thermal parameters the soil freezes faster in M2 than in M1, the different geometries are thus of influence on the freezing rate. In M2 the ring of freeze pipes is actually a continuous ring instead of separate freeze pipes, leading to more heat withdrawal from the soil.

During construction of the Westerschelde tunnel difficulties were encountered when freezing the soil directly behind the segments of the opposite tunnel, since the lining of the bored tunnel functioned as temperature boundary. That is why the frozen body did not make a watertight connection. To solve this problem dry ice was placed against the bored tunnel lining. That this problem can arise is demonstrated with model 2, when for this test the top boundary (representing the opposite bored tunnel)was given a temperature of 20^{o}C (Figure 5.7).

In Figure 5.8a the temperature measured by monitors SM4 and SM3 are presented in a timeline. The construction stages are also indicated. The monitors take measurements in multiple direction. Both monitors are located approximately at 1 m from the freeze pipes at a depth of -28.5 m. The monitored temperatures can be compared to the calculated temperatures at the same location in Figure 5.8b. Again it can be seen that the temperatures during the freezing phase are lower in M2 than in M1. The rate of freezing in M2 is more similar to monitor SM3-4, while the temperatures in M1 are approximating temperatures from SM3-2.

During the excavation phase a sudden temperature increase is observed in M1, but not in M2. When the excavation starts the frozen body becomes a structural element, increasing the load on the ice. This is where pressure melting kicks in, because ice under higher load melts. Due to the increase in water the temperature increases a few degrees. In M2 the stress conditions remain constant during all phases, therefore no additional loading of the ice occurs due to excavation and the temperature will remain constant. After the excavation phase the freeze capacity is reduced to 33%. In the monitoring data an slight increase in temperature can be seen, in contrast to the large increase in temperature in the models. The reduction in freeze capacity is modelled as an higher temperature (-13^{o}C) of the freezes pipes instead of a decrease in freeze capacity, leading to a higher temperature increase than in reality.

When the thawing phase begins the same pattern occurs in monitored temperatures and modelled temperatures. However, in the models thawing takes longer. The thawing process may be faster in reality due to external influences, such as higher surrounding temperatures, heat of hydration from curing concrete in the cross passage and a higher transfer of heat into the soil from the two bored tunnels. Also groundwater flow around the freeze pipes can make the soil thaw faster, in the model no additional water flow is taken into account. Apart from the longer thawing period, the temperatures in the different construction phases lie in the range of the measured temperatures.

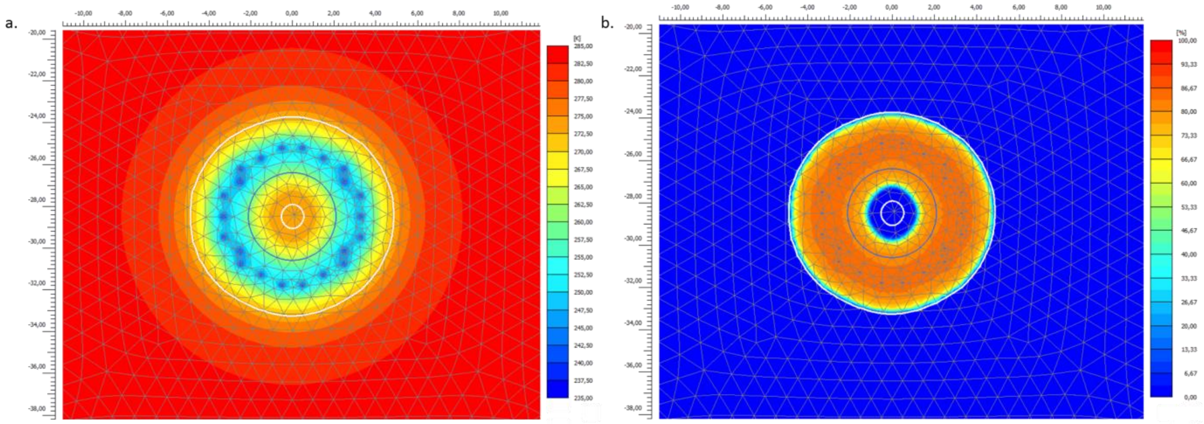

Figure 5.5: M1 after 73 days a. Temperature [k] b. Ice saturation [-]

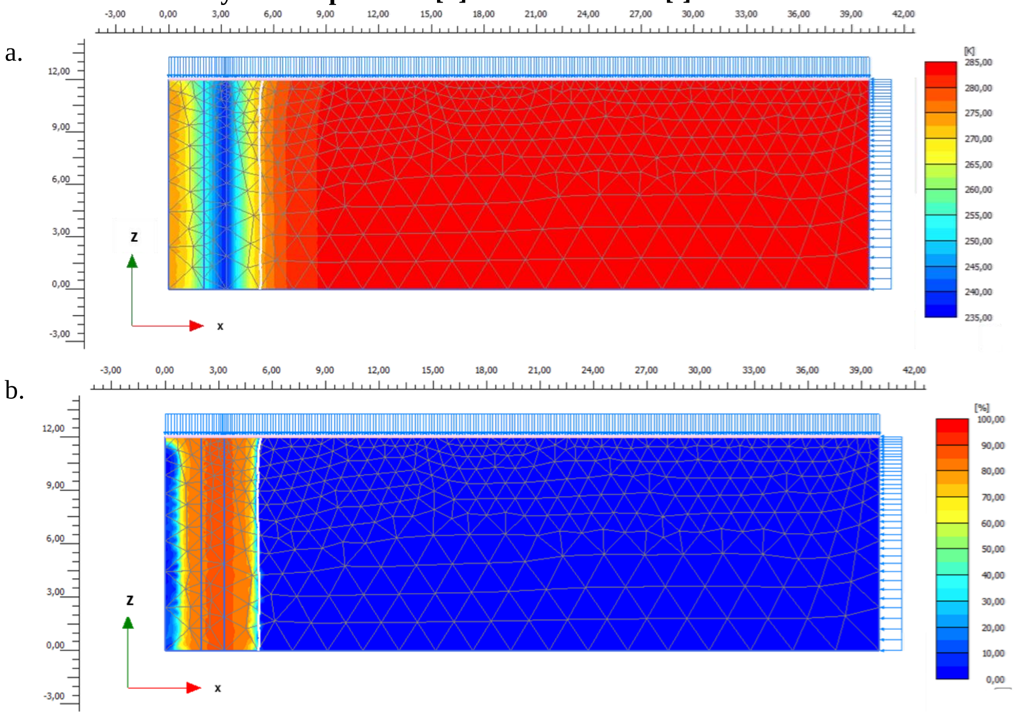

Figure 5.6: M2 after 73 days a. Temperature [k] b. Ice saturation [-]

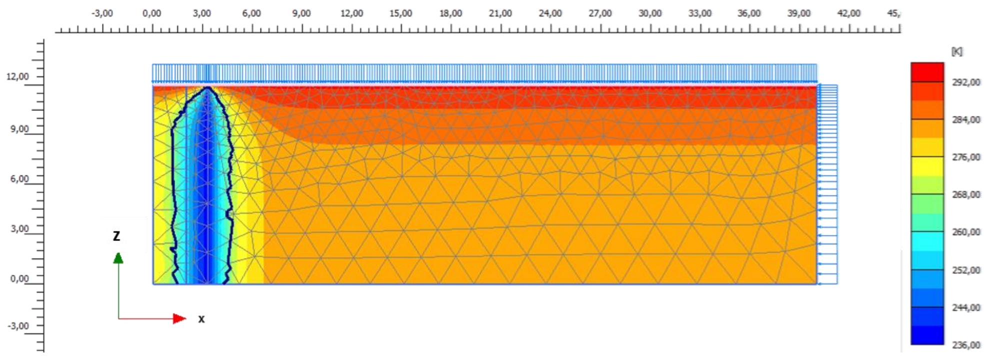

Figure 5.7: Temperature distribution in M2 when the top boundary has a temperature of 20^{o}C.

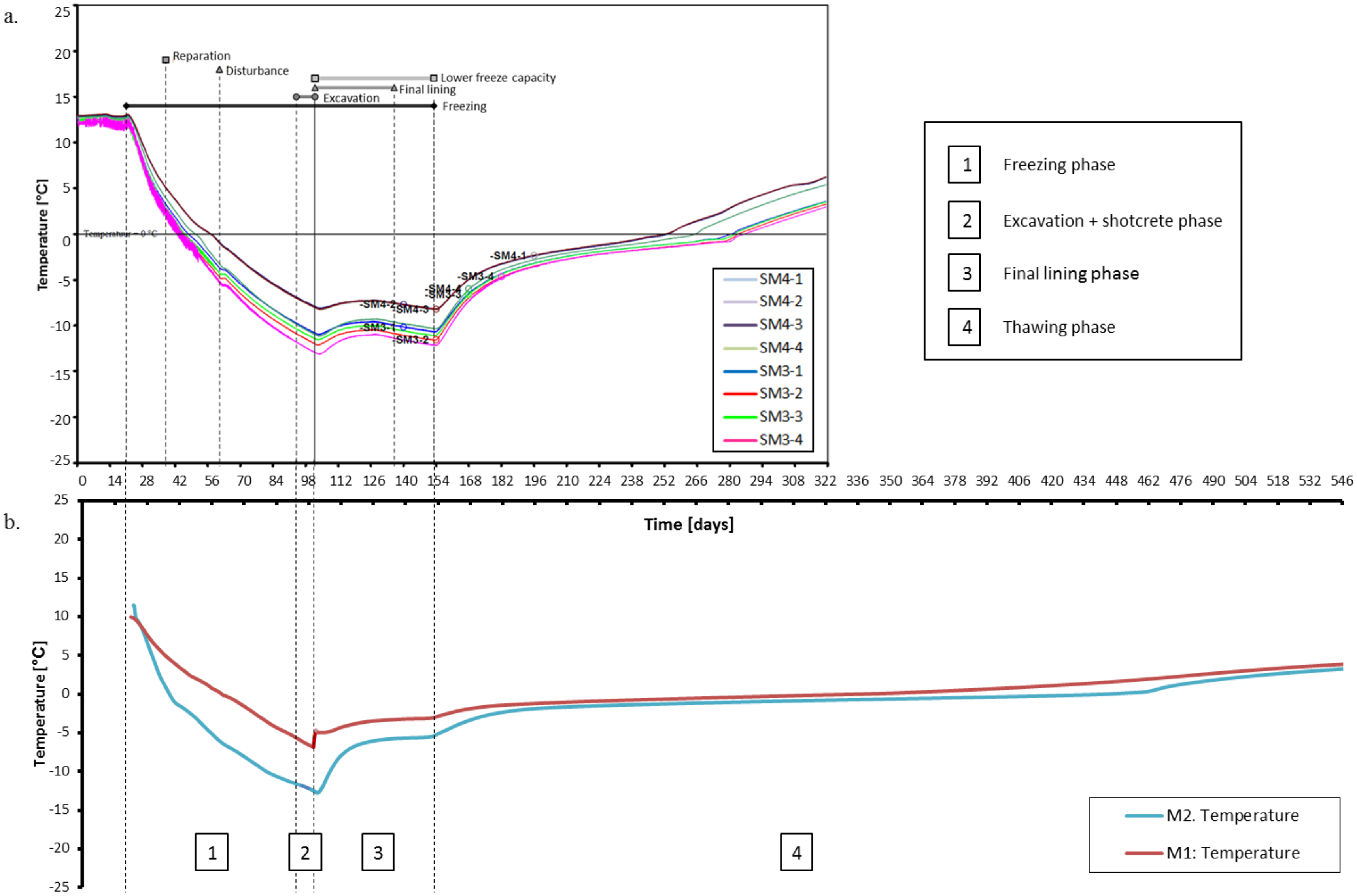

Figure 5.8: Temperature in different construction phases a. Measured temperatures at SM4 and SM3. b. Calculated temperatures in M1 and M2.

5.2.1 Water pressures

During freezing the pore water pressure decreases with increasing ice saturation. The calculated pore water pressures outside the freeze pipes are given in Figure 5.9b. Both models show very similar behaviour regarding the pore water pressures. When the temperature drops beneath 0^{o}C the pore water pressure gradually decreases. When the ice saturation becomes higher than 80% the water pressures diminishes all the way to zero. From the moment thawing starts, water pressures start to increase again, until they are at their original value. The decrease in pore water pressures only occur in the frozen soil and the surrounding pore water pressures are not influenced (Figure D1a and Figure D2a).

Figure 5.9a shows pore water pressures outside the freeze ring measured by monitor SM4 in pink. Before soil freezes an increase of approximately 50 kPa can be seen in the measured pore water pressures, while this does not occur in the calculated data. An increase in pore water pressures can occur due to expansion of the soil during freezing. The soil in the vicinity of the monitor is already frozen and expands due to the in-situ phase change of water or due to frost heave. Since the hydraulic conductivity in clay is low, the expansion causes excess pore water pressures. In the model the expansion is in the early stage of freezing very small, because the cryogenic suction has not passed the segregation threshold. Therefore, excess pore water pressures are not encountered before freezing. From the moment the soil freezes similar behaviour as in the calculated data is observed in the measured data. The pore water pressure decreases and although the thawing phase occurs faster the pore water pressures increase during thawing until the thawing point is reached.

One of the expected load situations is the increase of pore water pressures due to the enclosure of unfrozen water in the frozen cylinder (Section 3.2). In the measured pore water pressures in the middle of the frozen body by monitor VW3-1, an increase of pore water pressures of almost 400 kPa was measured before the pore water pressures started to decrease upon freezing (Figure 5.10a). Figure 5.10b shows that pore water pressures in the heart of M2 do show a slight increase in pore water pressures before freezing, only far less than measured. The heart of M1 was still unfrozen at the end of the freezing phase. To show the behaviour of the pore water pressures in the heart of M1 the freezing phase was extended with 25 days. In M1 no increase in pore water pressure is observed before freezing. The pore water pressures remain unchanged before freezing, just as outside the frozen cylinder. In both models, the pore water pressures give a slight dip before freezing. This is the influence of the suction of the approaching frost front. So, in both models no large pore water pressure is built up in the core of the frozen cylinder (Figure D1a and Figure D2a). What is often seen in frozen soils is that deformations occur in the direction of the temperature gradient, while in the model deformations occur in all directions. This means that the soil in between the freeze pipes expands as well, pressing the ring outward. The outward movement of the frozen ring is enough to keep the pore water pressures from building up. The volume expansion between the freeze pipes is shown in (Figure D1b and Figure D2b)

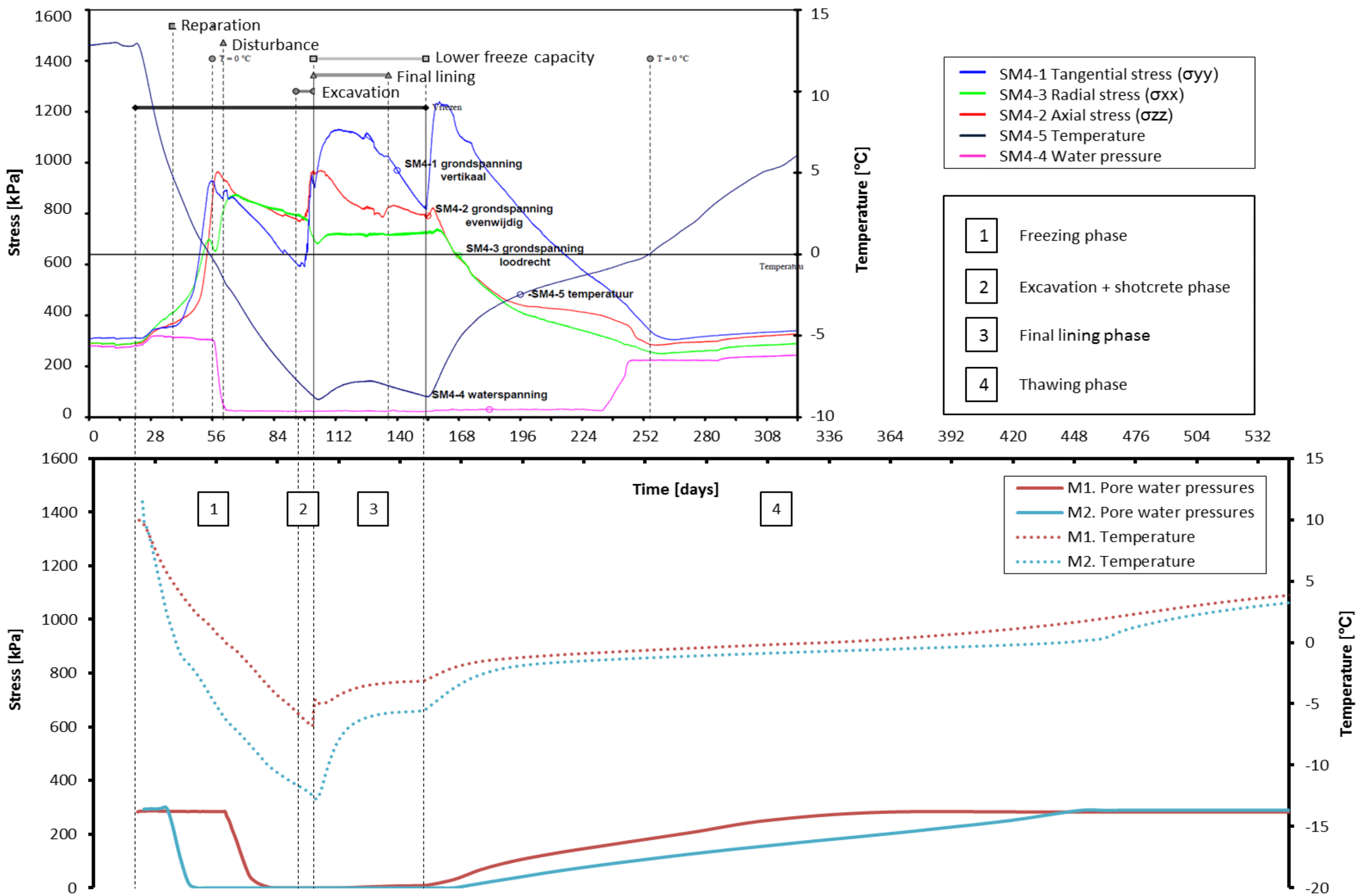

Figure 5.9: Pore water pressures outside the freeze pipes a. Measurements monitor SM4-4. b. Calculated (active) pore water pressures temperature of M1 & M2.

a.

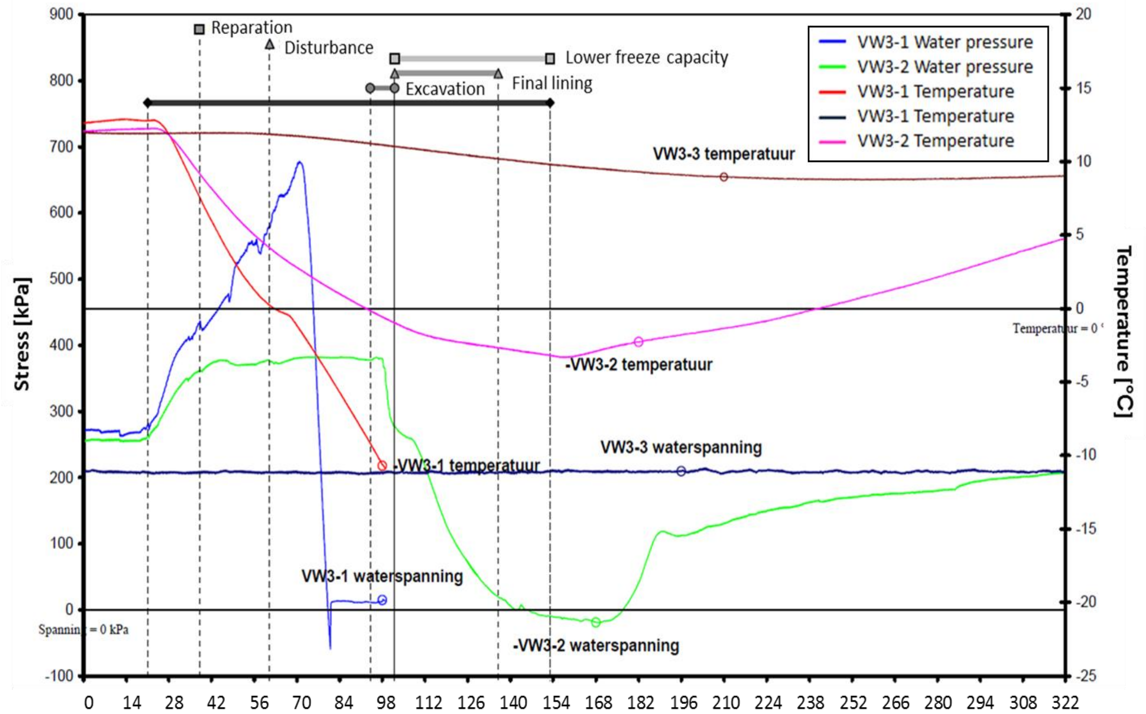

b.

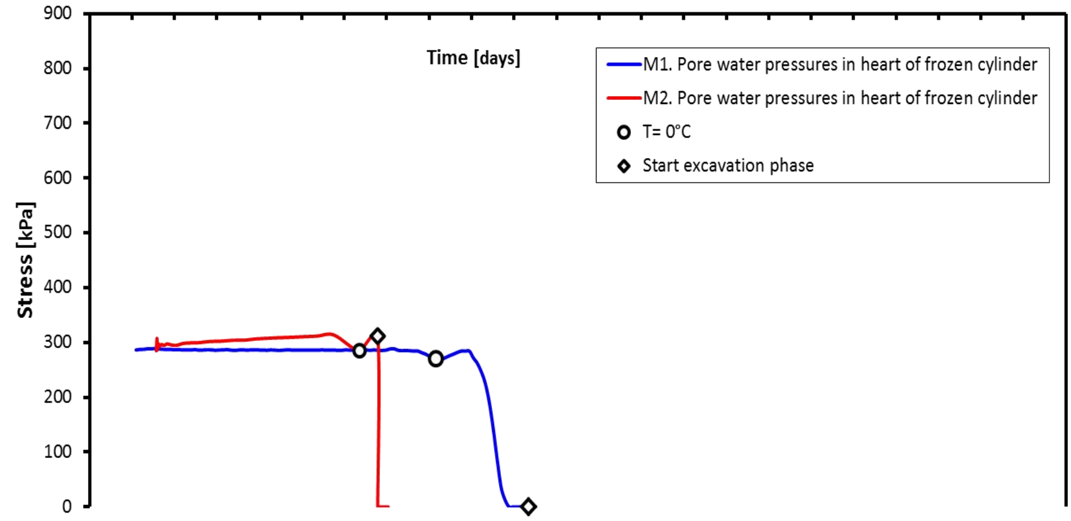

Figure 5.10: Pore water pressures in the heart of the cross passage a. Measurements monitor VW3 b. Calculations of M1 & M2.

5.2.2 Soil stresses

The monitoring results from monitor SM4 will be used again to compare the measured soil stresses to the calculated soil stresses in the model. The monitor registers three different stresses; vertical stress, perpendicular stress and parallel stress relative to the cross passage. Due to installation of the stress monitor a relaxation of the soil occurred. This local disturbance results in lower initial stresses measured by the SM4. Therefore the measured stresses should be seen relative to the initial measurement. Figure 5.11a shows the measured stresses with SM4, together with the pore water pressures and temperature. The same graph has been made for M1 and M2 (Figure 5.11b and Figure 5.11c). In M1 the parallel stress is the out-of-plane stress and in M2 the vertical stress (tangential stress) is the out-of-plane stress. As soon as the soil is at the location of the monitor the perpendicular stresses equal the radial stress, parallel stresses equal the axial stress and vertical stress equals the tangential stress in the frozen cylinder.

The measured stresses start to increase even before the temperature reaches 0^oC. The soil in the vicinity of the stress monitor expands upon freezing causing a stress increase in the surrounding unfrozen soil. After the soil is frozen the stresses start to decrease due to creep or volumetric contraction of ice at lower temperatures (Rijkers et. al. 2006). In the models the stresses also increase in the freezing phase. However this stress increase occurs after the soil is frozen and not before as in the measured stresses. Before the soil becomes cooler than 0^oC the tangential and axial stresses even decrease. Soil in the vicinity of the monitoring is freezing and already gaining a higher stiffness. In the unfrozen soil this can cause a redistribution of stresses. The stress decrease becomes even larger when the pore water pressures start to decrease due to an increase in ice saturation. Shortly after the fast decrease of stresses, the stresses start to increase again. At this point the low temperature causes a cryogenic suction higher than the segregation threshold, resulting in an expansion of the soil and thus an increase in stresses. In M1, in contrast to M2, the axial stresses become higher than the tangential. This can be caused by the plane strain conditions. In a plane strain model the strain and displacements in z-direction are assumed to be zero, whereas in reality, displacements can occur in z-direction, resulting in deformations of the main bored tunnel linings.

In both models the radial stress behaves a little differentlythan the two other stresses. It starts to increase before the soil freezes, just as in the measured stress. The dip in stress due to the decrease in pore water pressures is also encountered. When expansion due to ice segregation starts the stresses increase again, but not as much as the other two stresses. The radial stress is the only stress that is not restricted by boundary conditions (the bored tunnels) or by frozen soil. Therefore larger displacements can occur.

The frost heave pressure on the bored tunnel can be expected to be similar to the stress increase in axial direction. The maximum frost heave pressures measured at SM3 was approximately 625 kPa. Both models give a fair an approximation of the frost heave stresses. M1 and M2 respectively predict a frost heave pressure of 600 kPa and 530 kPa.

Excavation of the frozen body heart leads to a decrease in stress release in radial direction. The remaining frozen soil must compensate by increasing the axial and tangential stresses. This occurs in both measured stresses and calculated stresses, but is very small in M1. The stress changes in the excavation phase are the largest in M2, however they are still approximately two times smaller than the measured stresses.

During the installation of the final lining the freezing temperature was increased. Higher freezing temperatures result in a lower frozen soil stiffness. SM4 measures first a large increase in tangential and axial stresses when the temperature increases, after which they decrease again with decreasing temperature. The stress in the tangential direction becomes even larger in this phase than during freezing. Report F100 states that this sudden unexpected increased is caused by redistribution of stresses and calls it a local shock. Additional stresses in tangential direction can influence the shotcrete and the final lining that is being installed. The stresses in the model are less sensitive to temperature fluctuations, since the stresses barely change in this phase. The sensitivity of the measured stresses to temperature changes could also be caused by creep effects. Creep effects are not taken into account in the FUS model.

The measured axial and radial stresses show a decrease of stresses as soon as thawing start. The initial increase in tangential stress is also observed during the temperature increase during the final lining phase. When the soil is further thawed the soil stresses return to their original level. The calculated stresses during thawing deviate from the measured stresses. The stresses after thawing are still 200-400 kPa higher than the stresses before freezing. In M2, the stresses start to decrease before the pore water pressure return to their original value. Still, the stresses remain 100-200 kPa higher. This might be caused by the longer thawing period in the model. The stresses need more time to go to their original value. On the other hand the thaw test was the only test that could not be validated and this might be the effect of parameters that are not optimal for a thawing problem. The thaw process highly depends on the actual stress condition and the initial pre-consolidation stress. A small pre-consolidation stresses lead to larger thaw settlements in the model, thus a larger stress decrease. The chosen pre-consolidation stress is high, choosing a smaller value probably would benefit thaw behaviour. On the other hand, it would significantly influence the strength and stiffness.

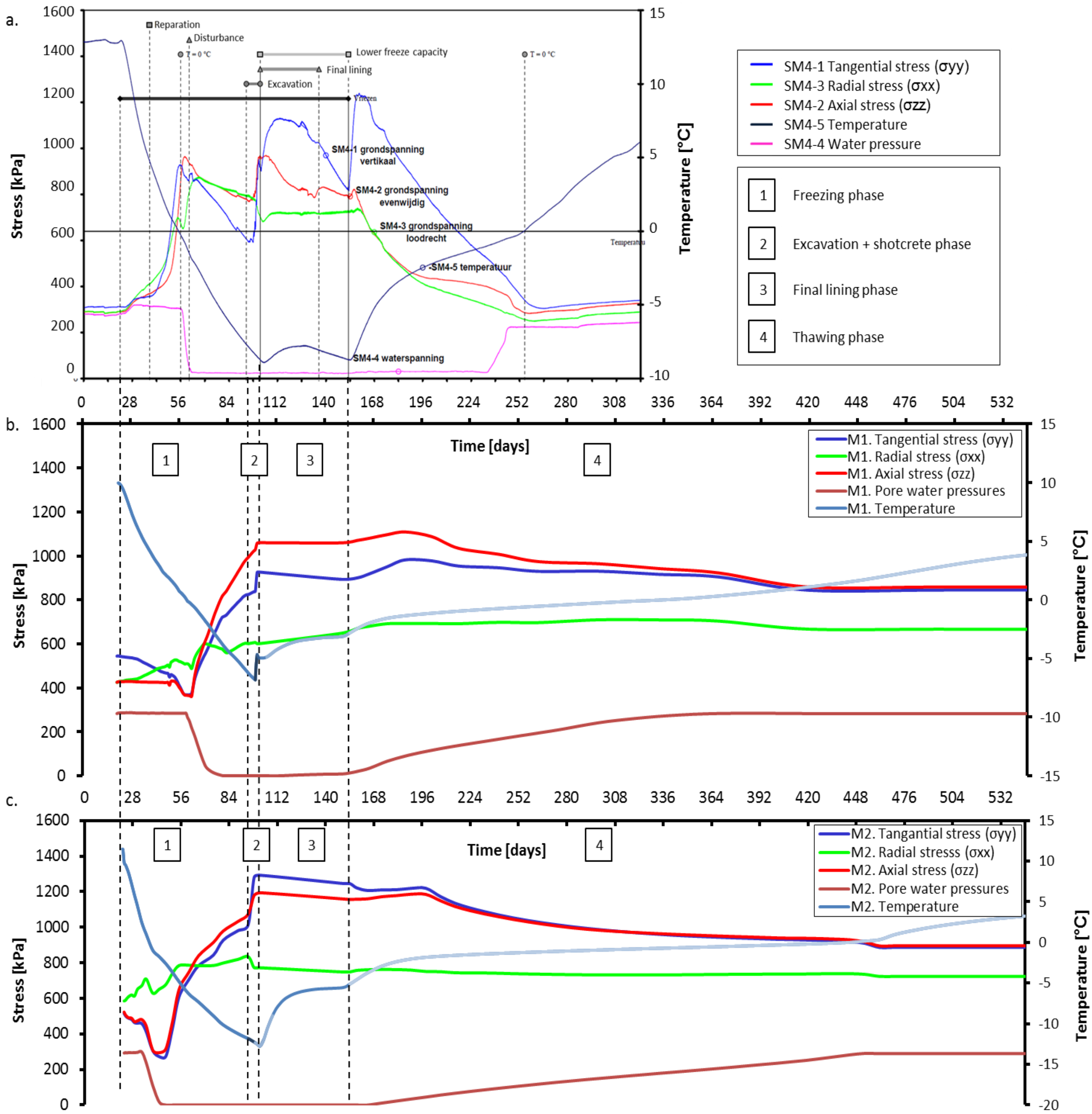

Figure 5.11: Total soil stresses in different orientations relative to the cross passage a. Measurements monitor SM4 b. Calculations of M1 c. Calculations of M2

5.2.3 Deformations

The deformations of the main bored tunnel's lining during the construction of the cross passage can only be evaluated in M2. The plate on the top boundary of M2 represents the bored tunnel. The bored tunnel is thus represented as a flat plate. The assumption was that when the lining of the bored tunnel was loaded with a force from one direction (i.e. the frost heave force), the stiffness response would be very weak. In the most inconvenient scenario the long term stiffness is 1/3 of the short term stiffness, and added to the reduction of 50% due to the presence of joints (Table 5.2: lining 1.0) (Blom, 2002). To investigate the results of scenarios with stiffer linings two other sets of lining properties have been made. One in which the short term stiffness is applied and stiffness reduction of 70% is applied for joints (Table 5.2: lining 2.0) and one in which the lining was made 100 times stiffer (Table 5.2: lining 3.0).

Table 5.2: Properties of the bored tunnel lining in M2

	Young's modulus (E) [N/m^2]	Bending stiffness (EI) [N/m^2/m]	Axial stiffness (EA) [N/m]	Plate thickness (d) [m]	Poisson ratio (ν) [-]
Lining 1.0	5.0E9	2.7E7 E6	2.0 E9	0.40	0.15
Lining 2.0	21.0E9	1.12 E8	8.4 E9	0.40	0.15
Lining 3.0	210.0E9	1.12 E10	8.4 E11	0.40	0.15

The measurement program of the Westerschelde tunnel included the displacements of the lining of the opposite tunnel. The largest displacements were measured during the freezing phase. Figure 5.12 shows the displacements in the freezing phase after 69 days of freezing relative to the position of the cross passage. A positive value gives an inward displacement of the circumference of the bored tunnel. The measured displacement graph has a ''camel'' shape, where two bumps are caused by frost heave at the tip of the freezes pipes. This camel shape is reflected in M2 when lining 1.0 is used. Due to the low stiffness, the displacements of the soil are followed by the lining. When the stiffness of the lining is increased the displacements become smaller and the camel shape disappears, notice that also the area of influence becomes larger. Lining 1.0 with the lowest stiffness gives the best representation of the lining behaviour compared to the measured displacements. However, the magnitude of the calculated displacement is more than four times larger than the measured displacement. This factor depends on the chosen solid thermal expansion coefficient, the ratio between the length of the frozen body and the radius and the temperature distribution in the frozen soil. To calculate displacements closer to the measured displacement the ratio between the expansion in radial and parallel direction should be considered.

This overestimation in displacements occurs for all construction stages. Figure 5.13a shows the measured displacement and the calculated at point A13 which corresponds to the location of the measured displacements. After excavation the displacements are reduced due to creep, while this reduction does not occur in the calculated displacement. Only a small reduction takes place during thawing, which can be also seen for some measured points.

In addition to the lining deformation a closer look is taken at the radial and axial deformation at the location of inclinometer HE4 (Figure A9) in M2. In the measured radial deformations (Figure A9a) a displacement away from the cross passage is seen, due to the expansion of the soil. This displacement increases during freezing to a maximum of 35 mm, after which it again slightly decreases in the excavation and final lining phase. Upon thawing the deformations decrease further, but not completely to its original position. Striking is that axial deformations change the most during the thawing phase.

In M2, a different trend between axial and radial deformation is seen. The axial deformations are twice as large as the radial deformations, while during the validation of the frost heave test this was the other way around (Figure A9b). The deformations in the model are independent of the temperature gradient, in contrast to reality (section 3.1). In order to simulate different expansion in axial and radial direction the solid thermal expansion coefficient was used. In the frost heave the solid thermal expansion coefficient in z-direction was enlarged, to get a larger shrinkage of the solids and compensate for the frost heave deformations. Although the chosen value of the solid thermal expansion coefficient worked well for the frost heave test, this value can clearly not be translated directly into a larger model where the ratio between the axial length and radial thickness of the frozen ice is different. The calculated radial displacements approximate the measured radial displacements better and are not overestimated (Figure A9).

In M1 the lining deformations of the main bored tunnels cannot be assessed due to the plane strain conditions. However, the radial deformations can be compared to measurements and M2. Figure 5.15a shows the deformations measured at the crown of the frozen body. Figure 5.15b shows the measured deformations at the crown of the frozen body and at the right edge at the location of HE4. The expansion of the soil during freezing is similar to the measured deformations. The radial expansion during freezing at the edge of the model can be compared to M2. Both calculated deformations are very similar 25 mm in M1 and 20 mm in M2. The slight difference could be caused by the constant stress condition in M2.

The radial deformations at the crown are approximately 10 mm larger than the radial deformation at the side of the frozen body. During the freezing phase it seems that the whole frozen body is pushed upward, leading to larger deformations in the vertical direction (Figure D3a and c). This could be caused by the boundary conditions of the model, even though the model boundaries are located almost 40 m out of the centre of the frozen body. Deformations at the crown reduce significantly at the crown, while at the side of the frozen body the calculated deformations approximate the measured deformations more closely in the excavation phase. It is odd that during the construction of the final lining deformations increase again, especially because the temperature increases. In the measured data this increase is not seen.

During the thawing phase a small reduction in displacements is seen at the crown, while the radial displacements at the side increase. This behaviour can be better visualised by looking at the bigger picture. Figure D3b and d show the phase displacements in the thawing phase. When the soil at the crown of the frozen body thaws displacements in vertical direction can be seen, while the soil is pushed outward at the edges.

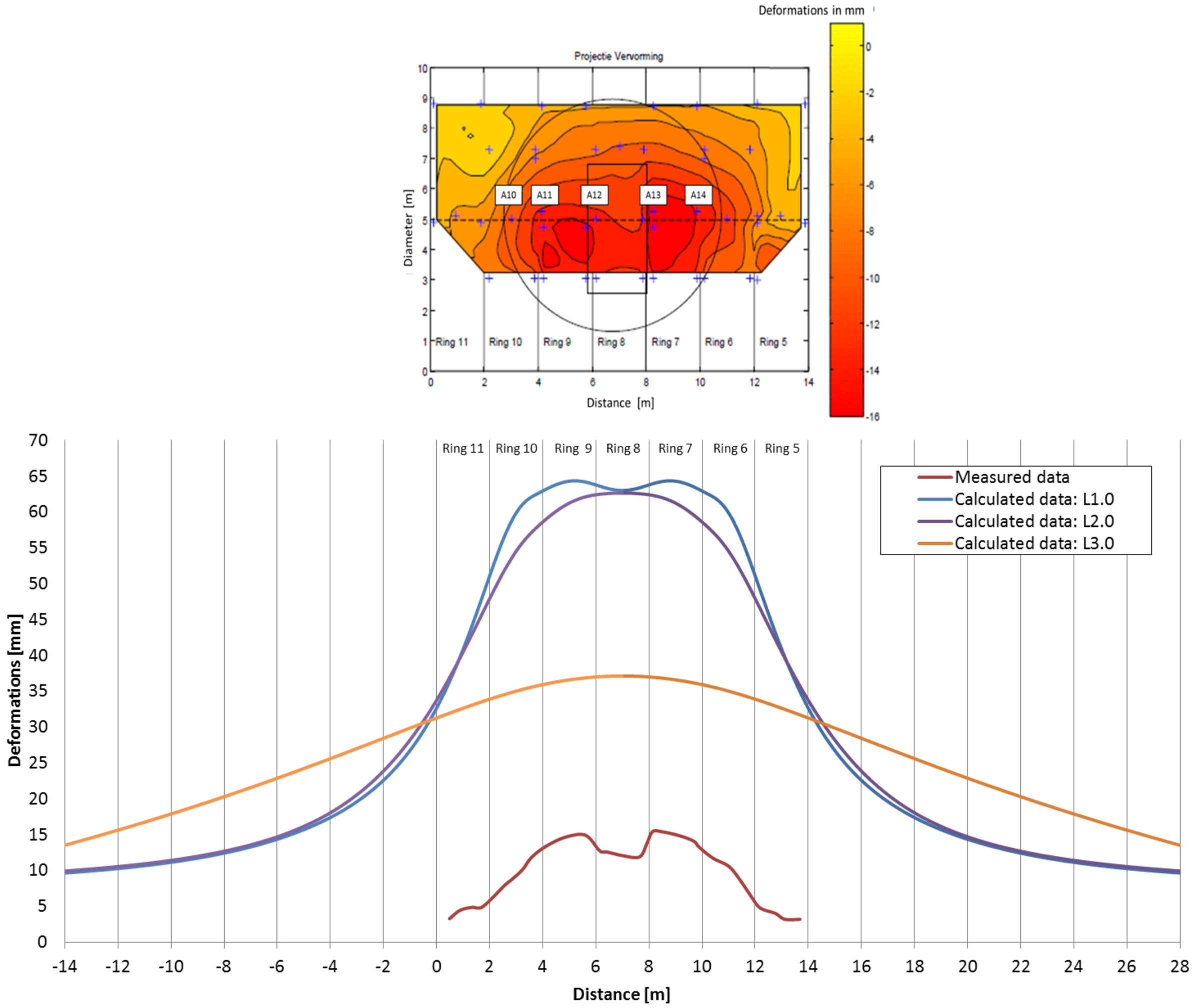

Figure 5.12: Joint displacements of the opposite tunnel measured after 69 days of freezing and calculated with model M2

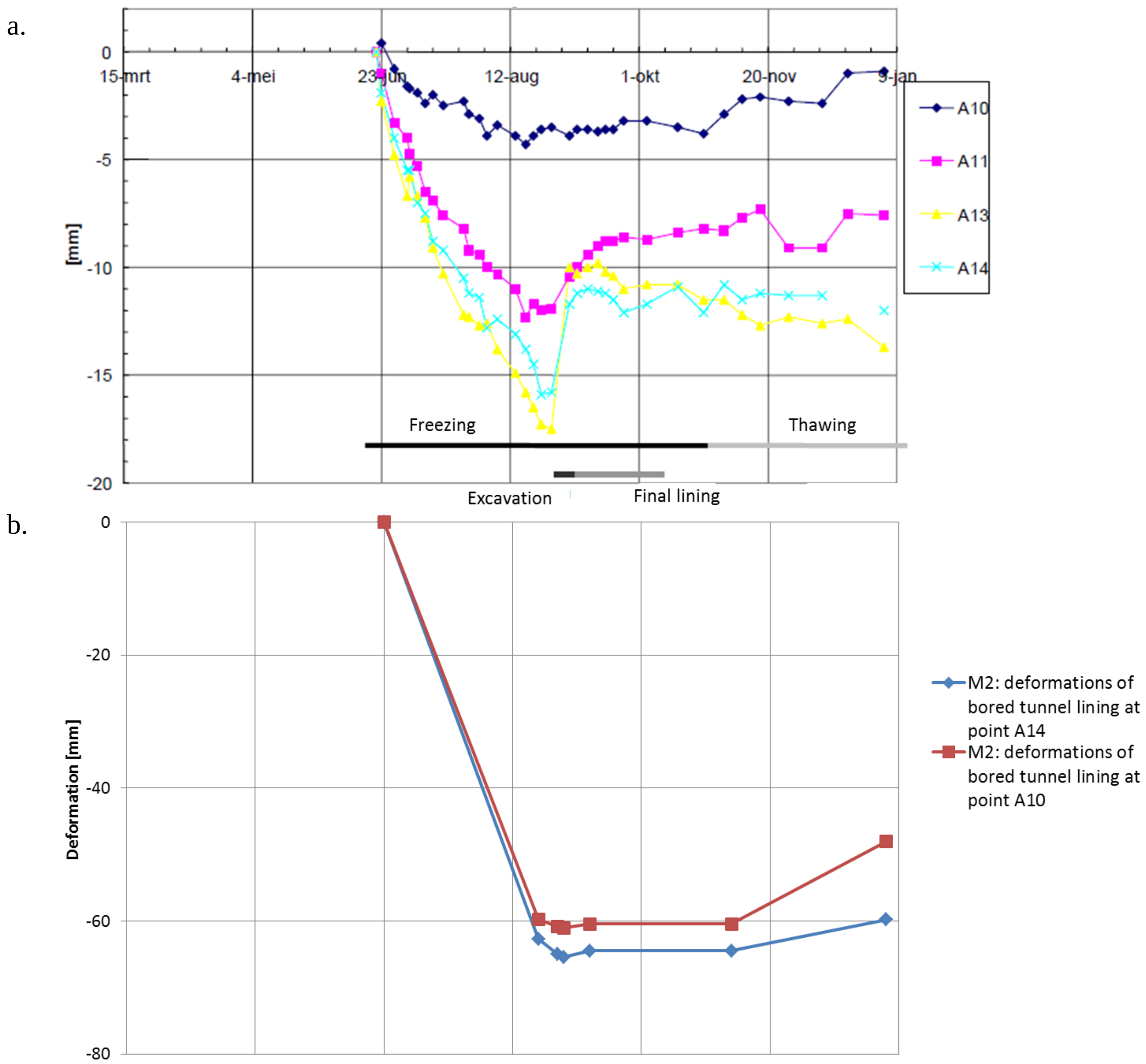

Figure 5.13: Displacements of the lining of the opposite tunnel during different construction phases a. measured displacements at different points b. calculated displacements at location A13.

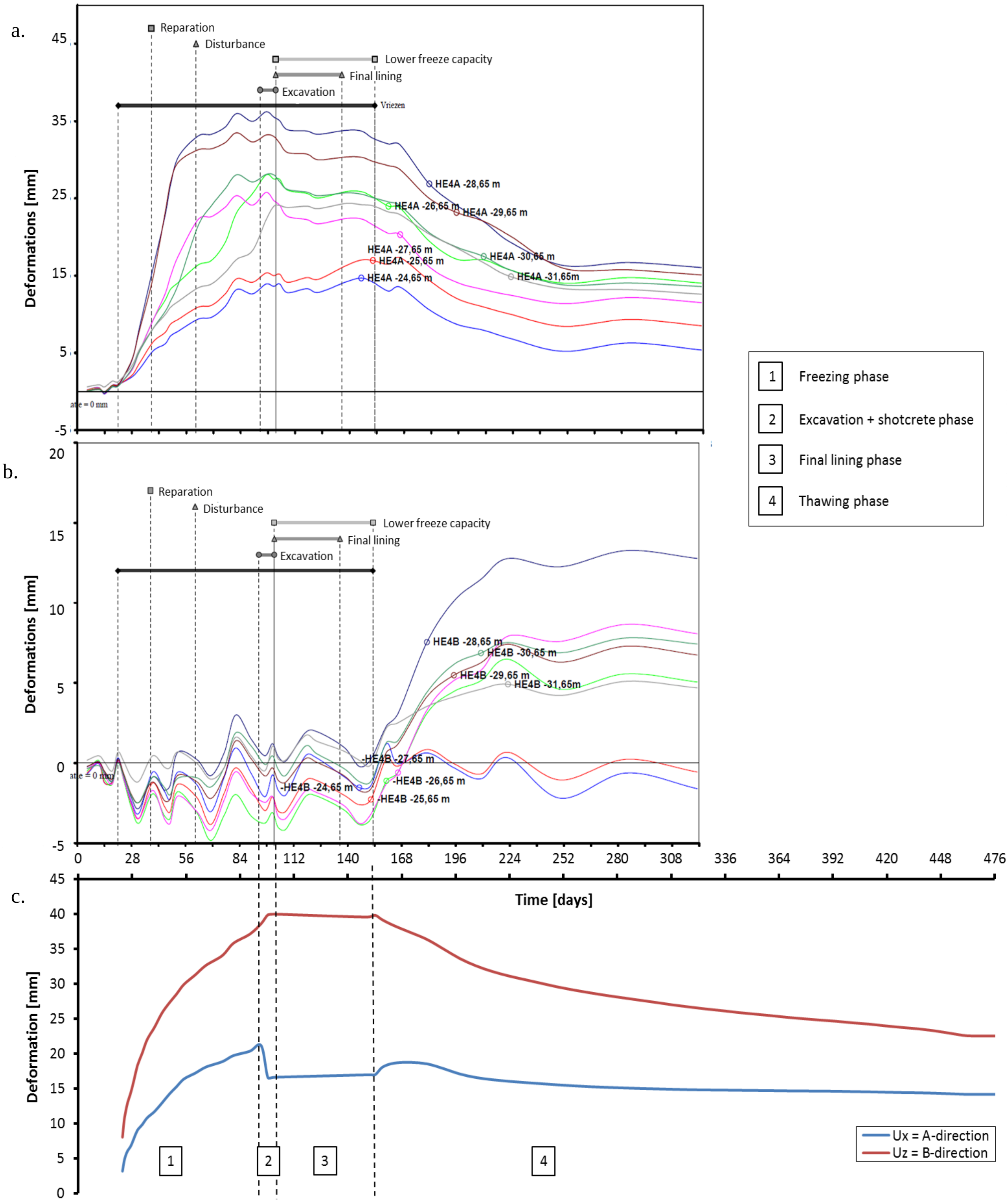

Figure 5.14: Deformations at the location of inclinometer HE4 a. Measurements in direction in radial direction b. Measurements in axial direction. c. Calculated in axial (z) and radial direction (x)

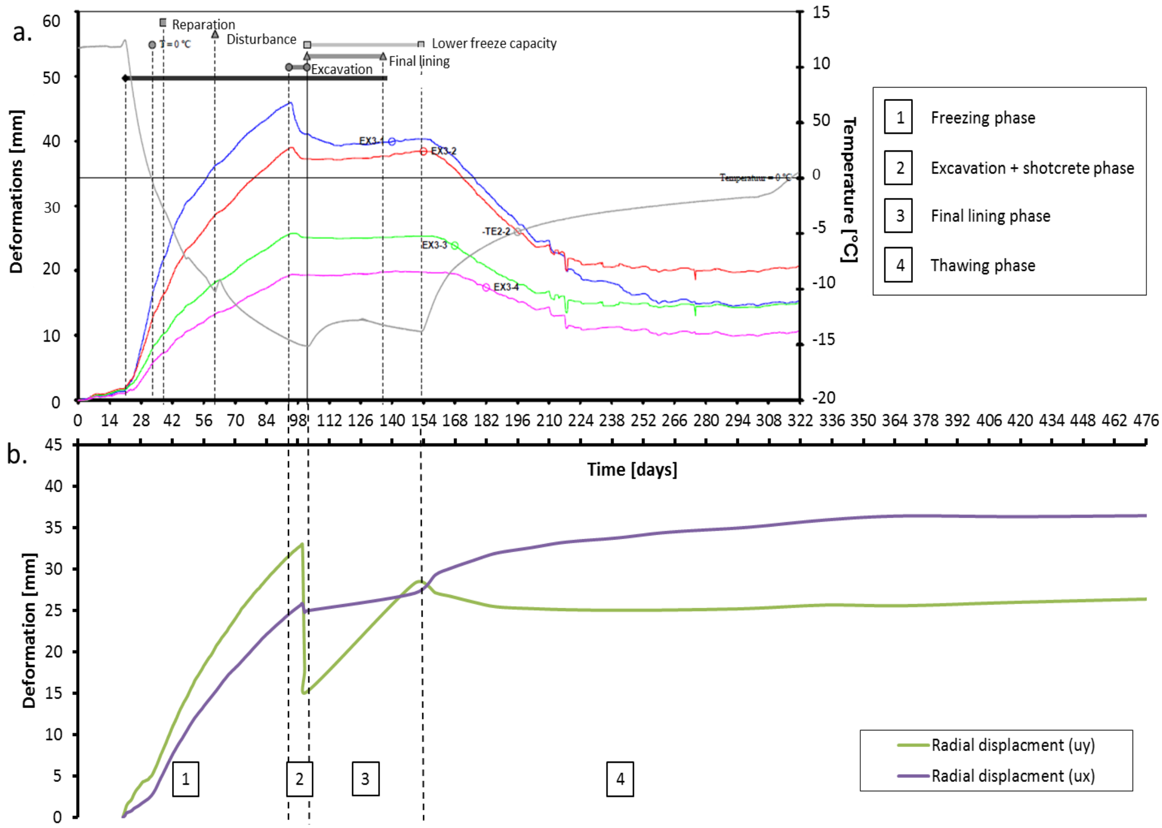

Figure 5.15: a. Measurements of deformations at the location of extensometer EX3. b. Calculated deformations in radial direction at location of EX3 and HE4.

5.3 Comparison between model 1 and model 2.

During the previous sections the similarities and differences out between the two models have been pointed. In this section the differences and similarities between the models are listed.

- Temperature: M1 generates a lower temperature field around the freeze pipes than M2 in the same amount of time. For both models the same thermal parameters have been used, so the geometry of the models has influence on the temperature. In M2 the ring of freeze pipes is a continuous ring instead of separate freeze pipes, consequently the freezing rate increases. Instead of the capacity of the individual freeze pipe, the freeze ring should be given an equivalent capacity.
- Water pressures: the generated water pressures are very similar in both models. However, in M1 the water pressures are hydrostatic with depth and in M2 the water pressures are constant. At the same depth they are equal to each other. The pore water pressures in the centre of the frozen cylinder stay constant during freezing in M1, while in M2 a slight increase is observed. The expansion between the freeze pipes in M1 causes a larger deformations than in M2, therefore pore pressures in M2 slightly build up.
- Stresses: at the same depth the stresses in the models behave similar. The stress changes in M1 are slightly lower than in M2. The temperature in M1 is a little lower and the soil contains less ice in the pores. Consequently, the stress increase due to ice pressure is lower in M1 than in M2.
- Deformations: the deformations of the bored tunnel linings due to frost actions in the soil can only be evaluated in M2, since de deformations in z-direction are zero in a plane strain model such as M1. However, a comparison can be made between the displacements in radial direction. The displacements in the freezing phase are very similar, only a small difference can be seen. This difference is probably caused by the different model conditions.

5.4 Comparison between predictive methods of frost heave.

The numerical models are able to predict qualitative behaviour of stresses induced by frost heave in the soil. There are some other methods and indications available to predict the consequences of frost heave. In this paragraph these methods will be compared to the model results and the measured results by the monitors of the Westerschelde tunnel.

5.4.1 U.S. Army corps of Engineers frost design and soil classification system

An indication of the amount of frost heaving and thaw weakening in the soil can be given in terms of frost-susceptibility. Frost-susceptibility index tests allow evaluation of the potential for frost heaving and thaw weakening in soils. Many classification systems are available for frost-susceptible soils, for example the U.S. Army corps of Engineers frost design and soil classification system. This index is presented in Figure 5.16, where the frost heave is indicated for different types of soil. Clay is given a frost-susceptibility classification between low and high, meaning an average rate of frost heave between 1.0 and 6.0 mm/day. This broad range of possible frost heave rates is an indication, but leaves a high uncertainty on the consequences of frost heave.

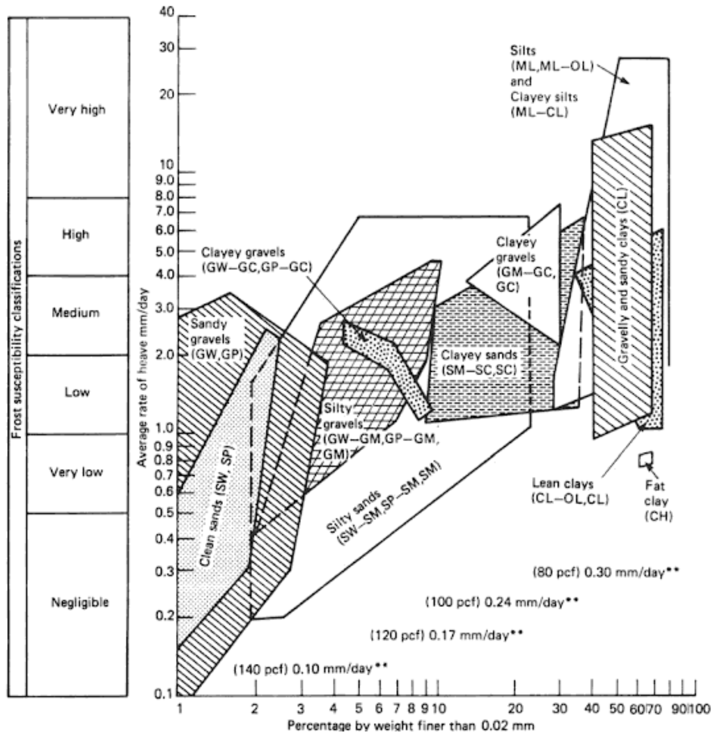

Figure 5.16: U.S. Army corps of Engineers frost design and soil classification system (Andersland & Landanyi, 2004)

5.4.2 Segregation potential

A more precise indication of the frost heave rate can be given with the segregation potential (SP). The SP value gives the relationship between the temperature gradient and the rate of water flow toward the frost front. The SP is based on an one-dimensional ground deformation model by Konrad & Morgenstern (1980). The one dimensional expansion of the soil occurs perpendicular to the frost front. The SP value can be determined with a laboratory test, after which the rate of heaving can be determined with and without extra overburden pressure:

$$h = SP * gradT \tag{5.4.1}$$

where:

h	rate of the water flow at the frost front	[m/s]
SP	segregation potential at the ice lens	[$m^2/(^oCs)$]
grad T	temperature gradient over the frozen fringe	[$^oC/m$]

and:

$$SP\ (\sigma_n) = SP_0 \ast e^{-a\sigma_n} \qquad 5.4.2$$

SP (p)	segregation potential under load (σ_n)	[m/s]
SP_0	segregation potential without extra load	[$m^2/(^oCs)$]
σ_n	stress perpendicular to the frost front	[$^oC/m$]
a	ground factor	-

The temperature gradient over the frozen fringe is taken into account in this equation, since the suction generated over the frozen fringe is the driving force for ice segregation. A simple linear analysis of the frozen fringe is assumed in this method (Figure 5.17). The temperature gradient varies from the bulk freezing temperature of water at the bottom of the fringe to the segregation temperature at the ice lens. The permeability is assumed to be constant. The suction over the frozen fringe is presented by the linear Clausius-Clapeyron equation, which was also used in the frozen and unfrozen soil model (eq. B2).

One dimensional frost heave tests have been done on BC for the Westerschelde project to determine the SP value. The SP value has been determined for different temperature gradients, from which the heave rates have been calculated with equation 5.4.1. The relationship between the rate of frost heave and the temperature is presented in Figure 5.18. The measured frost heave rates give the BC a frost-susceptibility classification between negligible and low, which is very different from the initial classification of low to high with the classification system of the U.S. Army corps of engineers. The classification system used for the Westerschelde project was the ISSMFE (1989), which also classified these frost heave rates from negligible to low. The classification systems compared the soils to one another, whether the actual frost heave is negligible or low for specific engineering problems still should be taken into consideration. Another note regarding the segregation potential is that these heave rates say little about heave in a three dimensional situation. This one dimensional test makes no distinction between soil displacements radial and axial direction relative to the freeze pipe. As discussed before, the difference between the radial and axial displacements around the freeze pipes are very significant during cross passage construction using AGF.

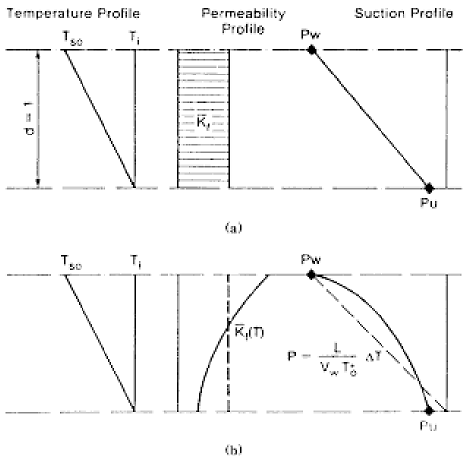

Figure 5.17: Characteristics of the frozen fringe a. Simplified by Konrad & Morgenstern (1980) b. Actual shape (Andersland & Ladanyi, 2004))

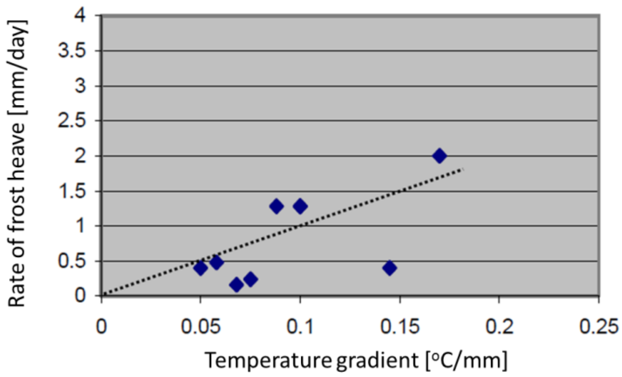

Figure 5.18: Relation between the temperature gradient and the rate of frost heave based on 1D frost heave tests on BC1 and BC2. (Report F100, 2002)

5.4.3 Three dimensional frost heave tests

For the Westerschelde project three dimensional frost heave tests were executed to obtain insight in the axial and radial deformations, which cannot be gained with SP values or one dimensional heave tests. These three dimensional heave test have also been modelled in section 4.3.3 and the test setup is given in Figure C2. The maximum strain obtained during the 3D frost heave test was 0.15% in axial direction and 2.9% in radial direction in tests with a freeze pipe temperature of -30°C. If these strains found in the laboratory are used for the situation of the cross passage and bored tunnel, an estimation can be given of the deformation of the tunnel segments:

0.15% *12000/2 = 9 mm at the east side
0.15% * 12000/2 + 2.9% *300 = 18 mm at the west side

Additional information:

- 12 000 mm = Length of the freeze pipe
- 300 mm = Distance between the tip of the freeze pipe and bored tunnel at the west side tube.

These displacement were obtained when the confining stress around the sample was 620 kPa. The stress necessary to prevent these displacements can also be calculated, with assuming a simple linear elastic relationship between the displacement and the stress. The assumption is made that the axial deformation is constant over the whole frozen body, For this simple calculation. The stiffness of the frozen body varies with temperature, therefore an equivalent stiffness is calculated. Furthermore, assumed is that the bored tunnel lining is a flat plate at the end of the frozen body, which approximates the situation where the cross passage diameter is small compared to the bored tunnel diameter (Figure 5.19). The following analytical calculation can be made to gain the stress to obstruct the displacements:

$E_{T=0}$ = 40.0 MPa
E_{inc} = 13.0 MPa/°C
$E_{quivalent} = (\sum_{i=1}^{n=37}(40 + 13 * i))/37$ = 287.0 MPa = 287 N/mm^2
$\varepsilon = \Delta L/L$ = 18 mm / 6300 mm = 2.86E-3
$\sigma = \varepsilon * E_{quivalent}$ = 521.0 * 2.86E-3 = 0.82 N/mm^2 = 820 kN/m^2

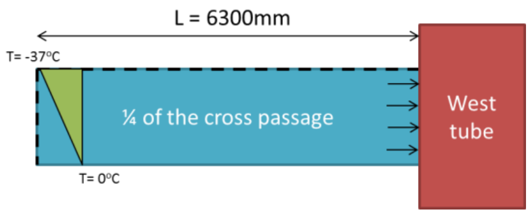

Figure 5.19: Schematization of the frost heave loads on the tunnel segments at the west tube

The extra stress necessary is 820 kN/m2, the total stress will become 620+820 = 1440 kN/m2. The linear relationship is shown in Figure 5 in blue. According to the analytical calculation, frost heave loads and deformations along the blue line are expected. The measured deformations are underestimated by the analytical calculation at the present frost heave loads. Striking is that the numerically calculated stresses are similar to the measured frost heave stresses, however the deformations are grossly overestimated. The numerical model can be used to obtain the frost heave loads imposed on the tunnel segments. The analytical calculation or another more advanced method can afterwards be used to compute the tunnel segment deformations.

One phenomenon might be overlooked up to this pointed: the friction between the freeze pipe and the soil. The axial deformations of the total triaxial cell during freezing was a contraction of 31 μm, so the upward heave soil must have sheared along the freeze pipe. In the laboratory a relative small area around the freeze pipe is frozen, consequently the shear between the freeze pipe and soil. The axial deformations of the total sample is likely to be restricted by the shearing. In reality this shear is present too, but the area frozen around the freeze pipe is much larger. Therefore, the area influenced by the shear is a small relative to the total frozen soil mass. In the numerical models the friction between freeze pipe and soil was not taken into account, contributing to the overestimation of the axial deformations.

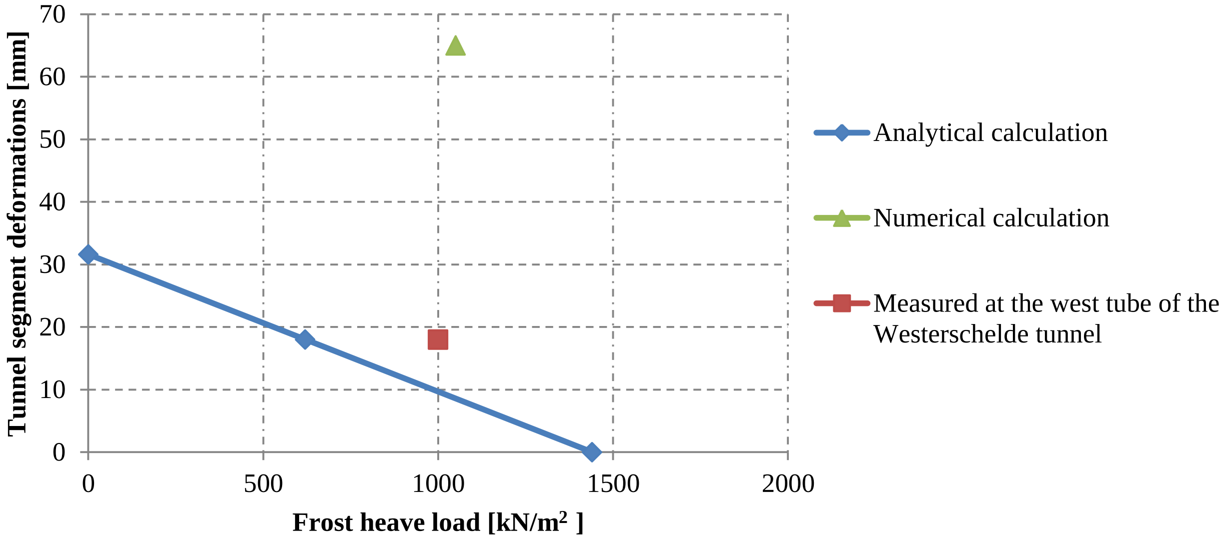

Figure 5.20: Relationship between the segment deformations and frost heave load

5.5 Conclusions of chapter 5

The third sub-question of this thesis is answered in this chapter:

> *What are the similarities and differences between modelled soil behaviour and the measured soil behaviour (stresses, pore water pressure, deformations and temperature)?*

The differences and similarities between the models and measured soil behaviour are summarized in Table 5.3 in terms of qualitative and quantitative behaviour. With qualitative behaviour is meant the ability to describe certain behaviour or phenomena regardless of their exact value of measure. Investigating qualitative behaviour gains understanding of the specific soil behaviour and trends can be discovered. The description of quantitative behaviour goes a step further, since specific soil behaviour or phenomena are described in realistic amounts.

Table 5.3: Differences and similarities between M1, M2 and measured data in the different load situation during cross passage construction with AGF.

	Model 1		**Model 2**	
	Qualitative	**Quantitative**	**Qualitative**	**Quantitative**
Load case 1: Frost heave				
Temperature				
Pore water pressures (Intern **)				
Stress (intern)				
Displacements of the tunnel segments	--	--		
Radial displacement around the frozen cylinder				
Load case 2: Enclosure of water				
Pore water pressures in the heart of frozen cylinder				
Stresses in het heart of frozen cylinder				
Displacements of the tunnel segments				
Load case 3: Excavation				
Temperature				
Stresses (Intern)				
Displacements of the tunnel segments	--	--		
Pore water pressures (Intern)				
Creep				
Load case 4: Construction of the lining				
Temperature				
Stresses (Intern)				
Displacements of the tunnel segments	--	--		
Pore water pressures (Intern)				
Creep				
Load case 5: Thawing weakening				
Temperature				
Stresses (Intern)				
Displacements of the tunnel segments	--	--		
Pore water pressures (Intern)				
Thaw settlement				

* Green cell = model is able to describe the behaviour. Red cell = model is not able to describe the behaviour. -- = behaviour cannot be evaluated. ** Intern = measured inside the frozen soil.

Similarities between the measured and calculated soil behaviour:

- *Temperature*: The temperature distribution as well as the pore water pressures at the edge of the frozen cylinder is captured equally well in both models. Only thawing takes longer.
- *Water pressures*: The water pressures at the edge of the frozen cylinder are very similar to the measured water pressures for both models at this location.
- *Soil stresses during freezing, excavation and construction of the lining*: The magnitude of the stress changes due to frost heave pressures (load situation 1) and excavation (load situation 3) are very similar to the measured stresses, especially in M2. Stress changes in radial direction are slightly underestimated for both models, while this is not the case for axial and tangential direction.

Differences between the measured and calculated soil behaviour:

- *Direction of deformation*: The deformations on the bored tunnel lining are overestimated in all construction phases.They are independent of the temperature gradient and layering of the soil, resulting in deformations more than four times larger than measured in the direction parallel to the freeze pipe. Although the magnitude of the deformation is overestimated, the response of the lining to frost heave pressures is very similar. It must be said that the deformations radial to the freeze pipes give a better approximation of the measured deformations.
- *Enclosure of water:* An increase of pore water pressure in the heart of the frozen cylinder, due to the entrapment of water was not observed (load situation 2). It seems that a build up of pressure is prevented by the deformations. In reality, the expansion of the soil is largest in the direction of the frost front while in the model the expansion is also present between the freeze pipes. The expanding soil between the freeze pipes presses the ring outward. The outward movement of the frozen ring is enough to keep the pore water pressures from building up.
- *Thaw behaviour:* Thaw behaviour in the numerical models differs from the measured data, since almost no deformations occur and stresses remain high (load situation 5). Lack of laboratory data restricts the optimisation and validation during thawing. The result is that thaw does not correspond to the measured data.
- *Time dependent behaviour*: The measured stresses show slight changes due to the influence of creep. The model is rate-independent and does not show such behaviour.

This chapter also gives an answer to the fourth and last sub-question:

Are there any unexpected phenomena noticed in the numerical models?

- *Thawing time:* the temperature distribution is better described for freezing than for thawing. The faster thawing in reality could be caused by external influences. Especially, the heat released by curing concrete can be significant. Additionally, hysterics of the SCFF curve may play a role. In reality the SCFF curve is hysteric, meaning that the unfrozen water saturation curve during freezing is not the same as during thawing. In this model the SCFF curve is the same for freezing and for thawing. When more unfrozen water would be present in the soil at lower temperatures, the temperatures could change faster.
- *Direction of deformations*: The frost heave test gives the impression that the amount of deformation is similar to the measured deformations. The ratio between the parallel and radial deformations were corrected with the solid thermal expansion coefficient, to obtain a good resemblance with the measured deformations. Calibrating the solid thermal expansion coefficient on a frost heave test may not be suitable in a larger scale model, due to different proportions of the frost heave sample and the dimensions of the frozen body.

- *Stress in axial direction*: The soil stress in axial direction i.e. the stress on the bored tunnels lining can be predicted not only qualitatively, but corresponded also qualitatively to the measured stresses. The increase in stress due to frost heave is unexpectedly well described in M1, regardless of the plain strain conditions. The numerical calculations can determine the stress changes, while the deformations of the segments of the tunnel lining can be computed with other methods (like the analytical method shown in section 5.4.3).

6 Discussion

In this chapter, the results of this thesis are discussed. In paragraph 6.1, the validation of the parameters is discussed. In paragraph 6.2, the results of the two numerical models of the cross passage 2 of the Westerschelde tunnel are discussed. Finally in paragraph 6.3, the validity of the models and the measured data are discussed.

6.1 Validation of the parameters

The parameter determination of boom clay was based on available laboratory tests, correlations and default values. All parameters can be determined with laboratory tests (Table 4.2). However the tests are not commonly executed for every project. The parameters that could be determined with laboratory tests and correlations for the Westerschelde project are the parameters that are often used in engineering practice and constitutive models. For the more difficult parameters, a default value had to be chosen because these parameters are hard to associate with specific soil behaviour. The correctness of the chosen default values is the biggest uncertainty. In order to reduce this uncertainty, the reliability of parameters was increased by optimizing them on the available laboratory tests. This process may not be as accurate as direct parameter determination from the appropriate test, but it gives the opportunity to redefine the initially chosen default values that overestimate or underestimate certain soil behaviour.

A single parameter does not necessarily control one feature of (frozen) soil behaviour, but combinations of these parameters often do. Aukenthaler(2016) and Ghoreishian Amiri et al. (2016) used different parameter sets to model specific (frozen) soil behaviour. It turned out to be a challenge to make one parameter set for an engineering problem where multiple features of the frozen soil behaviour have to be captured. This resulted in a parameter set in which compromises had to be made to capture all required soil behaviour.

The evaluation of the optimised parameters show the possibilities of the FUS model. Decreasing temperatures cause strength and stiffness increase. The increase in strength and stiffness depends on the temperature and the applied stress conditions. The results from the triaxial compression test and uniaxial compression test show that this behaviour is captured by the model. The increase in strength and stiffness also substantially depends on the unfrozen water content in the soil and thus on the relation between the unfrozen water content and temperature. Changes in the SFCC curve can cause large differences in strength and stiffness behaviour.

The volumetric expansion in the model is based on the two macroscopic phenomena of curvature-induced pre-melting and interfacial pre-melting. The interfacial pre-melting governs the volumetric increase in the plastic range, simulating the expansion due to ice segregation. No real ice lenses are simulated, only an expansion of the soil at the location where the segregation threshold is violated. In the elastic range the volumetric behaviour is controlled by the curvature induced pre-melting, a force that acts like capillary pressure and bonds the grains together. This will cause a volumetric decrease in the elastic range during freezing and a volumetric increase during thawing. The volumetric changes are governed by parameter k_s. The volumetric changes in the elastic range can be limited when selecting a small value of k_s. However, the volumetric increase is dominant when the stress state remains in the elastic range during thawing. Although these mechanisms might occur on macroscopic level, this behaviour is directly opposite of what is expected of frozen soils. The in-situ phase change of water and ice can cause a volume expansion in the soil upon freezing, while during thawing a volumetric decrease is observed. The volumetric changes due to the in-situ phase are not taken into account in this model. A volume expansion due to the in-situ phase change of water and ice can be observed in reality before ice lens formation occurs. Selecting a negative value of k_s assures a volumetric increase during freezing and volumetric decrease during thawing in the elastic range.

The direction of the deformation in reality depends on the direction of freezing and stratigraphy i.e. deformations are larger perpendicular to the temperature gradient and parallel to the layering of the soil. Although the direction of deformation is independent of the temperature gradient in the constitutive model, the direction of deformation can be influenced by changing the solid thermal expansion coefficients of the soil. By changing the solid thermal expansion coefficient in a direction parallel to the temperature gradient more shrinkage of the soil grains will be obtained in this direction, compensating for the actual deformations due to ice segregation. Using the solid thermal expansion coefficient is a means to obtain soil behaviour that cannot be simulated with the model directly.

6.2 Validation of the model results

Two 2D numerical models had to be modelled to evaluate the soil behaviour during cross passage construction with AGF, since the FUS model was not available in 3D. Both models have their possibilities and limitations. The interaction between the frozen soil and the lining of the main bored tunnels can best be evaluated in M2, an axisymmetric model in the XZ-plane. The biggest limitation is that the stress state must be constant in this axisymmetric model. The stress state in the middle of the cross passage was used. The influence of the stress state can be observed in M1, where the soil stresses and pore water pressure increase with depth. Due to plane strain conditions, strain in Z direction was assumed to be zero. Therefore M1 cannot be used to asses deformations on the lining of the main bored tunnels. Although both models have limitations, the results corresponded very well to the measured data from the Westerschelde project (apart from the lining deformations).

Both models have their own possibilities and limitations due to the assumptions and simplifications that had to be made. Surprising is how well the two model results correspond to one another. They both show the same qualitative behaviour and only quantitatively slight differences are observed. Despite the use of simple two-dimensional models, the frozen soil behaviour is captured quite well for the temperature distribution, pore water pressures and soil stresses. These results are general in agreement with the measured data. However, the calculated deformations largely deviate from the measured data and from the expected soil behaviour. Especially the deformations in axial direction are grossly overestimated. The direction of expanding is simplified by assuming an equal deformation in all directions. Therefore, the solid thermal expansion coefficient can be used to reduce the settlement parallel to the freeze pipe. The ratio between the deformations parallel and radial were corrected with the solid thermal expansion coefficient to obtain a good resemblance with the measured deformations. Calibrating the solid thermal expansion coefficient on a frost heave test may not be suitable in a larger scale model, due to different proportions of the frost heave sample and the dimensions of the frozen body. The fact that the deformations are independent of thermal gradient or layering limits the possibility to calculate reliable deformations. In addition to the lining deformations, the direction of expansion also influences the pore water pressures in the core of the frozen cylinder. No pore water pressure build up is seen, because the expansion of the soil between the freeze pipes prevents the pore water pressure build up.

It might seems strange that proper soil stresses can be obtained while the deformations are overestimated. An explanation that can be offered takes in to account the grout layer around the bored tunnel. In the model this layer has not been taken into account and soil are directly translated to the lining. In reality a grout layer is present between the bored tunnel lining and the end of the freeze pipes, which can compress more easily and reduce the soil deformations.

AGF is a 3D engineering challenge. In 2D models, many assumptions and simplifications have to be made that would not be necessary when 3D models could be made. However, in the current model the direction of deformation is the largest inaccuracy. The direction of deformation is independent of the temperature gradient and therefore the displacements on the tunnel lining are overestimated.

6.3 Validity of the measurements

The calculated data are compared to the actually measured data, as this is the best reference available. This does not mean that all measured values are exactly correct. For example, the installation of the stress monitors caused relaxation of the soil. The local stresses are disturbed and the initial measurement is not the original soil stress. Therefore the stress changes should be seen relative to the initial measurement.

In Report F100 (2002) doubts are raised about the measurements of the pore water pressures at temperatures around and below the freezing point. The pore water pressures are measured with so called vibrating wire pore water pressure monitors. The temperature dependency of the pore water pressure monitors was investigated for temperatures below $0^{o}C$ in the air in the climate chamber (report f100). In these test conditions, the monitor was almost independent of temperature. No tests were conducted in frozen soil. From the moment the soil around the instrument freezes, the oil in the filter and measuring chamber is enclosed. With decreasing temperatures, the oil and the casing shrink. When the casing shrinks harder than the oil, an increase in pressure will be registered. If it is the other way round, a decrease in pressure will occur. As soon as the temperature drops below zero, it is unknown whether the water pressures really decreased to zero (or below) or that the monitor was not able to measure water pressures. The stress monitors do not show this problem.

6.4 Conclusions of chapter 6

The most important conclusions from the discussion are listed below:

- Determination of parameters directly from soil tests is more accurate than optimizing the parameters on tests from which the parameters are not directly obtained from.
- It turned out to be a challenge to make one parameter set for an engineering problem where multiple features of the frozen soil behaviour have to be captured. Making one specific parameter set for one feature of frozen soil behaviour may give more accurate results.
- The increase in strength and stiffness also substantially depends on the unfrozen water content in the soil, thus the relation between the unfrozen water content and temperature. If optimal parameters cannot be found during calibration it could be due to the SCFF curve.
- Expansion due to frost heave is based on curvature-induced pre-melting and interfacial pre-melting. The first causes a volume decrease while the latter simulates a volume increase due to ice segregation. The expansion due to the in-situ phase change from water into ice is not part of the constitutive model.
- It is striking how well the models correspond to the measured data and to each other. The biggest deviations from the measured data are the deformations parallel to the freeze pipe, because they are independent of the temperature gradient.
- Calibrating the solid thermal expansion coefficient on a frost heave test may not be suitable in a larger scale model, due to different proportions of the frost heave sample and the dimensions of the frozen body.
- No grout layer has been modelled around the bored tunnel lining. The grout layer might reduce the settlements induced by the frozen soil.
- Both numerical models of the cross passage have assumptions and limitations. Many of these are caused by the fact that the models are 2D and not 3D. However, in the current model, this is not the largest inaccuracy. At the moment the direction of deformations due to frost heave is the biggest inconsistency in the mode.

7 Conclusions and recommendations

7.1 Conclusions

This thesis investigated the following problem statement '*Can a quantitative measure of loads due to frost actions on the bored tunnel lining be given with a numerical model, supporting the physical understanding of frozen soil.'*

Based on the physical understanding of frozen soil (chapter 2), five load situations were formulated that may occur due to frost action on the bored tunnel lining during construction with AGF (chapter 3). Four of these load cases could be qualitatively analysed with the two numerical models (Chapter 5). The enclosure of water in the heart of the frozen cylinder could not be simulated with the numerical models. On the other hand, soil stresses due to frost heave and excavation gave good a quantitative measure. In this research one case is extensively investigation, therefore this research is non-statistical. Henceforward, the conclusion cannot be drawn that this quantitative measure of frost heave stresses can also be obtained for other cases. A quantitative measure might be a step to far for now, but a qualitative measure of loads due to frost heave in construction with AGF can certainly be given with these numerical models.

The objective of the problem statement was: '*To determine if loads due to AGF may be a governing load case on the segments of a bored tunnel lining'*.

Although not all loads due to AGF could be taken into account (i.e. creep, enclosure of water in the frozen heart), one of the most important loads, frost heave, could be quantitatively defined for the BC of the Westerschelde tunnel. This load situation is worth investigation in AGF projects, since stresses can become 2.5 times higher than initially measured soil stresses. Beforehand the BC at the Westerschelde tunnel was given a frost-susceptibility index of negligible to low. Even with this mild index the stresses due to frost action increased significantly. This factor and index are probably not the same for other soil types. However, this study shows that such large stress increases are a real possibility during cross passage construction with AGF.

The following conclusions can be drawn from this research:

1. Stress changes in the soil during freezing and excavation can be calculated accurately for the studied cross passage of the Westerschelde tunnel. The stress increase due to both these load situations is approximately 2.5 times larger than the initial soil stress for both models. This number comes close the measured stress increase, which was approximately 3.0 times larger than the initially measured soil stresses.
2. The factor with which the stress changes is probably not the same for other soil types. However, this study shows that such large stress increases can occur during cross passage constructions with AGF. For other soil types the same procedure as in this thesis can be followed in order to gain an indication of the stress increase due to frost heave.
3. The frozen and unfrozen model is able to describe important features of frozen soil behaviour. For more complex numerical models, like cross passages, there are some assumptions in the model that influence capability of the model to simulate certain load situations. The fact that the deformations are independent of the temperature gradient has a major impact on the lining displacements but also on pore water pressures inside the frozen cylinder. At the moment the models are better capable of describing temperature distributions, stresses and pore water pressures at the edge of the frozen body instead of displacements.

4. The validation of the parameters against laboratory tests turned out to be crucial to obtain control of the frozen soil behaviour. With this constitutive model it is challenging to obtain a parameter set in which all frozen soil features are equally well described. The validation of the final parameter set against laboratory tests gives an indication which frozen soil behaviour is underestimated or overestimated.
5. AGF is a 3D engineering challenge. In 2D models many assumptions and simplifications have to be made that would not be necessary when 3D models could be made. However, in the current model this is not the largest inaccuracy. The direction of deformations due to frost heave is the largest inconsistency in the model.

7.2 Recommendations

Recommendations for further research are listed below:

1. The constitutive model could be improved by making the deformations dependent on the thermal gradient. The direction of deformations is crucial in cross passage construction with AGF. Not all the expected load situations could be seen due to the direction of deformations.

2. Creep has influence on the long term strength of the frozen soil. Currently, creep cannot be taken into account in the model. The evaluation of the exact influence of creep on the interaction between soil and lining is an interesting task for the future.

3. Determination of the many model parameters is a time consuming task, especially when not all laboratory tests are available to determine a parameter. It would be interesting to execute all necessary soil tests to determine complete parameter sets for different soils. The results give insight in the range and sensitivity of the model parameters for different features of frozen soil behaviour.

4. Be aware of the quantitative and qualitative behaviour the FUS model is able to describe, when using it as a AGF design tool (Table 5.3).

5. A standardized 3D frost heave test would be valuable for AGF projects, since they provide information about radial and axial displacements around the freeze pipe. Gathering more information about 3D frost deformations can even lead to a classification system or index for 3D deformations in frozen soil. That would be beneficial for all further AGF projects.

6. More measurements (Stress, deformations, temperature and pore water pressure) during AGF project would help to validate predictive methods for loads induced by frost actions. Pressure gauges on the tunnel segments like at the Shanghai Yangtze River Tunnel (section A.3) could give valuable information in further AGF projects and research.

Bibliography

Alonso, E.E, Gens, A. & Josa, A. (1990). A constitutive model for partially saturated soils. *Géotechnique 40(3)*, 405-430

Andersland, O. B., & Ladanyi, B. (2004). *Introduction to frozen ground engineering* (2nd ed.). New York, USA: Springer.

Arenson, L. U., Xia, D., Sego, D., & Biggar, K. (2005). Brine and Unfrozen Water Migration During the Freezing of Devon Silt. In K. Biggar, G. Cotta, M. Mulliek, N. Nahir, J. Buchko, A. Ho, S. Guigard. W. Gouldin (Eds.), *Prodeedings of the Fourth Biennial Workshop on Assessment and Remediation of Contaminated Sites in Artic and Cold climates* (4th ed., pp. 35-44). Edmonton, Canada: Lone Pine Publishing.

Aukenthaler, M (2016). The Frozen & Unfrozen Barcelona Basic Model, verification of a constitutive model. Master's thesis, Delft University of Technology, the Netherlands.

Aukenthaler, M., Brinkgreve, R. B. J., Haxaire, A. (2016) . A practical approach to obtain the soil freezing characteristic curve and the freezing/melting point of a soil-water system. *Proceeding GeoVancouver 2016*, Vancouver.

Azmatch, T. F., Sego, D. C., Arenson, L. U., & Biggar, K. W. (2012). New ice lens initiation condition for frost heave in fine-grained soils. *Cold Regions Science and Technology*, *82*, 8-13.

Baker, T. H. W. (1979). Strain rate effects on frozen sand. *Engineering Geology*, *13*, 223-231.

Blom, C.B.M. (2002). Design philosophy of concrete linings for tunnels in soft soils. Doctoral thesis, Delft University of Technology , The Netherlands.

Bourbonnais, J., & Ladanyi, B. (1985). The mechanical behaviour of frozen sand down to cryogenic temperatures. *International Symposium on Ground Freezing* (4^{th} ,pp. 235-244), Rotterdam, The Netherlands: Balkema.

Bragg, R.A. &Andersland, O.B. (1982) Strain rate, temperature, and sample size effects on compression and tensile properties of frozen sand. *Ground freezing 1980: Developments in Geotechnical Engineering* (pp. 34-46). Rotterdam, The Netherlands: Balkema.

Chang, D. K., & Lacy, H. S. (2008). Artificial Ground Freezing in Geotechnical Engineering. *International Conference on Case Histories in Geotechnical Engineering*, Arlington, VA.

COB. (2002). *Aanleg Dwarsverbindingen met Grondbeviezing bij de Westerscheldetunnel* (Report F100-E-02-0.79), COB.

Coté, H., Thimus, J. F., Rijkers, R., & Naakteboren, M. (2000). Soil behaviour during artificial freezing - Part 1: Frost Heaving 3D Tests. In J. F. Thimus (Red.), *ISGF2000 - Frost Action in Soils* (4e ed., pp. 69-74). Rotterdam, The Netherlands: Balkema.

Deng Y., Tang A.H., Cui Y., Nguyen X., Li X., Wouters, L. (2011). Laboratory Hydro-mechanical Characterisation of Boom Clay at Essen and Mol. *Physics and Chemistry of The Earth*, 36(17-18), 878-1890.

Gallipoli, D., D’Onza, F. & Wheeler, S.J. (2010). A Sequantial Method for Selectting Parameter Values in the Barcelona Basic Model. *Canadian Geotechnical Journal,* 47(11), 1175-1186.

Ghoreishian Amari, S. A., Grimstad, G., Kadivar, M., & Nordal, S. (2016). Constitutive model for rate-independent behaviour of frozen soils. *Canadian Geotechnical journal*, 53, 1646-1657.

Groot, A., Coffeng, P., Bulkmas, C., & Siegert, H. (2009). Dossier Verstikkingsgevaar in besloten ruimtes, Arboportaal.

Han, L., Ye, G., & Xia, X. (2016). In-situ monitoring of frost heave pressure during cross passage construction using ground freezing method. *Canadian Geotechnical journal*, *53*(3), 530-539.

Haß, H., & Schäfers, P. (2006). Application of ground freezing for underground construction in soft ground. In E. A. Kwast, K. J. Bakker, W. Broere, & A. Bezuijen (Red.), *Geotechnical Aspects of Underground Construction in Soft Soils* (5e ed., pp. 405-412). Londen, United Kingdom: Taylor & Francis.

Haynes, F.D., Karalius J. A., & Kalafut J. (1975). Strain Rate Effect on the Strength of Frozen Silt. *U.S. Army Cold Reg. Res. Eng. Lab. Res. Rep. RR 350.*

Heijboer, J., Van den Hoonaard, J., & Van de Linde, F. W. J. (2004). *The Westerschelde Tunnel: Approaching Limits*. Lisse, The Netherlands:.Balkema.

Hohmann, M. (1997). Soil freezing — the concept of soil water potential. State of the art. *Cold Regions Science and Technology*, *25*(2), 102-110.

ISSMFE(1989) Work report 1985-1989 of the technical committee on Frost TC8. *Frost in engineering* (ed. Rathmeyer, H) IS VTT94, Espoo, Finland, 15-70

Jessberger + Partners. (1998). *Westerschelde, Vereisung der Querschläge*, Kombinatie Middelplaat Westerchelde.

Johansen, O. (1975). *Thermal conductivity of soils.* Doctoral thesis, Norwegian Technical University, Norway.

Johansson, T. (2009). *Artificial Ground Freezing in Clayey Soils*. Royal Institute of Technology, Sweden.

Jones, J. S., & Brown, R. E. (1979). Design of Tunnel Support Systems using Ground Freezing. *Engineering Geology*, *13*(1-4), 375-395.

Kofoed, N., & Doran, S. R. (1996). Storebelt Eatern Railway Tunnel, Denmark - Ground freezing for tunnels and cross passages. In R.J. Mair & R.N. Taylor (Red.), *Geotechnical Aspects of Underground Construction in Soft Ground* (pp 391-398). Londen, United Kingdom: Taylor & Francis.

Konrad, J.M. & Morgenstern N.R. (1980). The Segregation Potential of a Freezing soil, *Canadian Geotechnical Journal,* 18, 482-491

Ladanyi, B & Paquin, J. (1978). Creep Behavior of Frozen Sand Under a Deep Circular Load. In D.C. Burell & D.W. Hood, *3rd International Conference on Port and Ocean Engineering Under Arctic Conditions* (3th ed., pp. 334-365), Fairbanks, USA.

Leroueil, S., Tardif, J., La Rochelle, P., & Konrad, J. M. (1991). Effects of Frost on the Mechanical Behaviour of Champlain Sea Clays. *Canadian Geotechnical Journal*, *28*(5), 690-697.

Meijers, P. (1998). *Westerschelde oeververbinding vriesbelasting op tunnellling* (Report CO-380950/11). Grondmechanica Delfr & TNO.

Liu, W.V., Apel, D.B., & Bindiganavile V.S. (2014). Thermal propertis of lightweight dry-mix shortcrete containing expanded perlite aggregate. *Coment & Concrete Composites, 53,* 44-51.

Kong, W.L. and Campbell, T.I. (1987). Thermal expansion due to an ice cap in an elevated water tank. *Canadian Journal of Civil Engineerg,14,* 519-526.

Mortier, H., & Tuunter, L. (2004). Cross Connections at Pannerdensch Canal Tunnel - Freezing soil Mass Design and Executional Comparison. *Engineering Geology for Infrastructure Planning in Europe* (pp 455-465). New York, USA: Springer

Muir Wood, D. (1991). *Soil behaviour and Critical State Soil Mechanics*. Cambridge University Press.

Nishimura, S.A., Gens, S. & Jardine, R. (2016). Thm-coupled finite element analyses of frozen soil: formulation and application. *Géotechnique 59,* 159 – 171.

O'Neill, K., & Miller, R. D. (1985). Exploration of a ridig ice model of frost heave. *Water Resources Research*, *21*(3), 281-296.

Ortiz, J., Serra, J., Oteo, C. (1986). *Curso Aplicado de Cimentaciones* (Third Edition ed.). Madrid: Colegio de Arquitectos de Madrid.

Qi, J., Vermeer, P. A., & Cheng, G. (2006). A Review of the Infuence of Freeze-thaw cycles on Soil Geotechnical properties. *Permafrost and Periglacial Processes*, *17*, 245-252.

Qi, J., Ma, W., & Song, C. (2008). Influence of Freeze-thaw on Engineering Properties of a Silty Soil. *Cold Regions Science and Technology*, *53*, 397-404.

Othman, M. A., & Benson, C. H. (1993). Effect of Freeze Thaw on the Hydraulic Conductivity and Morphology of Compacted Clay. *Canadian Geotechnical Journal*, *30*(2), 236-246.

Rempel, A. W. (2007). Formation of ice lenses and frost heave. *Journal of Geophysical Research: Earth Surface*, *112*(F2).

Rempel, A. W. (2010). Frost heave. *Journal of Glaciology*, *56*(200), 1122-1128.

Rijkers, R., Naakgeboren, M., Coté, H., & Thimus, J. F., Visschedijk, M. (2000). Soil behaviour during artificial freezing - Part 2: Application in bored tunnels. In J. F. Thimus (Red.), *ISGF2000 - Frost Action in Soils* (4e ed., pp. 69-74). Rotterdam, The Netherlands: Balkema.

Rijkers, R. H. B. (1998). *Het effect van een vries-dooi cyclus op het mechanisch gedrag van de klein van boom bij de Westerscheldetunnel* (Report NITG 98-22-B), TNO

Rijkers, R. H. B., De Lange, G., Coté, H., Thimus, J. F., Vervuurt, A. H. J. M., & Visschedijk, M. (2000). *Het vervormingsgedrag van bevroren grond* (Report NITG-99-232-B), TNO.

Rijkers, R. H. B., Hemmen, B., Naaktgeboren, N. M., & Weigl, H. (2006). In-situ frost heave loads in artificially frozen ground for tunnelling. In H. van Lottum and A. Bezuijen, *Tunnelling: A Decade of Progress(pp.* 51-60), Londen, United Kingdom: Taylor & Francis.

Sayles, F. H. (1968). Creep in frozen sands, Technical Report 190,. U.S. Army Hanover, New Hampsire.

Sayles, F. H. (1973). Triaxial and Creep Tests on Frozen Ottawa Sand. *Permafrost: North American contribution to the 2nd International Conference on Permafrost (*2th ed, pp. 984-99). Washington, USA, National Academy of Sciences.

Sayles, F.H. & D.L.Carbee (1981) Strength of Frozen Silt as Function of Ice Content and Dry Unit Weight. *Engineering geology*, *18(1-),* 55-66.

Shelman, A., Tantalla, J., Shritharan, S., Nikolaou, S., & Lacy, H. (2014). Characterization of Seasonally Frozen Soils for Seismic Design of Foundation. *Journal of Geotechnical Engineering*, *140*, 1-10.

Sheng, D., Zhang, S., Yu., Z., & Zhang, J. (2013). Assessing frost susceptibility of soils using PCHeave. *Cold Regions Science and Technology*, *95*, 27-38.

Shuster, J. A. (1981). Engineering quality assurance for construction ground freezing. *Engineering Geology*, *18*, 333-350.

Shuster, J. A. (2000). Ground freezing failures: Causes & preventions. In J. F. Thimus (Red.), *ISGF2000 - Frost Action in Soils* (4e ed., pp. 333-338). Rotterdam, The Netherlands: Balkema.

Steiner, A. (2016). The influence of Freeze-thaw Cycles on the Shear Strength of Illite Clay. Master’s thesis, Delft University of Technology, the Netherlands

Stoss, K. & Valk J. (1979). Uses and limitations of ground freezing with liquid nitrogen. *Engineering Geology*, *13*(1), 485-494

Van der Meer, T. (1999). *Dwarsverbindingen in boortunnels*. Master’s Thesis, Delft University of Technology, the Netherlands

Van der Meiden, V. (2003). *Thermisch rekenmodel voor cilindrische vrieslichamen voor de bouw van dwarsverbindingen tussen tunnelconstructies*. Master’s thesis, Delft University of Technology, the Netherlands.

Wang, Y., Wang, D., Ma, W., Wen, Z., Chen, S. & Xu, X. (2017). Laboratory Observation and Analyses of Frost Heave Progression in Clay from the Qinghai-Tibet Plateau. *Applied Thermal Engineering.* (In press)

Wettlaufer, J. S., & Worster, M. G. (2006). Premelting Dynamics. *Annual Review of Fluid Mechanics*, *38*(1), 427-452.

Wheeler, S.J., Gallipoli, D., Karstunen, M. (2002) Comments on use of the barcelona basic model for unsaturated soils. *International Journal for Numerical and Analytical Methods in Geomechanics 25(15),* 1561-1571

Zhang, L., Ma, W., Yang, C., When, Z., & Dong, S. (2016). An investigation of pore water pressure and consolidation phenomenon in the unfrozen zone during soil freezing. *Cold Regions Science and Technology*, *130*, 21-32.

Zhou, J., & Tang, Y. (2015). Artificial ground freezing of fully saturated muck clay: Thawing problem by centrifuge modelling. *Cold Regions Science and Technology*, *117*, 1-11.

APPENDIX A: CASE STUDIES

A.1 Westerschelde Tunnel

The Westerschelde tunnel consists of two 6.6 km long bored tunnels (D=11.30) with 26 cross passages one constructed at every 250 m. The cross passages were constructed with the use of AGF in 2000 and the tunnel was opened in 2003. Detailed information can be found in Report F100 (2002). This appendix gives a summary of the information that important is for this thesis.

The Westerschelde tunnel connects Zuid-Beveland and Zeeuws Vlaanderen (Figure A1). The tunnel improves the connection that in the past had to be crossed by ferry, without interrupting the shipping through the Westerschelde to and from Antwerp. Large part of the tunnel lies in boom clay (BK1 & BK2), whereas the rest of the route consists of different compositions of sand (Z1 & GZ1). Due to the depth of the tunnel water pressures up to 6.5 bar had to be overcome during construction (Figure A2).

AGF was realisd by placing 22 freeze pipes trough the main tunnel lining in an oval shape with a surface area of 6.25 m^2 (Figure A3 & Figure A4). Brine was used as a cooling medium with a temperature of approximately -36 to -38^oC. Temperature, soil stresses, water pressures and deformations were measured at cross passage 1(located in sand) and cross passage 2 (located in boom clay). The location of these cross passages in relation to the geology is shown in Figure A5.

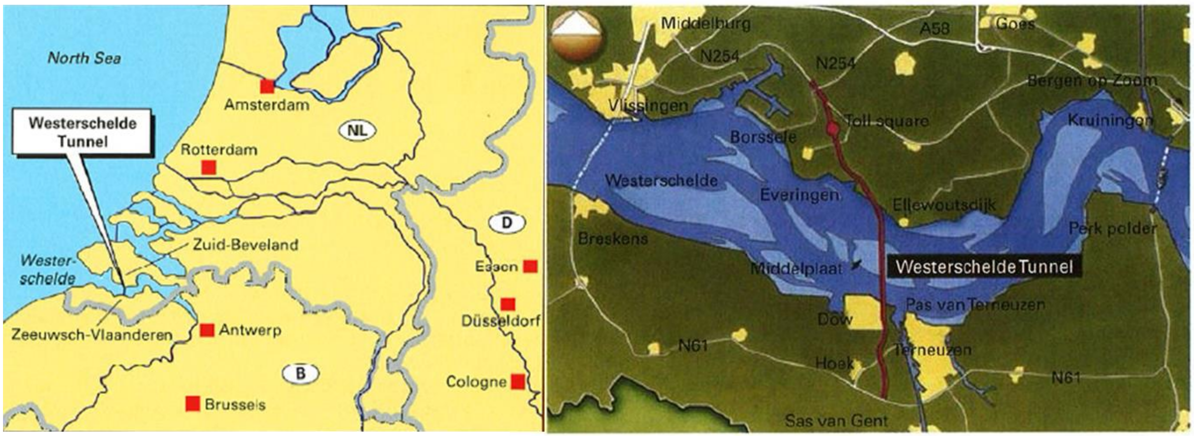

Figure A1: Location Westerschelde tunnel (Heijboer, Van den Hoonaard, & Van de Linde, 2004)

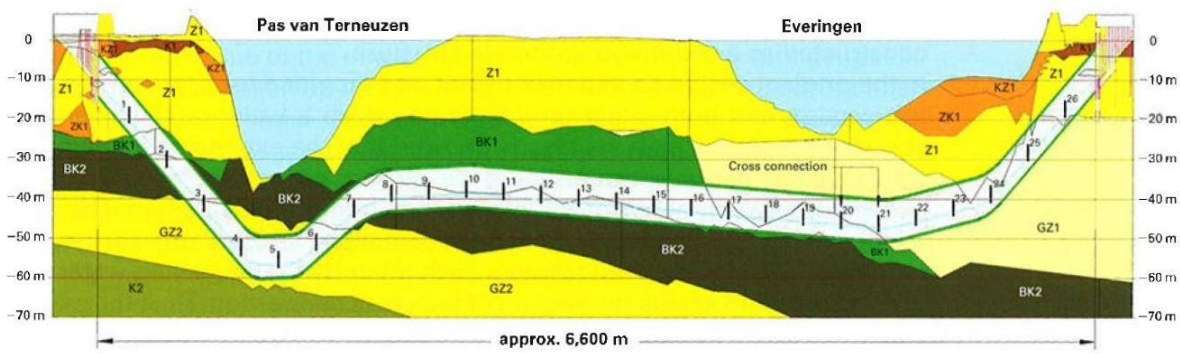

Figure A2: Soil profile Westerschelde tunnel (Heijboer, Van den Hoonaard, & Van de Linde, 2004)

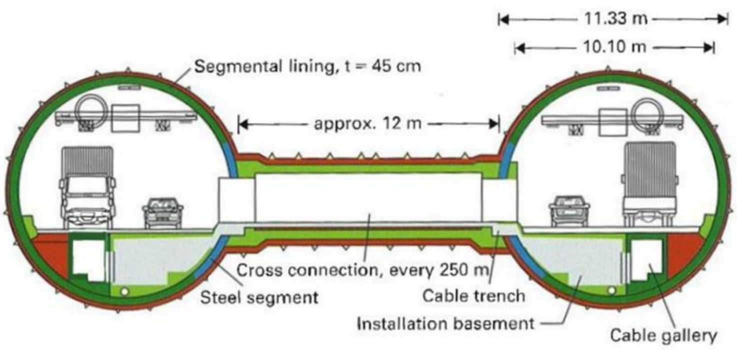

Figure A3: Cross section the cross passage

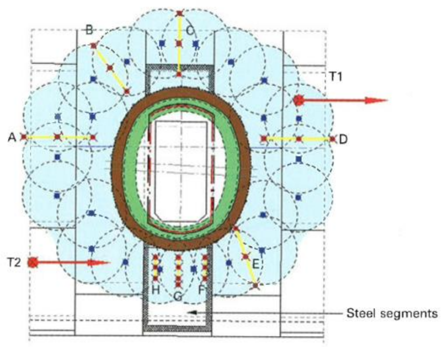

Figure A4: Frozen soil around the cross passage

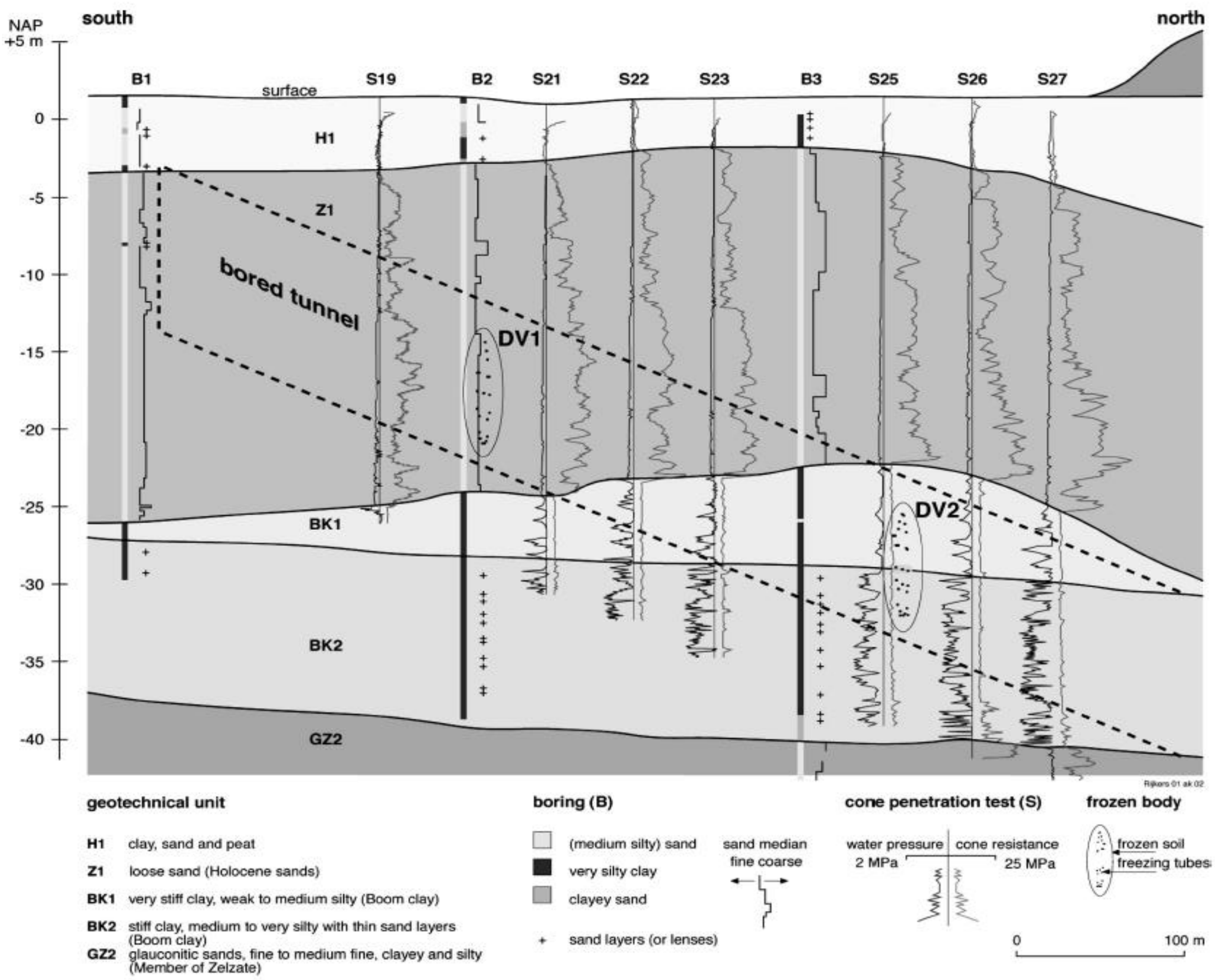

Figure A5: Soil profile with position and depth of cross passage DV1 and DV2. (Rijkers, Hemmen, Naaktgeboren, Weigl, 2006)

A1.1 Characteristics of Boom Clay

Boom clay (BC)) is part of the formation of Rupel, a marine deposit from the Oligocene. From the South-west of the Netherlands the boom clay layer dips towards Belgium in a South-East plane. The thickness of the deposit gets larger towards Belgium, where it is approximately 100 m thick. Due to erosion the thickness of the BC at the trajectory of the Westerschelde tunnel is only 4 to 40 m. The BC is considered overconsolidated since oedometer tests show a pre-consolidation stress between 1000 - 2000 kPa. Implying an over consolidation ratio between 5-10 along the tunnel trajectory(Report NITG 98-22-B).

The BC is generally very homogenous over the total deposit. Therefore is the BC at the Westerschelde is only divided in two geotechnical layers, BK1 and BK2. BK1 is the upper part of the deposit and is weak to moderately silty clay with thin sand lenses (< 2mm). BK2 is moderate to highly silty with thin sand lenses (<2mm) and locally thicker sand lances (≈0.5m). Due to the larger amount of silt and sand in BK2 the permeability is approximately a factor 10 to 100 times larger than the permeability of BK1.

Figure A6 is the salinity over the depth shown near cross passage 2. The largest salinity content can be found at the top of the frozen body in BK1 and goes to almost zero at the bottom of the frozen body in BK2. The maximum salinity will be approximately be 7000 mg/l. The freezing point depreciation can be calculated with formula 2.3.5 and comes down to 0.04 ^{o}C. Since the influence of the salt on the freezing temperature is so small, the depreciation is not taken into account in lab tests and calculations. An overview of important properties of BK1 and BK2 is given in Table A1.

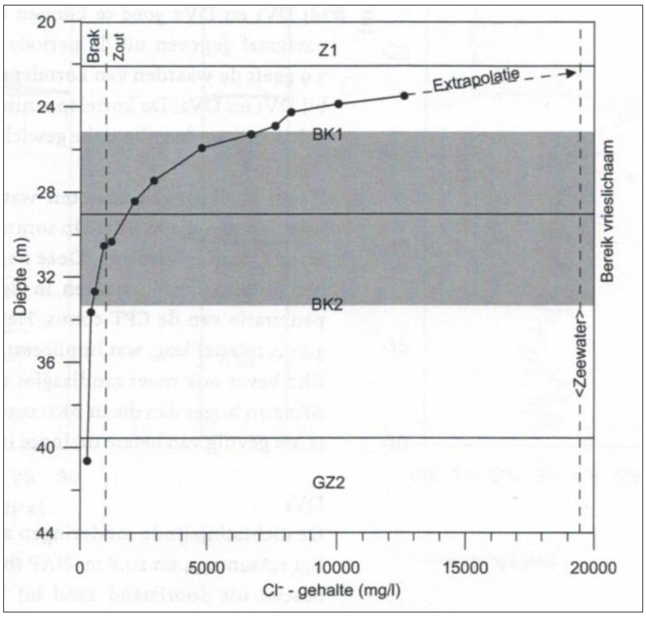

Figure A6: Salinity content at DV2 (Report F100-E-02-0.79, 2002).

Table A1: Properties boom clay (After Report F100-E-02-0.79, 2002)

Property	BK1	BK2	Unit
Lithology	silty Clay	silty Clay with sand layers	
Saturated unit weight (γ_{sat})	19.4	19.3	kN/m^3
Water content	25.3	23.8	%
Porosity (n)	~50	~50	%
Horizontal hydraulic conductivity (k_h)	1.5E-9 – 2.4E-11	-0.17E-9	
Vertical hydraulic conductivity (k_v)	2.7E-11 – 5.8E-18	-	m/s
Pre-consolidation stress	1000-2000	1000-2000	kPa
Over consolidation ratio	5-10	5-10	-
Specific heat (c_s)	920	920	J/kg/K
Thermal conductivity (λ)	1.9	1.9	W/m/K

A1.2 Monitoring at cross passage 2

Various monitors have been placed in the ground before the construction of the cross passage started. Table A1gives an overview of the different monitors and what they measured. The locations of the monitors relative to the bored tunnels and cross passage are visualised in Figure A5, Figure A7, Figure A8, Figure A9. The exact coordinates of the monitors can be found in Report F100-E-02-0.79, 2002.

Spade cells are 1D stress monitors and stress monitoring stations are 3D stress monitors. It is important to realise that the initial measured stresses do not represent the original vertical and horizontal soil stresses, because the installation locally changes the stresses in the soil. The installation of the spade cells and stress monitors results in respectively a stress increase due to soil displacements and a stress decrease due to relaxation of the soil. Therefore the stresses should be seen relative to the initial measurement.

Table A2: Overview monitor types at cross passage 2.

Type monitor	Units	Abbreviation	Accuracy
Inclinometer		HE2/ HE4	0.25mm/m
- Horizontal movements	mm		
Extensometers		EX2/EX4	0.2 mm
- Vertical movements	mm		
Temperature sensors	^oC	TE2	0.1 ^oC
Spade cell		SC5, SC6, SC7, SC8	2 kPa
- Total horizontal soil stress	kN/m^2		
- Temperature	^oC		
Stress monitoring station		SM3, SM4	2 kPa
- Total soil stress	kN/m^2		
- Water pressure	kN/m^2		
- Temperature	^oC		
Water pressure	kN/m^2	VW3, VW4	0.5 kPa

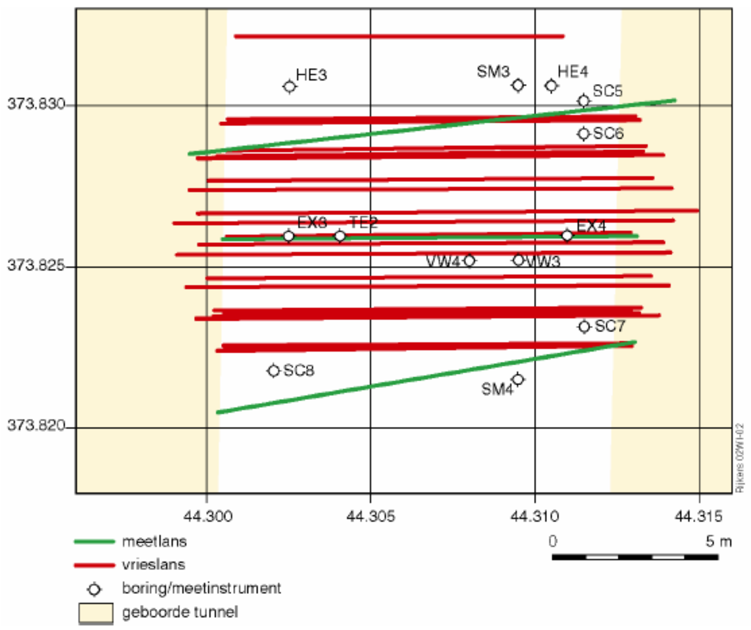

Figure A7: Top view location freeze pipes (red), measuring rods(green) and monitors

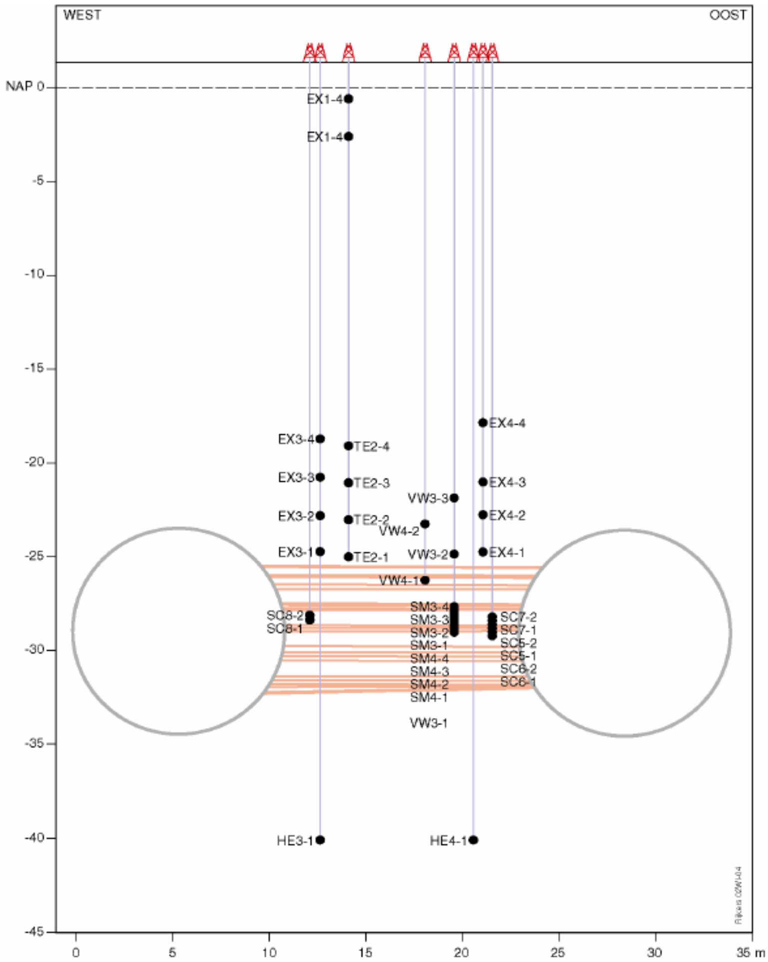

Figure A8: Side view location freeze pipes (red) and monitors

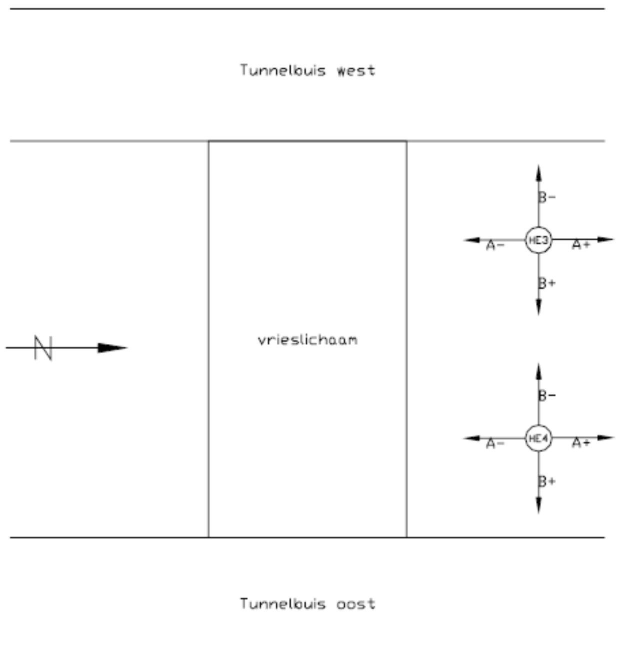

Figure A9: Location of the inclinometers at cross passage 2 and the direction of measurements.

A.2 Pannerdensch Canal tunnel

The Pannerdensch Canal tunnel is the third bored tunnel in the Betuwe route, the traffic connection between the North Sea and German border. Construction took place between 2000 and 2004 and the tunnel has a length of 2700 m. For the construction of two cross connections AGF was used. AGF was used in the first cross passage to make a connection between a previous sunken shaft and the two tunnel tubes (Figure A10). In the second cross passage AGF was used to make a temporary load barring structure between the north and south tube (Figure A12). Liquid nitrogen with a temperature of-196 ^{o}C was used to freeze the soil. 36 freeze pipes were placed in the shaft and an extra 4 extra to install thermocouples. Freezing with liquid nitrogen took approximately 9 to14 days. Using semi-empirical methods the necessary thickness of the ice varied between 0.560 m to 0.950 m. Eventually a thickness of 0.9 m at a temperature of -20^{o}C was chosen to use at the first cross and a thickness of 0.7 m at a temperature of -10^{o}C at the second cross passage. In the end it took only 7 days to acquire a wall thickness of 1.40m. Mortier & Tuunter (2004) described the design and construction of the Pannerdensch canal tunnel.

Excavation started at cross passage 1 (CP1) at the shaft with an opening of 140x240 cm^2. At cross passage 2 (CP2), excavations started at the south tube. Because of freezing with liquid nitrogen, the soil was very stiff and hard to excavate. Risk of excessive deformation of the tunnel lining of the main tubes during excavation of the soil body was considered to be high. Therefore strutting systems were designed to avoid excessive deformations of the tunnel lining. At CP 1, struts inside the future cross passage were applied between the tunnel lining and shaft (Figure A11). Near CP 2 pre-stressed steel rings were applied (Figure A13). Pre-stressing the rings up to a level that the longitudinal joints between the segments nearly opened gave the certainty that all forces went into the steel rings.

After excavation, a temporary lining of 200 mm shotcrete was used at CP1 and 145 mm at CP2. An attempt was made to spray the shotcrete directly against the frozen wall at CP1, however approximately 75% fell off. Lack of space due to internal struts made it necessary to install the final lining at CP1 in three phases and at CP2 in two phases. Insulation and lattice girders were necessary for the concrete to stick to the wall. The lining at the opposite side of the cross passage was opened after placement of the final lining.

The soil at the first cross passage was silty with characteristic strengths of 1.87 to 3.40 MPa, for temperature ranging between -10^{o}C to -20^{o}C. At the second cross passage, the strength values ranged from 2.50 to 4.35 MPa for a fine to medium sand in the same temperature range. The strength of the frozen mass that was taken into consideration was the long term strength of the frozen soil. The long term strength was taken into account since ice deforms at low stress and transfers its stress to the soil skeleton up to the limit of its frictional resistance. Therefore, the short term (high) strength due to the cohesive strength of the ice matrix was not considered but divided by 2.0 to obtain the long term strength. Over this reduced strength, a safety factor of 1.5 was used to obtain the characteristic strength. The assumption was made that the long-term elastic modulus was approximately 145 MPa for every load case.

The displacements of the tube diameters were also measured during construction of the cross passage. The horizontal diameter increased 7-9 mm, while the vertical diameter decreased 6-8 mm. So, a horizontal ovalisation developed due to artificial ground freezing. The differential displacements between two adjacent rings was 4 – 6 mm This was below the required value of 10 mm. The change in distance between the two tubes differs from 3 mm at CP1 to 9 mm at CP2. This can be explained by the difference in excavation. At CP1 excavation started at the shaft and the tunnel lining was opened after the final lining was finished. This opportunity was not present at CP2 and the southern tube lining was opening to excavate the cross passage.

The compression forces and bending moments in the strutting systems were monitored with strain gauges at CP1. The measured forces and moments were 20 to 80% smaller than the calculated forces. At CP2 axial forces in the ring were far below the calculated ones and the forces in the three inner struts was equal to zero.

All these safety factors, creep effects and not taking into account the possibility of arching resulted in a very conservative design for the frozen body especially with the requirement that all along the ice wall a minimum temperature had to be reached. This led to an ice wall thickness of almost twice the calculated thickness.

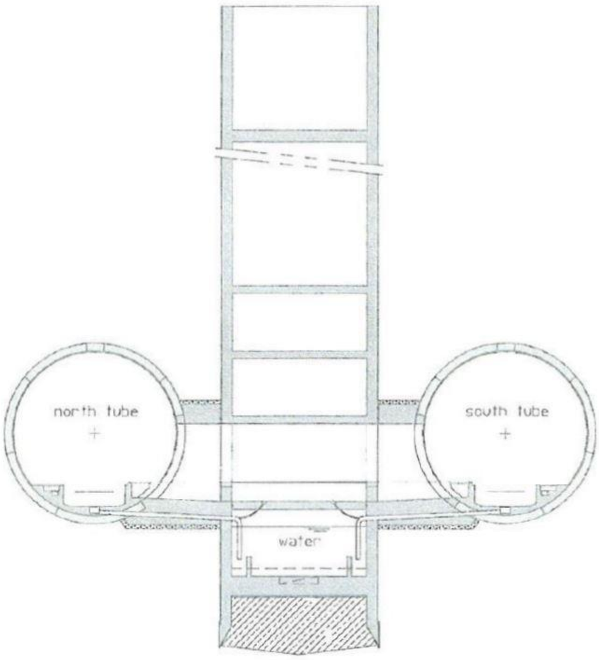

Figure A10: Cross passage 1 (Mortier & Tuunter, 2004)

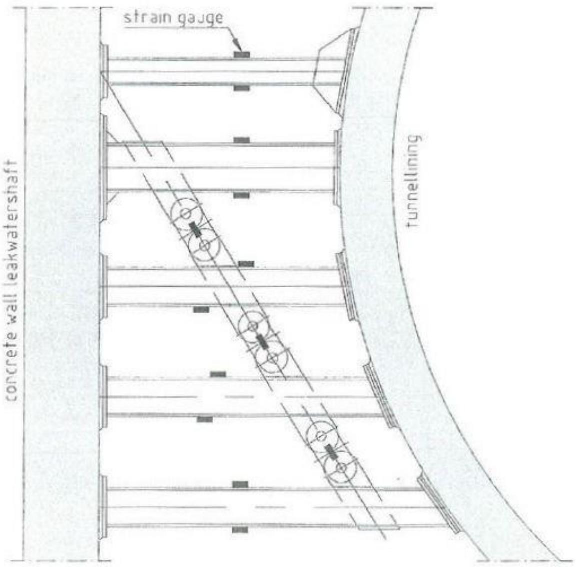

Figure A11: Steel struts at cross passage 1 (Mortier & Tuunter, 2004)

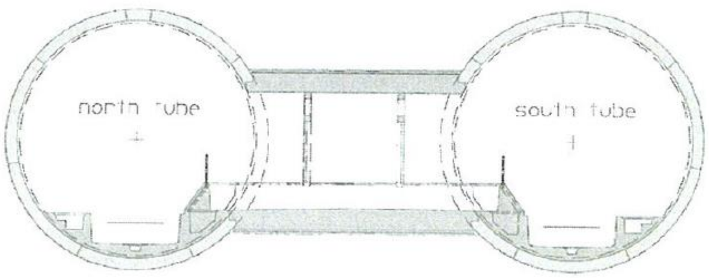

‘

Figure A12: Cross passage 2 (Mortier & Tuunter, 2004)

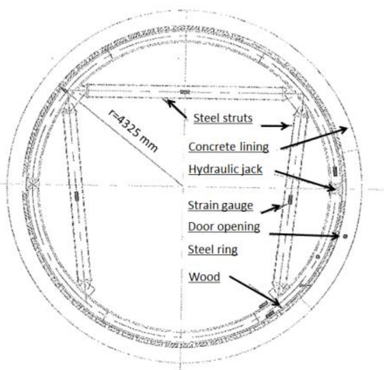

Figure A13: Strutting system at cross passage 2. (Mortier & Tuunter, 2004)

A.2 Bothnia line

Johansson (2009) did extensive research regarding AGF in clay soil and had the possibility to do research at the AGF site of the Bothnia line. The Bothnia line is a single track railway tunnel constructed near Stranneberget, Sweden. Most of the tunnel goes through rock and is built with shotcrete and rock bolts. A length of 100 m goes through clay and AGF is used as construction method (Figure A14). Effects of ground freezing were investigated by many in situ measurements of temperature, stress on tunnel roof and deformations of the ground surface.

Indirect freezing with brine at -35°C was used to cool the soil for 90 days. The freeze pipe configuration can be seen in Figure A15. The frozen body was designed to be an arch of 3m out of the tunnel contour with an average temperature of -15°C. The soil inside the frozen arch was frozen and the tunnel was excavated the same as the rock part of the tunnel, with drill and blast.

Special are the measurements of the load-cells on the tunnel roof upon thawing. During thawing, the frozen soil changes from a load bearing structure to a load on the tunnel roof. Not much is known about how the load is building up gradually, stepwise or something in between. The expected total load on the tunnel roof is the overlaying soil with pore water pressures. Thawing already starts during excavation, since convection is possible between the relative warm air in the tunnel and the inside of the frozen arch. Complete thawing of the soil above the tunnel takes over a year (Figure A16). Temperatures of -0.5°C were even measured after four years of stopping the freezing process. In the first year the largest temperature increase is encountered and the largest pressure built up. In later years the pressure is gradually increasing (Figure A17).

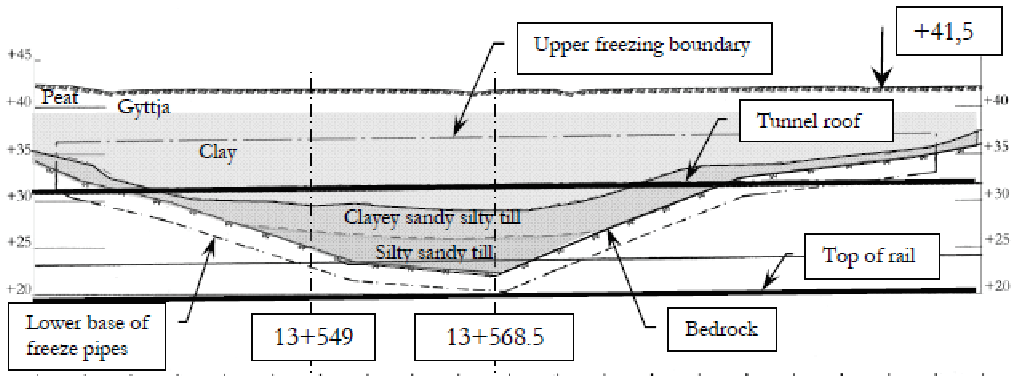

Figure A14: Alignment of the Bothnia line through clay. (Johansson, 2009)

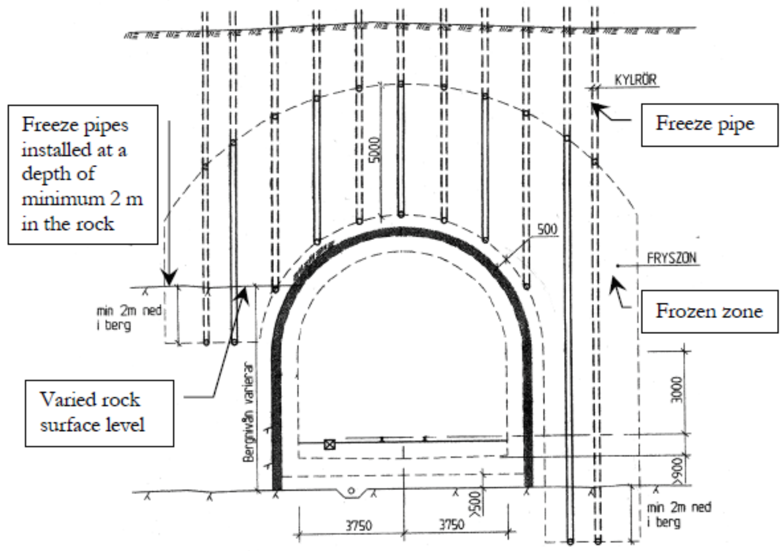

Figure A15: Freeze pipe configuration Bothnia line (Johansson, 2009).

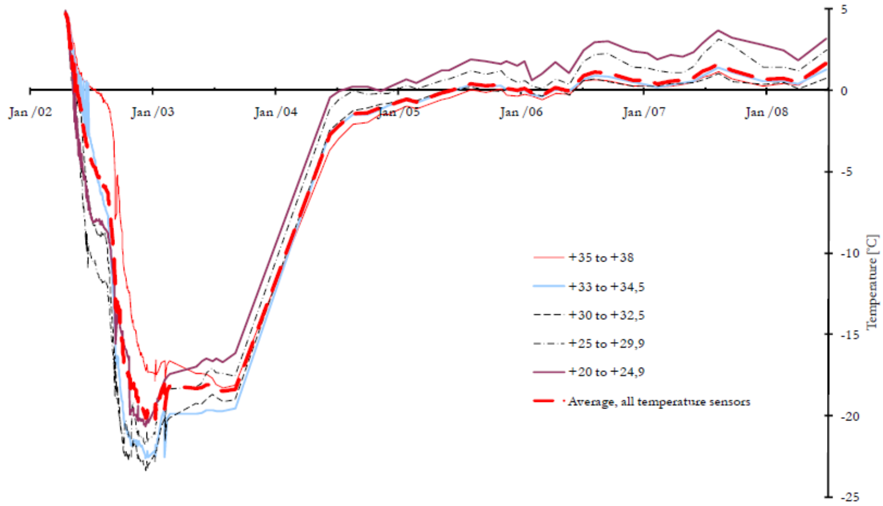

Figure A16: Temperature on top of the tunnel roof

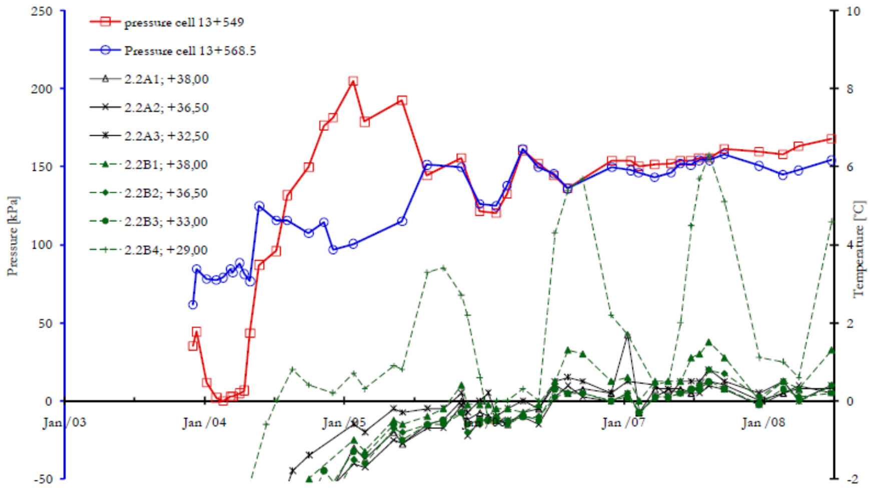

Figure A17: Pressure built up on tunnel roof at the Bothnia line relative to the temperature. (Johansson, 2009). Temperature control pipes (2.2&2.3) are located approximately 2m. south of the tunnel center.

A.3 Shanghai Yangtze River tunnel

The Shanghai Yangtze River Tunnel is one of the largest bored tunnels in the world with an external diameter of 15.0m. The eight cross passages are constructed with artificial ground freezing in silty clay. A steel lining is used for the bored tunnel at the positions at the cross passages instead of concrete. The distance between the tunnel tubes is approximately 15m and the frozen wall is designed with a thickness of 2.7 m (Figure A18). The average temperature of the frozen ring was chosen to be -15°C. In order to obtain this frozen body, freeze pipes were placed from both tunnel tubes in a fan shape (Figure A19). During the construction of the Yangtze river tunnel, frost heave pressures could be measured on the tunnel lining, with a pad type pressure gauge. The deformations of the tunnel lining and the temperature changes could be measured as well. Han, Ye & Xia (2016) analysed the monitoring data.

Figure A20a shows the heave pressures of the lining in different construction stages, freezing, excavation, construction of the lining and during thawing. The different lines correspond to different pressure gauges on the segments. These can be seen in Figure A20, together with the distribution of the heave pressures around the frozen cylinder. During the first freezing period almost all pressures in the gauges increased before decreasing almost to zero. During excavation and construction of the cross passage pressures remained approximately stable. They started increasing again when freezing stopped, but did not reach the initial pressures. It is noteworthy that although the frozen cylinder is circular, the pressure distribution is not completely circular.

The frost heave pressures were much lower than at the inside of the frozen soil measured in previous studies. Han et al. (2016) gave three possible explanations for the difference. Firstly, he suggested that water migrated to the middle of the tunnel, since there is where freezing occurs sooner than near the tunnels. The soil remains warmer near the segments, because of heat dissipation (Figure A22). Thus, the water near the segments migrates to the central part as shown in Figure A23. Frost heave near the segments is reduced as well as the pressures. Secondly, he suggested that the ground reacting pressure to the tunnel is relatively small in soft ground and the tunnel moves laterally. This may also release pressure. The third reason he gave is that during construction measures were taken to reduce frost heave pressure. Two holes were made in the steel segments to release earth pressure. They were opened during periods of the freezing process.

Besides the frost heave measures, deformations were measured. Figure A24 shows the cross-sectional deformations relative to the construction stages. Deformations slowly change in the early stage of freezing and remain approximately stable afterwards. During freezing an ovalisation can be observed, since a horizontal extension (max 4mm) and vertical shrinkage (max 5 mm) are measured. This matches with the pressures that are seen on the segments.

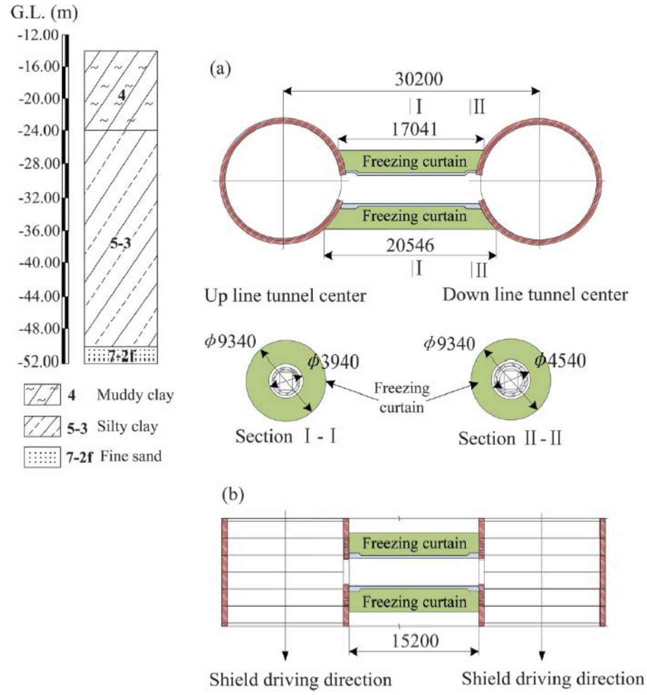

Figure A18: Cross passage at the Shanghai Yangtze River Tunnel. (Han et al., 2016)

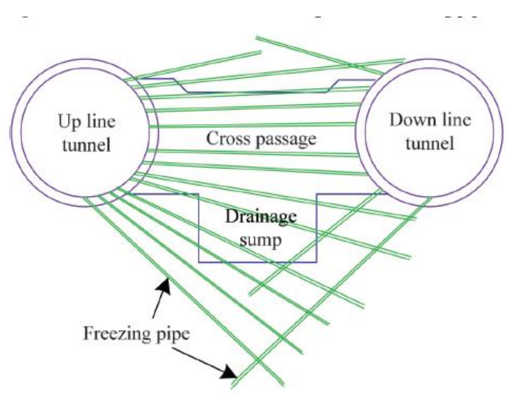

Figure A19: Freeze pipe configuration at the Shanghai Yangtze River Tunnel. . (Han et al., 2016)

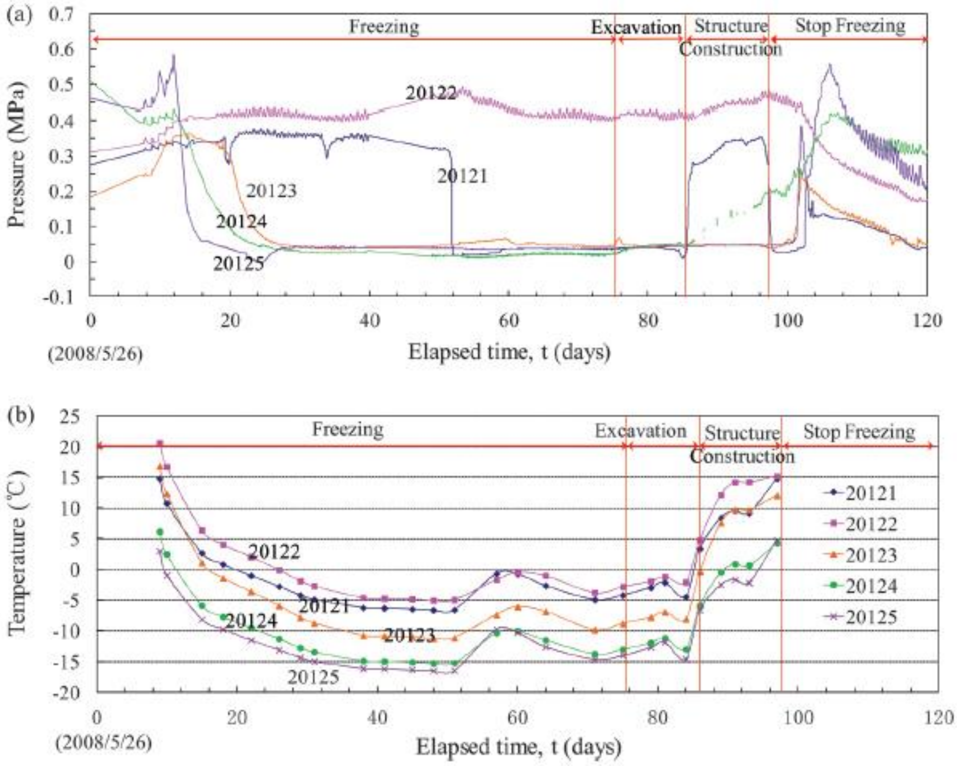

Figure A20: Timeline of (a) heave pressure measurements (b) temperature. . (Han et al., 2016)

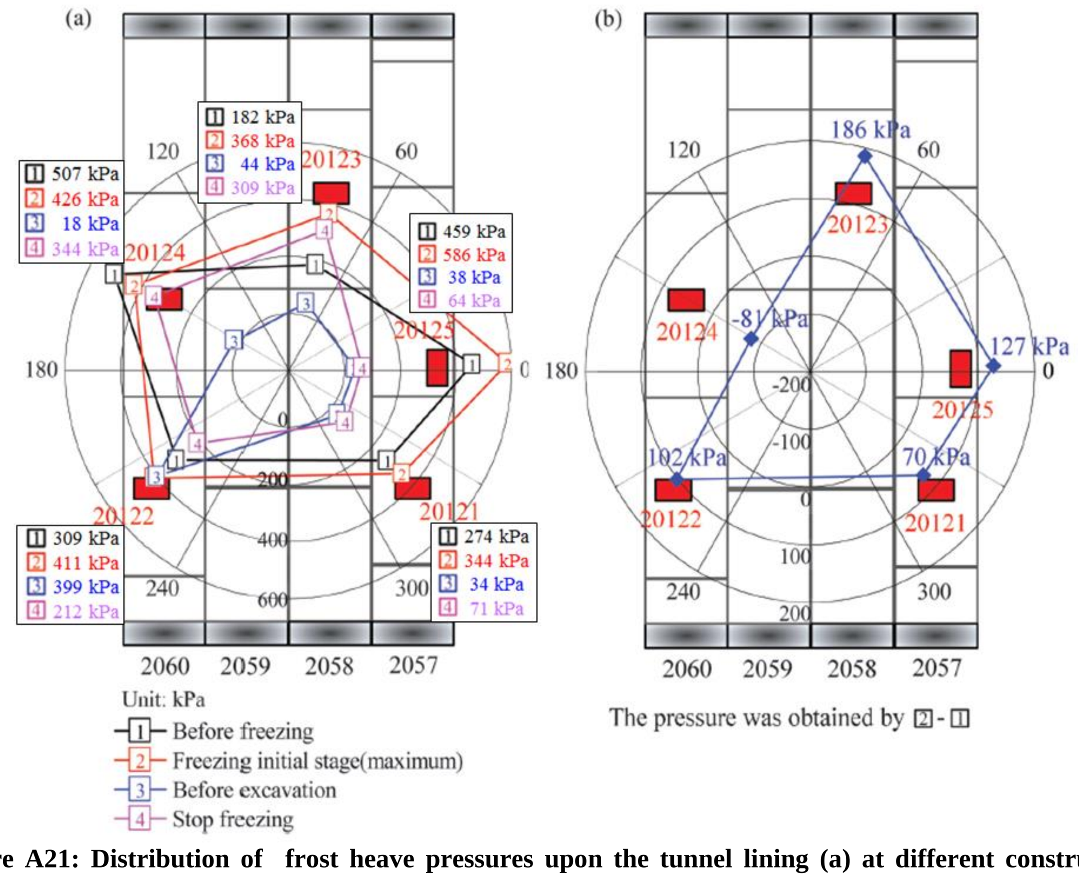

Figure A21: Distribution of frost heave pressures upon the tunnel lining (a) at different construction stages and (b) the largest pressure measured. . (After Han et al., 2016)

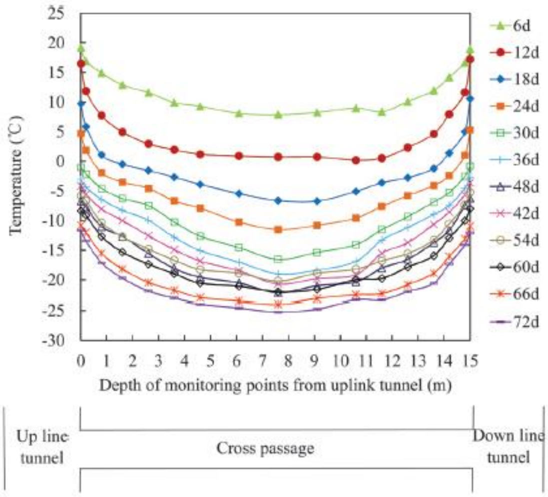

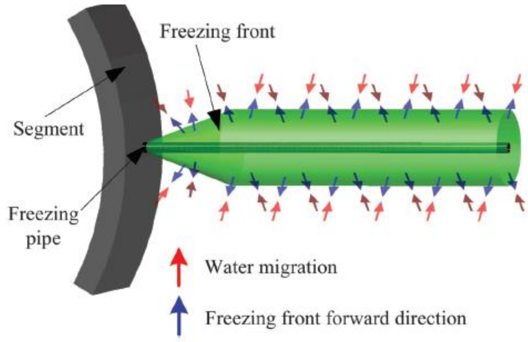

Figure A22: Temperature distribution over the length of the cross pasage

Figure A23: Water migration in the early stage of freezing

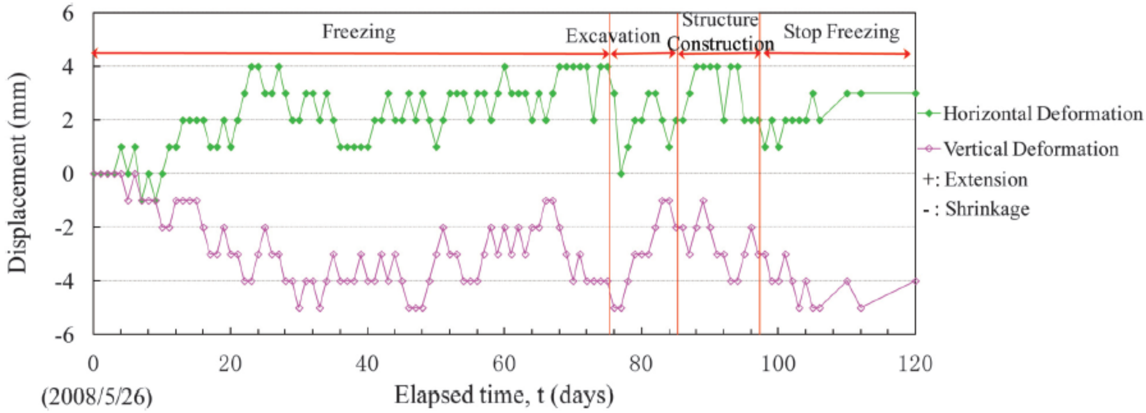

Figure A24: Cross-sectional deformation of the up line tunnel in time.

APPENDIX B: THE FROZEN AND UNFROZEN SOIL MODEL

The main concepts of the frozen and unfrozen soil (FUS) model are summarised in this appendix. This constitutive model for rate-independent behaviour of saturated frozen and unfrozen soil is developed by Ghoreishian Amiri et al. (2016). The summary is based on their work and the description of the model by Aukenthaler (2016), Alonso, Gens & Josa (1990), Wheeler, Gallipoli & Karstunen (2002) and Gallipoli, D'Onza & Wheeler (2010).

The FUS model is based on the Barcelona Basic model (BBM), which is a soil model for saturated and unsaturated soils. An unsaturated soil has an increased strength and stiffness due to suction. The FUS works in a similar way, because an increase in cryogenic suction with decreasing temperatures causes the (frozen) soil to become stiffer and stronger. The BBM also describes volume changes due to changes in suction, which is convenient for the expansion of frozen soils. The FUS model is capable of describing the mechanical behaviour of saturated soils as function of temperature, thus also the transition between frozen and unfrozen soils. In case the suction becomes zero, the BBM adapts to the behaviour of the modified cam clay model. The FUS model uses two stress-state variables; the solid phase stress and cryogenic suction. Throughout this whole appendix compression is positive and suction is negative. The solid phase refers to the soil grains and ice. Consequently, the pores contain only water. The solid phase stress tensor(σ^*) is expressed as:

$$\sigma^* = \sigma - S_{uw} p_w I \qquad B.1$$

where σ is total stress, S_{uw} the unfrozen water content, p_w water pressure and I denotes the unit-tensor. The ice is able to bear shear stresses, just as the soil grains. The formulation of stress is based on a Bishop single effective stress, where the S_{uw} is used as the effective stress parameter or Bishop's parameter. The effect of the unfrozen water content is taken into account on the mechanical behaviour through the solid phase stress. A hydro-mechanical coupling can be made with the cryogenic suction as second state variable. The cryogenic suction (s_c) is defined as the difference between water pressure and ice pressure (p_{ice}) and can estimated with the Clausius-Clapeyron equation:

$$s_c = p_w - p_{ice} \approx -\rho_{ice} L_w \frac{T}{T_f} \qquad B.2$$

where ρ_{ice} is the density of ice, L_w is the latent heat of water, T is the current temperature and T_f is the freeze/melt temperature at the given pressure. When the constants in this formula are filled in equation B.2 gives a linear increase in cryogenic suction with decreasing temperatures (Figure B1). The strain increments are composed of the elastic and plastic part of the solid phase stress ($d\varepsilon^{me}$ and $d\varepsilon^{mp}$) and the cryogenic suction ($d\varepsilon^{se}$ and $d\varepsilon^{sp}$)

$$d\varepsilon = d\varepsilon^{me} + d\varepsilon^{se} + d\varepsilon^{mp} + d\varepsilon^{sp} \qquad B.3$$

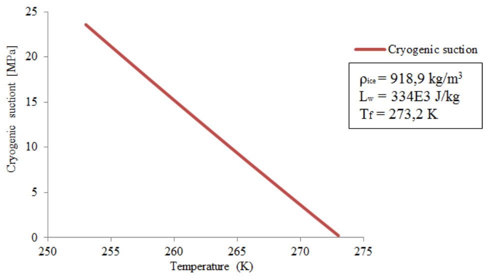

Figure B1: Cryogenic suction variation over temperature

B.1. Elastic strains

The elastic part of the strains to due variations in solid phase stress can be calculated based on the equivalent parameters of the mixture:

$$G = (1 - S_{ice})G_0 + \frac{S_{ice}E_f}{2(1+2v_f)} \qquad B.4$$

$$K = (1 - S_{ice})\frac{(1+e)p^*_{y0}}{\kappa_0} + \frac{S_{ice}E_f}{2(1-2v_f)} \qquad B.5$$

$$S_{ice} = 1 - S_{uw} \qquad B.6$$

where G en K are the equivalent shear modulus and bulk modulus of the mixture, S_{ice} is the ice saturation , e is the void ratio. G_0 and κ_0 stand for the shear modulus and compressibility coefficient of the soil in unfrozen and state. E_f and v_f are Young's modulus and poisons ratio in fully frozen state. P^*_{y0} is the pre-consolidation stress for unfrozen conditions. The stiffness of frozen soil increases with decreasing temperatures, the amount the Young's modulus increases depends on the factor $E_{f,ref}$. A linear equation is adopted for the frozen Young's modulus with decreases temperatures:

$$E_f = E_{f,ref} - E_{f,inc}(T - T_{ref}) \qquad B.7$$

The elastic part of strain due to suction variation and solid phase stress variation can be calculated with the following expressions:

$$d\varepsilon^{se} = \frac{k_s}{3(1-e)}\frac{ds_c}{s_c - p_{at}} - \qquad B.8$$

where κ_s is the compressibility coefficient due to suction variation within the elastic region, p_{at} is the atmospheric pressure and κ is the elastic compressibility coefficient of the soil mixture. The volumetric and shear elastic components of strain can be written as:

$$d\varepsilon^e_v = \frac{1}{K}dp^* \frac{k_s}{3(1-e)}\frac{ds_c}{s_c - p_{at}} \qquad B.9$$

$$d\varepsilon^e_q = \frac{1}{3G}dq^* \qquad B.10$$

where dp^* is the change in solid phase mean stress and dq^* is the change in solid phase deviatoric stress.

B.2 Yield surfaces

At temperatures above zero, the cryogenic suction equals zero and soil behaviour is defined by the modified Cam-clay model. In a frozen state there are two yield functions dependent on the cryogenic suction originating from the BBM. The LC yield surface due to variation of solid phase stress is described as:

$$F_1 = (p^* + k_t s_c)\left[(p^* + k_t + s_c){S_{uw}}^m - \left(p^*_y + k_t s_c\right)\right] + \frac{(q^*)^2}{M^2} = 0 \qquad B.11$$

where

$$p^*_y = p^*_c\left(\frac{p^*_{y0}}{p^*_c}\right)^{\frac{\lambda_0 - \kappa}{\lambda - \kappa}} \qquad B.12$$

$$\lambda(s_c) = \lambda_0[(1-r)\exp(-\beta s_c) + r] \qquad B.13$$

$$\kappa = \frac{1+e}{K} p_{y0}^{*} \qquad B.14$$

and p^* is the solid phase mean stress, q^* in the solid phase deviatoric stress, M is the slope of the critical state line, k_t parameter describing the increase in apparent cohesion with cryogenic suction, p_c^* is the critical stress, m is the yield parameter, λ_0 is the compressibility coefficient for the unfrozen state along the virgin loading, ß is a parameter controlling the rate of change in soil stiffness with suction. The yield parameter (m) influences the strength of the ice in the pores, should the ice behave like ice rubble or like pure ice. Ice rubble (m=0) can only yield upon shearing and pure ice can also yield during isotropic compression (m=1.0).

Cryogenic suction leads also to grain segregation and the formation of ice lenses. The second suction dependent yield criterion is the grain segregation (GS) yield criterion:

$$F_2 = s_c - s_{c,seg} = 0 \qquad B.15$$

where $s_{c,seg}$ is the threshold value of suction for ice segregation phenomenon and bounds the transition from the elastic to the virgin range when cryogenic suction is increased. The three dimensional yield surface is shown in Figure B2.

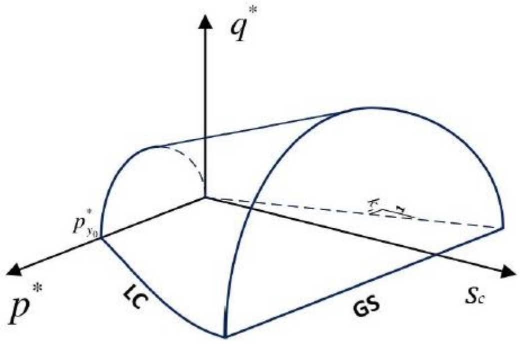

Figure B2: Three-dimensional view of the yield surface in the p*-q-sc space. (Ghoreishian Amiri et al.,2016)

B.3 Strain hardening

The FUS model uses coupled hardening rules. This way the LC yield surface can move outward when soil becomes stiffer during plastic compression. The GS yield surface shifts downward when plastic compression is encountered, since the pore space becomes smaller and ice segregation threshold value gets lower (Figure B3). The GS yield surface shifts upward when plastic dilation due to ice segregation occurs. This results in softer behaviour and an inward movement of the LC curve is taken into account (Figure B4). The two yield surfaces are coupled by the total plastic volumetric strain of the solid phase stress ($d\varepsilon_v^{mp}$) and the cryogenic suction ($d\varepsilon_v^{sp}$):

$$d\varepsilon_v^p = d\varepsilon_v^{mp} + d\varepsilon_v^{sp} \qquad B.16$$

Where

$$d\varepsilon_v^{mp} = \frac{\lambda_0 + \kappa}{(1-e)} \frac{dp_{y0}^*}{p_{y0}^*} \qquad B.17$$

$$d\varepsilon_v^{sp} = \frac{-\lambda_s + \kappa_s}{(1-e)} \frac{ds_{seg}}{s_{seg} + p_{at}} \qquad B.18$$

Combining equation B.17 with B.12 gives the hardening rule adopted for the LC yield surface:

$$\frac{dp_{y0}^*}{p_{y0}^*} = \frac{1-e}{\lambda_0 - \kappa_0} d\varepsilon_v^{mp} + \frac{1-e}{\lambda_0 - \kappa_0} d\varepsilon_v^{sp} \qquad B.19$$

Assuming a similar effect for the plastic formation due to variation in suction and taking into account equation B.18. The hardening rule for the GS yield surface becomes:

$$\frac{ds_{c,seg}}{s_{c,seg}+p_{at}} = -\frac{1+e}{(\lambda_s+\kappa_s)}d\varepsilon_v^{sp} - \frac{1+e}{(\lambda_s+\kappa_s)}d\varepsilon_v^{mp} \qquad B.20$$

The hardening rule for the GS yield surface is based on equation B.20, but adapted to take into account the unfrozen water content. The hardening rule takes into account the unfrozen water saturation. The lower the unfrozen water saturation, the lower the permeability for water to be sucked in, the smaller the strain due to increase of cryogenic suction. Thus, the resistance against plastic strains increases with a decreasing unfrozen water content. Furthermore, when suction increases and grain segregation starts to occur, the effect of plastic deformation due to mechanical loading becomes. relatively small to the effect of plastic deformation due to ice segregation. Taking this into account the hardening rule of the GS yield surface becomes:

$$\frac{ds_{c,seg}}{s_{c,seg}+p_{at}} = -\frac{1+e}{S_{uw}(\lambda_s+\kappa_s)}d\varepsilon_v^{sp} - \frac{1+e}{(\lambda_s+\kappa_s)}(1-\frac{s_c}{s_{c,seg}})d\varepsilon_v^{mp} \qquad B.21$$

where λ_s is the elastoplastic compressibility coefficient for suction variation.

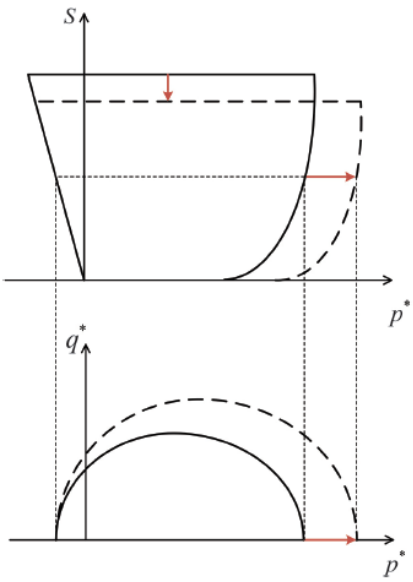

Figure B3: Evolution of yield surfaces due to plastic compression (Ghoreishian Amiri et al., 2016).

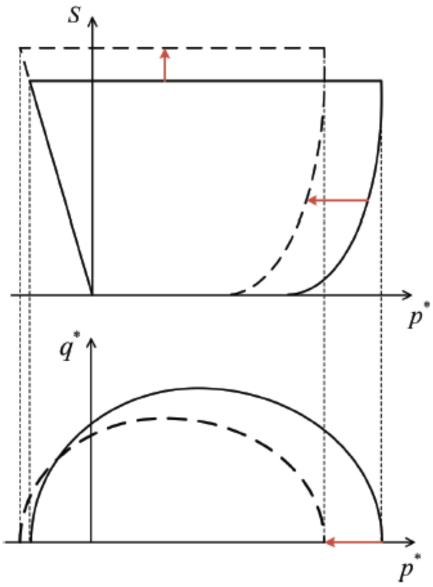

Figure B4: Evolution of yield surfaces due to ice segregation phenomenon (Ghoreishian Amiri et al., 2016).

B.4 Flow rules

The flow rule for the LC yield surface is non-associated expressed as:

$$d\varepsilon^{mp} = d\lambda_1\frac{\partial Q^1}{\partial\sigma^*} \qquad B.22$$

$$Q_1 = S_{uw}^{y}(p^* - \frac{p_y^* + k_t s_c}{2})^2 + (\frac{q^*}{M})^2 \qquad B.23$$

where y is the plastic potential parameter. The plastic potential parameter (γ) influences the volumetric behaviour of the soil. The soil behaves like a non-porous medium when very little unfrozen water is taken into account at γ=0. When γ=1.0, the unfrozen water content will be taken into account in its full extent, giving the possibility for water to move between the pores and cause plastic strains. The flow rule for the GS yield surface is associated:

$$d\varepsilon^{sp} = -d\lambda_2 \frac{\partial F_2}{\partial \sigma^*} I \qquad B.24$$

B.5. Influence of model specific parameters

A lot of parameters have been mentioned in the last 4 sections and seventeen of them are required in the numerical model. Some of these parameters are well known and can be easily associated with specific soil behaviour, like E_f, $E_{f,inc}$, v_f, k_t, G_0, M. Other parameters are difficult to grasp. Most of these difficult parameters belong the BBM for example β, $\lambda_{0,}$ r, p_c^*, p_{y0}^*, $\lambda_{s,}$ $\kappa_{s,}$. They are often hard to determine, since a single parameter does not control one feature of the soil behaviour, often combinations of these parameters control specific soil behaviour. This section is used to make these parameters more understandable and to see their influence on the soil behaviour.

Gallipoli et al. (2010) developed a sequential method to select parameters for the BBM based on experimental data from a isotropic compression test at saturated an unsaturated conditions. Since the FUS model is based on the BBM, the isotropic compression test of Gallipoli et al. (2010) can also clarify what the FUS model parameters mean and which influence they have on the soil behaviour.

During a frozen virgin isotropic compression test of a soil sample at a constant suction (s), the BBM gives a linear variation of specific volume (v) with the logarithm of mean net stress (p). The specific volume can be expressed as:

$$v = N(s) - \lambda(s) ln \frac{P}{P_c{}^*} \qquad B.25$$

At a constant suction equation B.21 defines a normal compression line in the BBM, with a slope λ(s). A normal compression line is visualised in the v:lnp plane in figure B5a. Normal compression lines at different suctions intersect each other in the critical pressure (p_c^*), thus p_c^* is the x-value of the intersection point between the normal compression lines. At p_c^*, the specific volume of the sample is N(s), so N(s) corresponds with the y-value at the intersection. The slope and interception between the normal compression lines with and without cryogenic suction depend upon the following relationships:

$$\lambda(s) = \lambda_0[(1-r)\exp(-\beta s) + r] \qquad B.26$$

$$\mathrm{N(s)} = \mathrm{N(0)} - \kappa_s \ln \frac{s + p_{at}}{p_{at}} \qquad B.27$$

where β is the parameter controlling the relative spacing between the normal compression lines with suction, λ_0 is the slope of the normal compression line at a suction of zero, N(0) specific volume at the critical pressure with zero suction, r is the ratio between the slopes of normal compression lines at suctions of infinity and zero ($r=\lambda(\infty)/\lambda(0)$), κ_s is the elastic compressibility coefficient associated with changes in suction and p_{at} is the atmospheric pressure. Combining equation B.25 and B.27 gives loading collapse (LC) yield locus according to the equation:

$$\frac{p_y^*}{p_c^*} = \left(\frac{p_{y0}^*}{p_c^*}\right)^{\frac{\lambda_0 - \kappa}{\lambda(s) - \kappa}} \qquad B.28$$

where p_{y0} is the pre-consolidation stress, which coincides with the yield stress at zero suction and defining the size of the unfrozen domain. κ is the elastic compressibility coefficient of the soil mixture (eq. B14). The LC yield curve in the p: s plane is visualises in Figure B.5b.

The conclusion from equation B.21, B.22, B.23 and B.24 is that the position of the normal compression at constant suction (the shape of the LC yield locus and how this shape develops as the yield surface expands) are determined by five parameters β, λ_0, r, p_c^*, and N(0). The positions of the normal compression lines at constant suction and the evolution of the LC yield locus are also influenced by the parameters κ_s and κ_0. Gallipoli et al (2010) assumed these parameters known. They can be defined by the elastic paths of loading-unloading (Figure B5) and wetting and drying (Figure B8).

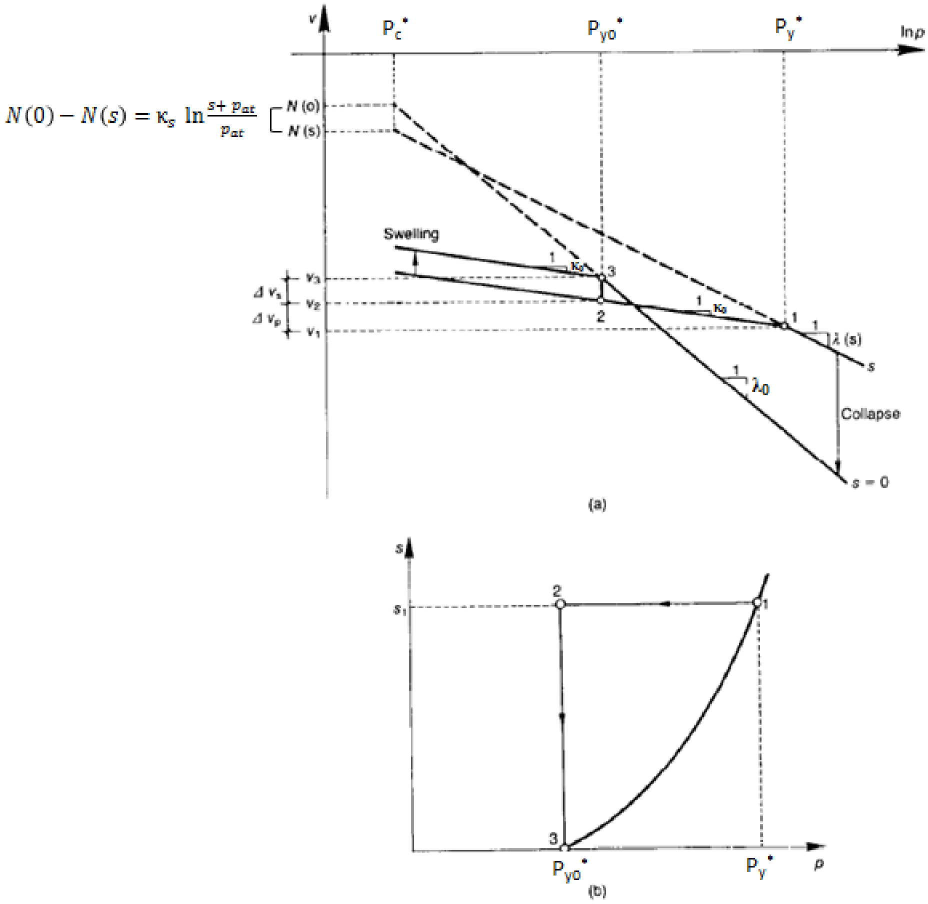

Figure B5: (a) Normal compression line for frozen and unfrozen (s=0) soil. (b) Stress path and LC yield curve in (p, s). (after Alonso et al., 1990)

The explanation and determination of the five parameters β, λ_0, r, p_c^*, and N(0) can be made easier with the mapped specific volume. Wheeler, Gallipoli and Karstunen (2002) defined the mapped specific volume (v^*) according to the following equation:

$$v^* = v + \lambda(s_c) \ln\frac{s+p_{at}}{p_{at}} \qquad B.29$$

Filling in equations B.21 an B.23 in equation B.26 shifts the v-ln p plane by a distance of along the vertical axis to the v*-ln p plane:

$$v^* = N(0) - \lambda(s_c) ln\frac{P}{P_c{}^*} \qquad B.30$$

When visualising this equation in a v^*-ln p plane the constant suction normal compression lines intersect all at the coordinates (p_c^*, N(0)) (Figure B.5a). The positions of the normal compression lines when using the mapped specific volume are fully defined by the five parameters β, λ_0, r, p_c^*, and N(0) and independent of the elastic parameter k_s.

Gallipoli et al. (2002) showed the effect of variation of a single parameter in the v*-lnp plane. In these variations it is assumed that r<1 and that the p_c* is smaller than the used pressure range in the BBM.

Otherwise, the v*;lnp space would like Figure B.5b. Figure B.6a shows the variation of parameter β, while the other four parameters are kept constant. The slopes of normal compression lines at a suction of infinity and zero are fixed. The spacing between the normal compression lines at other suctions is only controlled by the parameter β, according to formula B.26.. Variations in the parameter λ_0 affect the slope of the normal compression line at zero suction. This has also influence on the slope at other suctions, except for the slope of the normal compression line at infinite suction (Figure B.6b). Since parameter r is the ratio between the slope at zero suction and at infinite suction, the influence of parameter r can best be demonstrated by showing the change in $r\lambda_0$ i.e. the slope of the normal compression line at infinite suction ($\lambda(\infty)$).Just as the λ_0 has also $r\lambda_0$ influence on the slopes of the normal compression lines at other suctions, except for the slope of the normal compression line at zero suction (Figure B.6c). Changing the critical pressure p_c*, let all the normal compression lines at constant suction move over the x-axis, as shown in Figure B.6d. This works the same for changes in the intersection point on the y-axis, N(0). Variations are shown in Figure B.6d. In the FUS model the parameter of N(0) cannot be chosen. N(0) is chosen to be the initial specific volume (1+e).

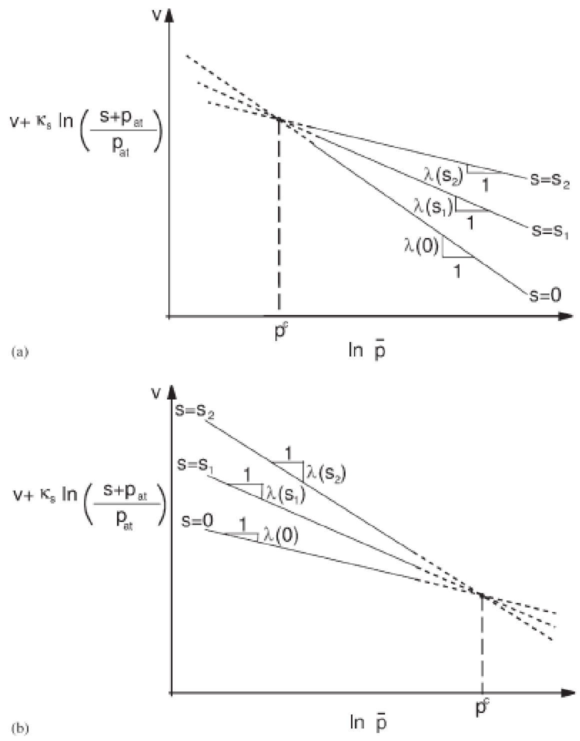

Figure B6: Visualization of the constant suction normal compression lines in the v*-lnp plane (a) r<1 (b) r>1 (Wheeler et al., 2002).

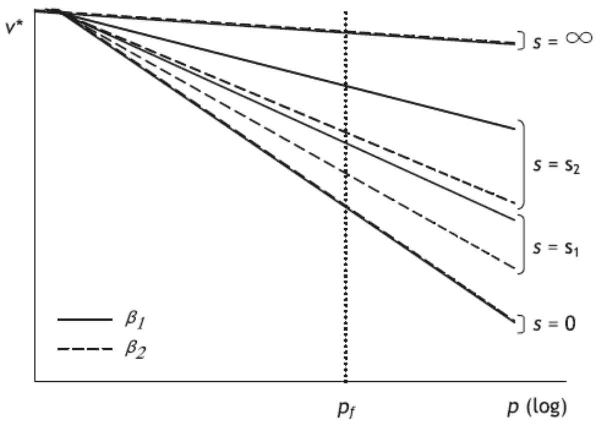

(a) Effect of variation of relative spacing , β.

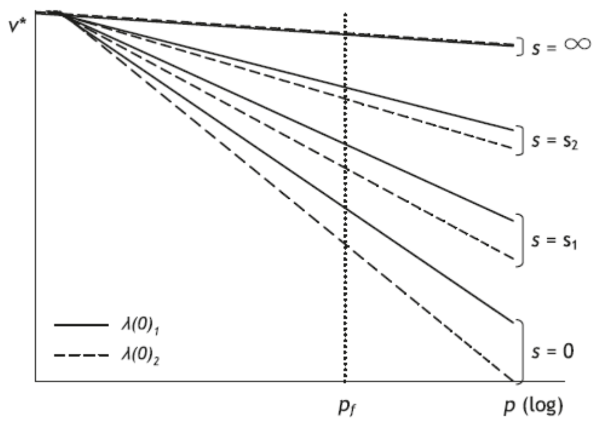

(b) Effect of variation of the slope of the normal compression line at zero suction, λ_0.

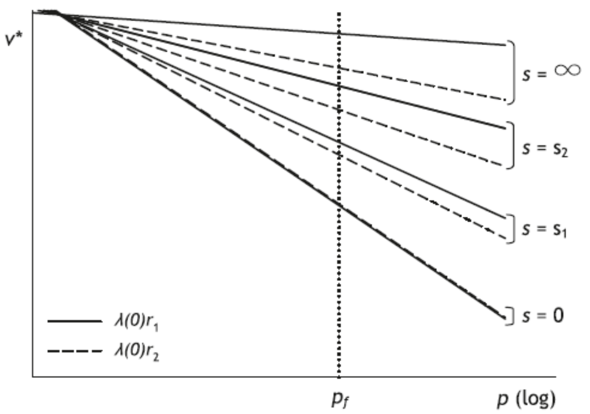

(c) Effect of variation of the slope of the normal compression line at infinite suction, λr.

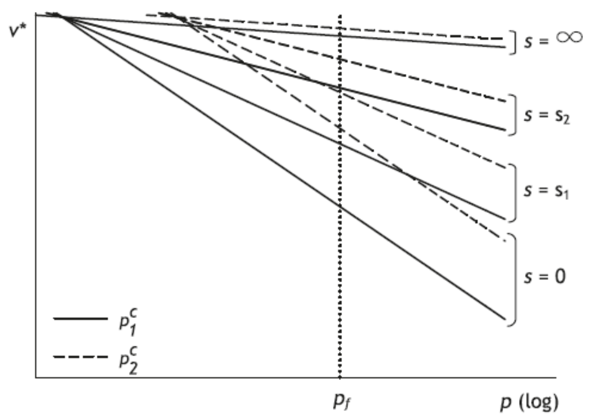

(d) Effect of variation of the intersection with the x-axis, p_c*

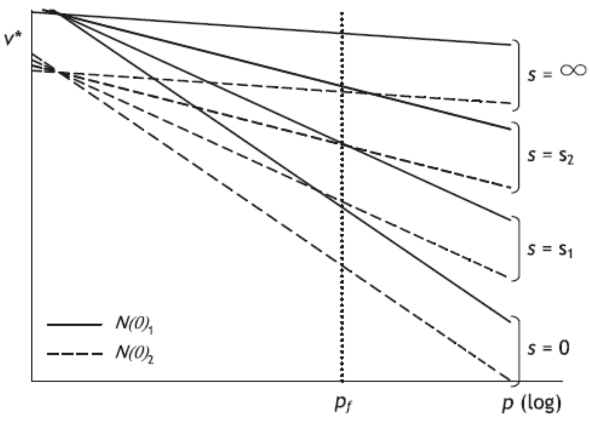

(e) Effect of variation of the intersection with the y-axis, N(0).

Figure B7: Effect of different parameters on the position of constant suction normal compression lines. (Gallipoli, 2010)

Alonso et al. (1990) described the changes in the shape of the LC yield curve with changing parameter β, r and p_{y0}^*. In this situation the parameters are: $p_c^* = 0.1$ MPa, $\lambda_0 = 0.2$, κ=0.02. The change in shape is visualised in Figure B8:

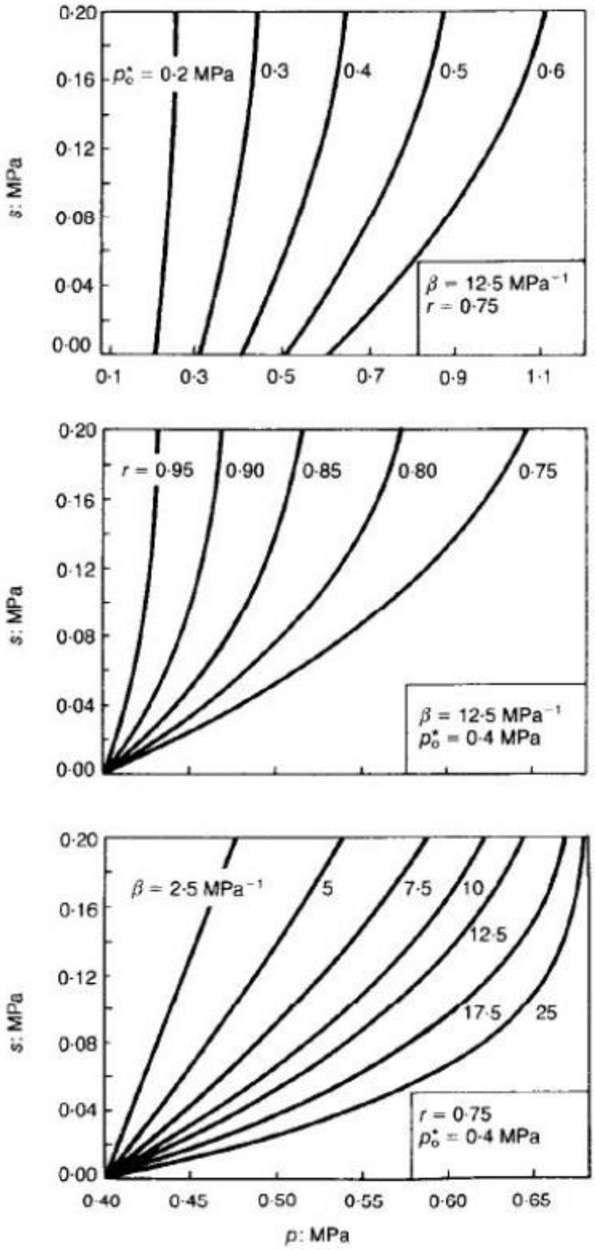

Figure B8: Shapes of the LC yield curve for variation in parameters P_{y0}^*($=p_0^*$), β and r. (Alonso et al., 1990)

An increase in net mean stress not only can cause irreversible strains, also an increase in suction can induce irrecoverable strains. The suction at which these irrecoverable strains start is the maximum suction ever experienced by the soil, s_{seg}. Although some dependence of the stiffness parameters elastic (κ_s) region and virgin state (λ_s) can be expected on the mean net stress, they are assumed to be constant. The v:lns plane is shown in Figure B9. The corresponding yield surface is called the suction increase (SI) surface in the BBM, or grain segregation (GS) surface in the FUS model (Figure B10). In the original BBM an increase in suction above the s_{seg} value causes a volume decrease of the soil (Figure B9a) according to the following equations:

$$d\varepsilon_v^{se} = \frac{k_s}{(1-e)}\frac{ds}{s-p_{at}} - \qquad B.31$$

$$d\varepsilon_v^{s} = \frac{\lambda_s}{(1-e)}\frac{ds_{seg}}{s_{seg}-p_{at}} - \qquad B.32$$

$$d\varepsilon_v^{sp} = \frac{\lambda_s + \kappa_s}{(1-e)}\frac{ds_{seg}}{s_{seg}+p_{at}} \qquad B.33$$

where $d\varepsilon_v^s$ is the increment of strain due to suction variation. In the FUS model, an increase in cryogenic suction above the s_{seg} value leads to more ice segregation i.e. a volume increase. To obtain the opposite effect and let the soil expand with suction, the value of λ_s is made negative in equation B.32 and B.33, the formula is then expressed as equation B.18. The value of k_s is kept positive in the model and thus in the elastic region the soil volume decreases with suction (Figure B9b).

The choice to make the elastoplastic compressibility coefficient in frozen state (λ_s) negative and the elastic compressibility coefficient in frozen state k_s positive is based on two mechanisms from pre-melting dynamics described by Wettlaufer and Worster (2006), namely curvature-induced pre-melting and interfacial pre-melting (Figure B11). The curvature induced pre-melting is a result of surface tension, acts like capillary suction and bonds grains together. At low ice contents this force leads to high soil strengths by bonding the gains together. Low ice contents mean low values of cryogenic suction and corresponds to the elastic region where k_s dominates the volumetric behaviour. The second pre-melting mechanism is the interfacial pre-melting, which can be seen as a repelling force between the ice and water. This disjointing pressure tends to widen the gap by sucking in more water (Ghoreishian Amiri et al., 2016). This phenomenon occurs at high ice contents, when the soil is weakened by grain segregation. High ice content means high values of cryogenic suction and corresponds to the plastic region where λ_s dominates the behaviour. Thus curvature induced pre-melting leads to a volume decrease by bonding the grains together and interfacial pre-melting causes the soil to expand due to repelling forces.

On the other hand, when cryogenic suction decreases, i.e. the soil thaws, a volumetric decrease of the soil is expected due to the volume decrease of water. The volume decrease will occur in the plastic region however, when it is situated in the elastic region no volume decrease will occur due to the positive value of k_s. When the value of k_s is made negative, a volume decrease will also occur in the elastic region upon thawing this is shown in Figure B9c (NOTE: the sign convention is different in Plaxis, the k_s is in this case positive. To make a negative variable positive, a negative value has to be entered).

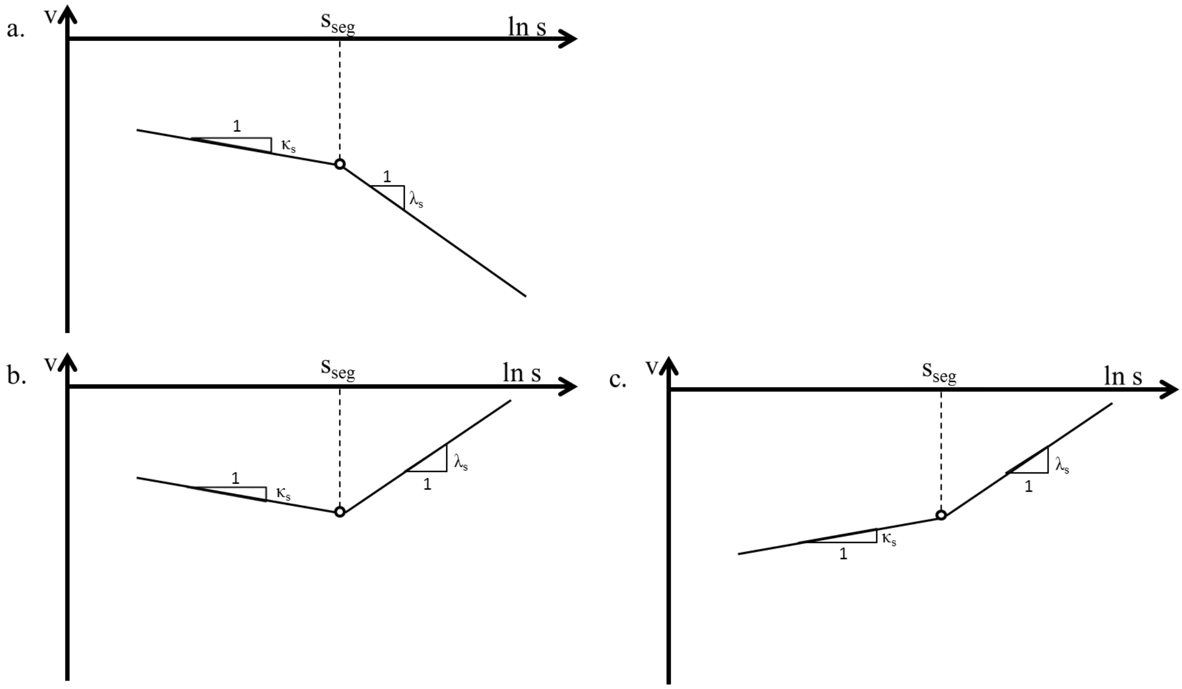

Figure B9: Change in v:lnp plane with choice of k_s and λ_s. (a) Compression curve in the original barcelona basic model (k_s & λ_s are negative). (b) Compression curve in the frozen and unfrozen soil model (k_s is negative & λ_s is positive). (c) Compression curve in the frozen and unfrozen soil model when k_s is positive (k_s & λ_s are positive).

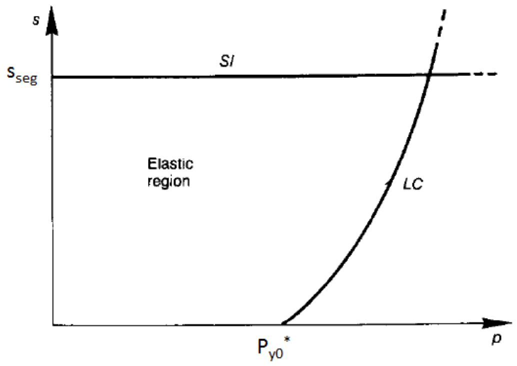

Figure B10: Loading collapse yield surface and the suction increase yield surface (after Alonso et al., 1990)

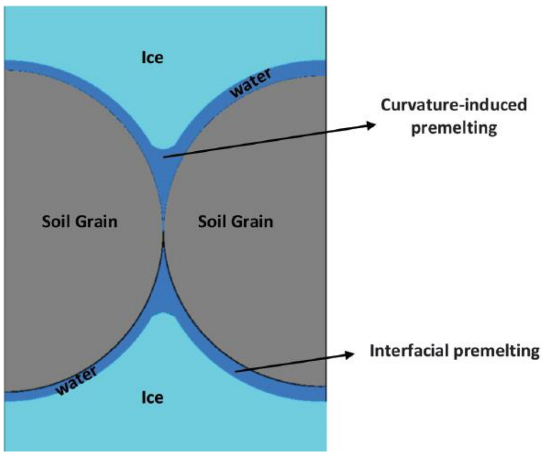

Figure B11: Schematic representation of curvature-induced premelting and interfacial premelting (Ghoreishian Amiri et al., 2016)

APPENDIX C: SOIL TESTS

C.1 Final parameter set

Elastic parameters	Symbol		Unit
Stiffness frozen	$E_{f,ref}$	40.00E6	N/m^2
Stiffness increase with temperature	$E_{f,inc}$	13.00E6	N/m^2
Poisson ratio frozen soil	ν_f	0.31	-
Unfrozen shear modulus	G_o	14.80E6	N/m^2
Elastic compressibility coefficient for cryogenic suction variation	κ_s	-5.00E-3	-
Unfrozen elastic compressibility coefficient	κ_0	0.13	-
Strength parameters			
Slope of the critical state line	M	0.77	-
Increase in apparent cohesion	k_t	0.17	-
Segregation potential	$(S_{c,seg})_{in}$	3.50E6	N/m^2
Yield parameter	m	1.0	-
Plastic potential parameter	γ	1.0	-
Parameters controlling virgin loading under isotropic stress state and cryogenic suction variation			
Rate of change in soil stiffness with cryogenic suction	ß	0.60E-6	m^2/N
Elasto-plastic compressibility coefficient for unfrozen state	λ_0	0.15	-
Coefficient related to the maximum soil stiffness	r	0.60	-
Reference stress	p^*_c	5.00E5	N/m^2
Elasto-plastic compressibility coefficient for cryogenic suction variation	λ_s	0.1	-
Initial pre-consolidation stress for unfrozen conditions	P^*_{y0}	-1.50E6	N/m^2
Thermal parameters			
Thermal conductivity	λ_{s1}	920	W/m/K
Specific heat capacity	c_s	1.90	J/kg/K
Density of solid material	ρ_s	2700	Kg/m^3
Solid thermal expansion coefficient, x-direction	α_x	5.2E-6	1/K
Solid thermal expansion coefficient, y-direction	α_y	2.0E-6	1/K
Solid thermal expansion coefficient, z-direction	α_z	5.2E-6	1/K
Parameters for fitting the SCFF curve			
Parameter for fitting the SCFF curve	λ_r	0.25	-
Parameter for fitting the SCFF curve	ρ_r	1.30E5	N/m^3
Parameter for the pressure dependency of ice thawing temperature ($7 \leq \alpha \leq 9$)	α	9.0	-

C.2 Uniaxial compression test

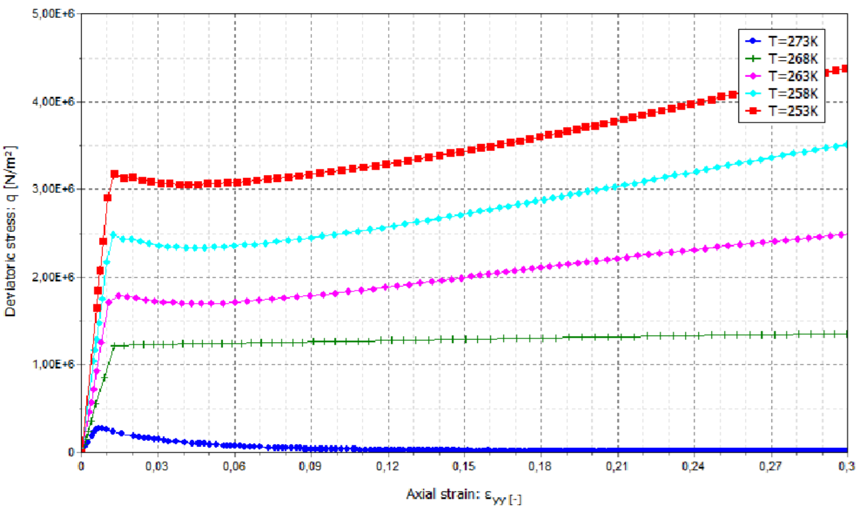

Figure C1: Stress-strain diagram of uniaxial compression test for different temperatures

C.3 Heave test

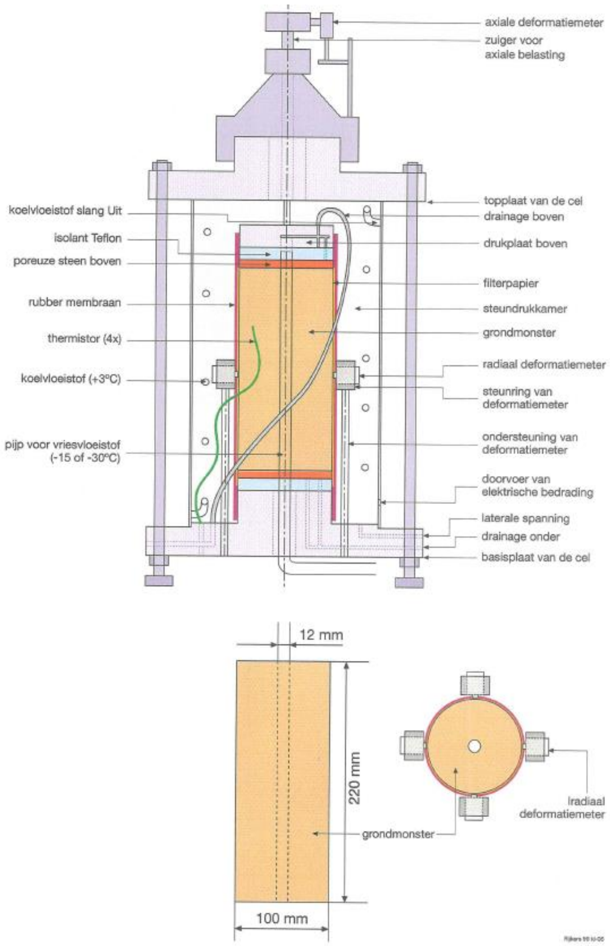

Figure C2: Special triaxial cell with freeze pipe (Report NITG 99-232-B, 2000).

APPENDIX D: CROSS PASSAGE MODELS

D1: Water pressures

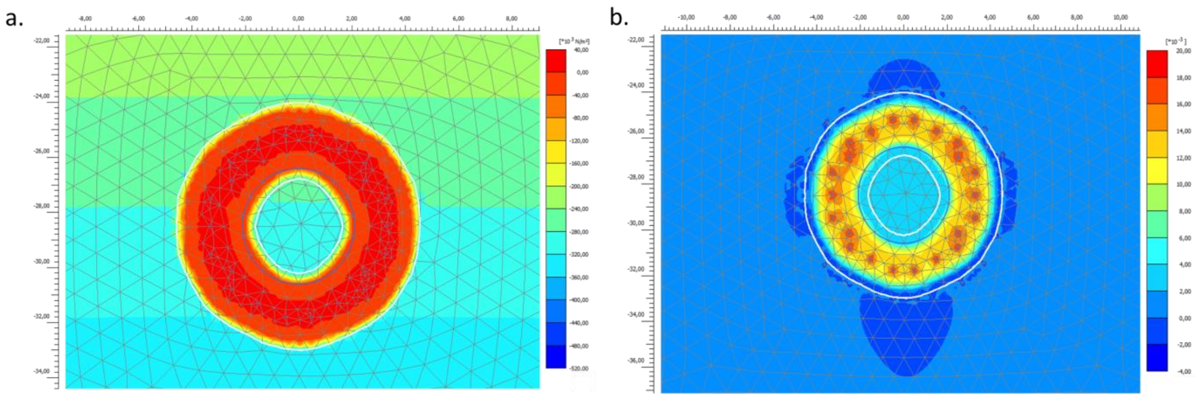

Figure D1: 55 days of freezing in M1a. Active pore water pressures b. Volumetric strain

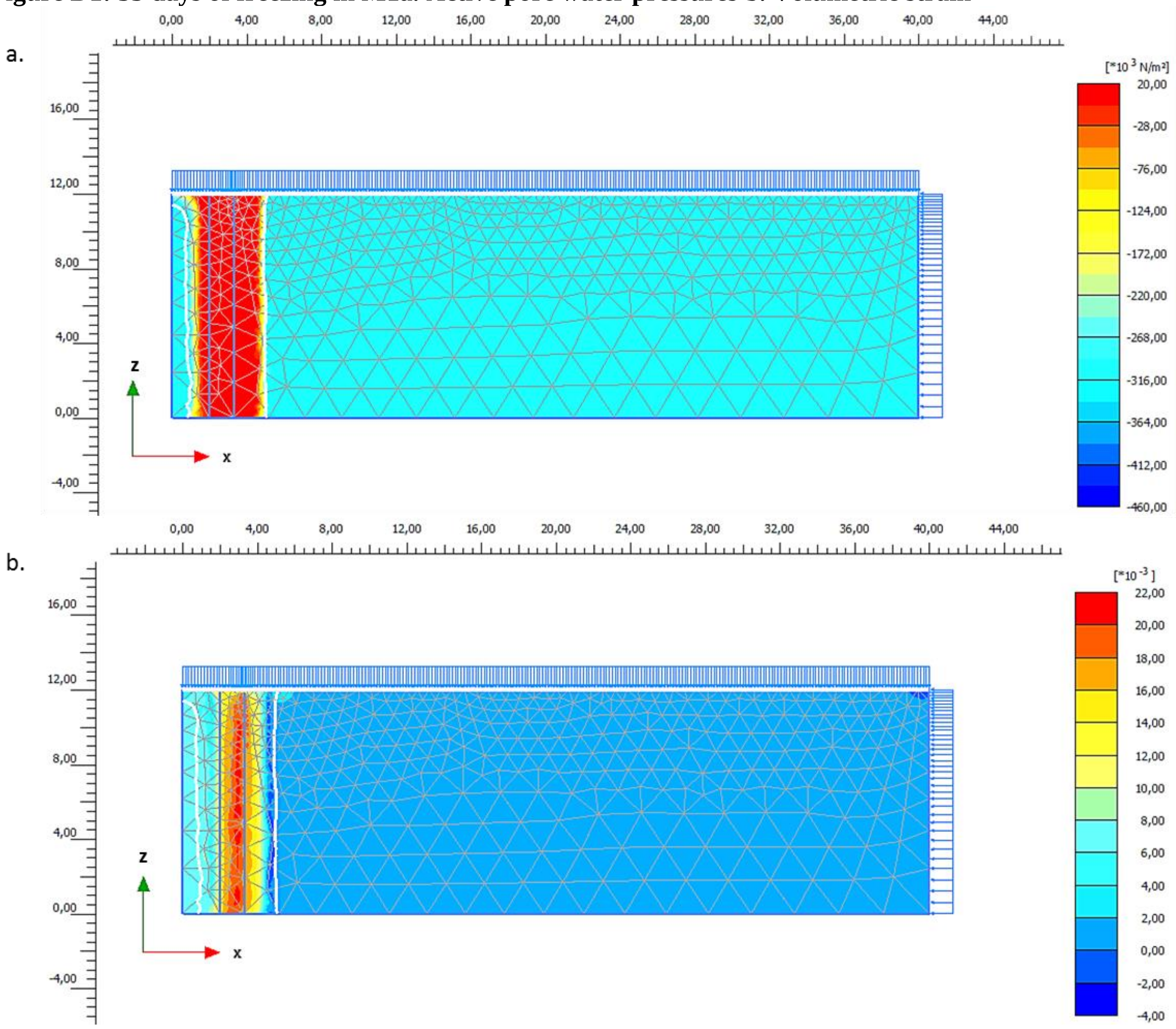

Figure D2: 55 days of freezing in M2 a. Active pore water pressures b. Volumetric strain

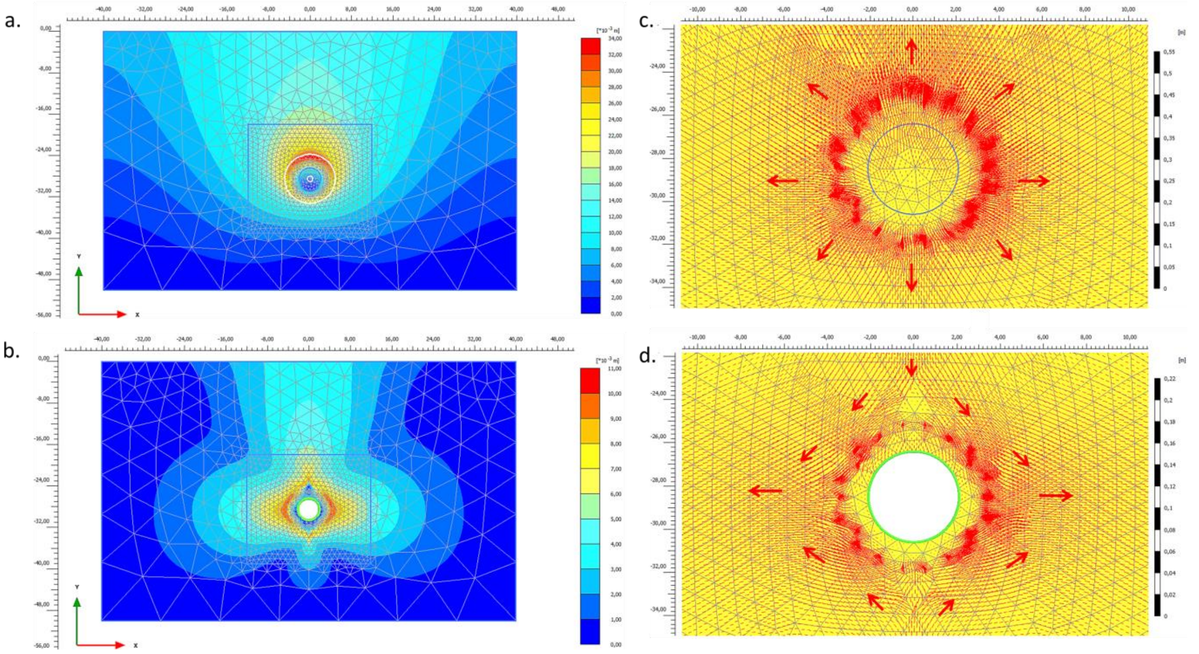

Figure D3: Deformations in M1 a. Contour plot total phase freezing phase b. Contour plot displacements in the thawing phase c. Indication direction of deformation freezing phase d. Indication direction of deformations thawing phase